UNIVERSITY OF CALIFORNIA SAN DIEGO

Cortex drives orofacial behaviors through distinct brainstem networks

A dissertation submitted in partial satisfaction of the
requirements for the degree Doctor of Philosophy

in

Biology

by

Nicole Mercer Lindsay

Committee in charge:

Professor David Kleinfeld, Chair
Professor Brenda Bloodgood
Professor Daniel Gibbs
Professor Harvey J. Karten
Professor Takaki Komiyama

2018

The Dissertation of Nicole Mercer Lindsay is approved, and it is acceptable in quality and form for publication on microfilm and electronically:

_____

_____

_____

_____

_____

Chair

University of California San Diego

2018

DEDICATION

I would like to dedicate this work to Adam and James and Samson for their continuous excitement, encouragement, and support. This would have been a lonelier journey without them.

TABLE OF CONTENTS

LIST OF TABLES AND FIGURES

ACKNOWLEDGEMENTS

I would like to thank my committee, Professors Harvey Karten, Brenda Bloodgood, Daniel Gibbs, and Takaki Komiyama. Each has been a source of critical feedback that shaped the project. I would especially like to thank Harvey Karten for being a mentor throughout my project and for sharing his unique insights into neuroscience and anatomy in particular.

I would especially like to thank my advisor David Kleinfeld. He has helped formulate this project from the beginning and was willing to let me take risks to see what we could find. He continuously made sure the resources were present for this project to proceed and went above and beyond to obtain new, cutting edge technologies that would push the boundaries of what we could find.

Chapter 2 of this work is a manuscript in preparation: Mercer Lindsay N, Knutsen, Per M, and Kleinfeld D. "Motor cortex drives orofacial behaviors through distinct brainstem networks." Under final preparation. The dissertation author is the primary author of this work.

Chapter 3 of this work is currently published in "Moore JD, Mercer Lindsay N, Deschénes M, and Kleinfeld D. "Vibrissa Self-Motion and Touch Are Reiably Encoded along the Same Somatosensory Pathway from Brainstem through Thalamus." PLoS Biology, 13(9):e1002253, 2015. It is used here with the consent of all authors and the journal. I contributed figure 2 of the paper.

VITA

2018 Ph.D., Biology
University of California San Diego

2011 Bachelor of Arts in Biological Sciences with a concentration in Neurobiology and Behavior
Cornell University

2010 Summer Undergraduate Research Intern
University of Utah

PUBLICATIONS

Moore, J.D., Mercer Lindsay, N.A., Deschénes, M., & Kleinfeld, D. (2015). Vibrissa self-motion and touch are reliably encoded along the same somatosensory pathway from brainstem through thalamus. *PLoS Biol*, 13(9): e1002253.

ABSTRACT OF THE DISSERTATION

Cortex drives orofacial behaviors through distinct brainstem networks

by

Nicole Mercer Lindsay

Doctor of Philosophy in Biology

University of California San Diego, 2018

Professor David Kleinfeld, Chair

Sensorimotor circuits are the base of how we experience and interact with the world. Voluntary movement is initiated from the motor cortex through descending inputs to premotor circuits in the brainstem and spinal cord. The descending cortical cells send collateral axons to many of the same brainstem regions regardless of where in motor cortex they originate. While it is clear that distinct regions of motor cortex initiate specific movements, it is unknown how these movements arise given the largely similar projection targets. Here, we closely examine the cortical inputs to two premotor nuclei found within the spinal trigeminal nucleus by using projection-

specific optogenetics in concordance with anterograde and retrograde tracing methods. We next consider how the sensory perception of self-motion are transmitted up to the cortex through the thalamus. It was previously proposed that the two distinct trigemino-thalamic pathways separately transmit information for touch and self-motion respectively. Here we show that the premotor nucleus that receives input from motor cortex does not transmit information for the self-motion but instead the more strictly sensory principal sensory nucleus is responsible for transmission of both touch and self-motion to somatosensory cortex through VPM thalamus.

Chapter 1. Introduction

Sensorimotor circuits are the basis for animals experiencing and interacting with the world. Incoming sensory information for vision, touch, audition, olfaction, and taste define our surroundings while vestibular and proprioceptive information grounds our bodies. In turn, we move through activation of motor circuits. These circuits are essential for survival and critical for decision making, learning, and other higher order circuits. Sensorimotor circuits are continuous loops of sensory information and motor output. Here we start with the motor output and work out way back to the sensory input.

Movement, the output of motor circuits, is ultimately enacted through motoneurons contacting muscles (Buchthal and Schmalbruch, 1980). Motoneurons are integrators of many incoming signals; in some cases, these signals are peripheral sensory inputs (Buchthal and Schmalbruch, 1980; Sherwood, 2005). These circuits are reflexive. Some reflex circuits utilize secondary sensory neurons as intermediaries between the ganglion input and the motoneuron (Gonzalez-Joekes and Schreurs, 2012).

Here we examine how higher order motor circuits contact brainstem sensory premotor areas and then then how these same brainstem nuclei send information to the thalamus.

1.1 The three types of motor cortex maps

Volitional movement typically requires a vast array of muscles activated in precise harmony (Miri et al., 2017; Wang et al., 2017). In addition to the muscles utilized for the action component of the movement, there are muscles recruited for postural control and reflexive adjustments (Massion, 1994). Both the action and postural movements arise from the interface between the motor cortex and brainstem and spinal cord premotor circuits and, in the case of

primates, motoneurons directly. How the volitional controller, the motor cortex, interfaces with these downstream motor circuits is largely unknown (Alstermark and Isa, 2012; Azim et al., 2014; Lemon, 2008, 2016; Rathelot and Strick, 2009).

Motor cortex was defined in the late nineteenth century, first in dogs (Fritsch and Hitzig, 2009) and later in nonhuman and human primates (F. and S., 1917; Frederick, 1953), as the part of the cortex in which muscle twitches were evoked from electrical stimulation at the lowest threshold. These types of experiments led to the first type of map found in motor cortex: a muscle map. This map emerged from studies in each of these animals that showed the muscle twitches roughly exist in a representation of the body (Brecht et al., 2004; Tennant et al., 2011). The map itself was not a 1:1 representation of the body, but rather distorted. In humans, for example, the digits and hand representations are relatively larger than the trunk and legs (Brecht et al., 2004; F. and S., 1917; Frederick, 1953). The dexterous movements taken up by the digits and hand are thought to explain this enlargement. Similarly in rodents, the representation of the vibrissa, the facial touch sensors, and forelimb are larger than other representations (Brecht et al., 2004; Ferezou et al., 2007).

As histological studies progressed alongside stimulation studies, a second map emerged: a cytoarchitectural map. While sensory and prefrontal cortices have a thick layer 4, a cytoarchitecture referred to as granular, primary motor cortex was agranular, or lacking a distinct layer 4 (Donoghue and Wise, 1982; Tennant et al., 2011). In primates, an additional map was eventually proposed and motor cortex, M1, was added upon. The new area, M2 is more commonly called the supplemental motor area (SMA) (Graziano, 2016). SMA has a dysgranular structure with a thin layer 4. Other additional premotor structures were later identified in close proximity to SMA and follow its variable granular structure (Graziano, 2016). The distinction between the

presence, absence, or weak appearance of L4 is relevant to the incoming sensory inputs from the thalamus (Moore et al., 2015a).

That motor cortex controls individual muscles alone was challenged by later electrophysiology studies. These studies found that excitatory neurons in motor cortex are active throughout a movement, typically for at least 500 ms (Georgopoulos et al., 1982; Graziano et al., 2002; Peters et al., 2014). The duration of activity indicated the possibility that motor cortex muscle maps were an artifact of short pulse (<50 ms) stimulation. Studies performed by Graziano and colleagues attempted to mimic the cellular firing in motor cortex by stimulating with electrical trains lasting for 500 ms (Graziano et al., 2002). With these parameters, ethological, or behaviorally relevant, movements were evoked. A third map was defined: a map of distinct movements. These movements ranged from reaching to grasp to climbing to hand to mouth (Graziano et al., 2002). Many of the movements they found utilize context of where the forelimb is in space prior to the movement to orient the following movements. For example, the movement to the mouth followed a different trajectory to reach the mouth, depending upon where the forelimb was in space prior to the stimulation. They clearly identified contralateral, ipsilateral, and bilateral forelimb region over the traditional forelimb muscle representation (Graziano et al., 2002). Other studies in primates identified the cortical masticatory area (CMA) (Huang et al., 1989). When stimulated, the CMA evokes rhythmic chewing movements. The CMA was in the same region as the jaw twitching region of primate motor cortex (Graziano and Aflalo, 2007). The movement map is very similar to the muscle map in terms of body region representation but instead of representing single muscles, is a map of overlapped muscles that result in distinct movements.

Mouse motor cortex also has these three maps. The muscle and movement maps have the head oriented rostrally with the trunk, hindlimb, and tail stretching caudally (Ferezou et al., 2007;

Tennant et al., 2011). Two distinct types of cytoarchitecture are seen: the agranular medial (AG_m) and lateral (AG_l) areas (Donoghue and Wise, 1982; Tennant et al., 2011). The AG_m has a denser layer II with a pale layer III while AG_l layers II and III look relatively similar. In the Paxinos atlas, AG_m and AG_l are called M2 and M1 respectively (Donoghue and Wise, 1982). The rostral pole of the mouse, sometimes called Fra, is a part of motor cortex whose cytoarchitecture looks similar to AG_m but has a less distinctive layer II, raising the possibility that this region is a third cytoarchitectural area (Donoghue and Wise, 1982).

The muscle map of the mouse has been defined in a series of papers ((Ferezou et al., 2007; Hollis et al., 2016; Tennant et al., 2011; Wang et al., 2017)). While instructive, these studies were mostly done in anesthetized animals with observations performed by eye. Studies have found that that vibrissa representation can only be detected under the lightest anesthesia and, when the mice were more deeply, the same region became the neck representation (Tennant et al., 2011). This sensitivity to ketamine makes it difficult to accurately map mouse motor cortex while anesthetized. Additionally, these studies mostly observed movements by eye. The small nature of mice makes it difficult to observe their movements (e.g. jaw, tongue, and nose movements). From these studies we can see the general location of different motor regions (Ferezou et al., 2007). The forelimb is clearly present in two clusters: the rostral and caudal forelimb areas (the RFA and CFA respectively). Note the location of the RFA and CFA can also be observed by injecting retrograde tracers in the spinal cord (Wang et al., 2017). Vibrissa and neck movements were found medial and lateral than the RFA while jaw opening has been found more lateral and rostral (Ferezou et al., 2007; Hira et al., 2013; Tennant et al., 2011).

The third motor map in the mouse, the movement map, has shown a direct overlay on the muscle map. Mice genetics have added an advantage to studying this map: the Thy1-ChR2 line, a

mouse line with ChR2 in all excitatory neurons in layer 5 of cortex (Harrison et al., 2012), can be used for stimulation of the solely the cortical output cells. Stimulation studies on this mouse line have found that the RFA roughly corresponds to a region that abducts or elevates the forelimb (Harrison et al., 2012). This directive movement of the forelimb towards the direction of the mouth is in close proximity to the coordinates defining the anterior lateral motor cortex (ALM) where rhythmic licking has been identified (Komiyama et al., 2010).

1.2 The descending projections of motor cortex in rodents and brainstem premotor nuclei

The output of motor cortex has four major targets: neighboring regions of cortex, the basal ganglia, the thalamus, and brainstem and spinal cord premotor circuits (Oswald et al., 2013). The last of these are called corticofugal cells and are the motor cortex's shortest pathway to orchestrating movement.

The corticofugal projections are part of the corticobulbar and corticospinal tracts that compose the pyramidal tract. While these two tracts travel through the internal capsule and down through the pyramids in the medulla, a major distinction is in the pattern at which the axons separate from the main tract, anatomically called the desiccation pattern (Young et al., 2015). In humans, 90% of the corticospinal tract cross the midline to the contralateral side at the level of the medulla (Young et al., 2015). In humans, the corticobulbar tract, on the other hand, projects bilaterally to many brain targets, including the facial, trigeminal, hypoglossal, and ambiguus motor nuclei (Sherwood, 2005; Young et al., 2015). These bilateral projections are typically found for face and head muscles that are part of bilateral unison motor systems like the tongue and jaw (Young et al., 2015). In rodents, direct projections to cranial motor nerve nuclei have been identified for the facial, trigeminal, and ambiguus motor nuclei (Arriaga et al., 2015; Grinevich et al., 2005a; Takatoh et al., 2013a) but are typically contralateral only (Grinevich et al., 2005b).

Direct projections from cortex to motor nerve nuclei are thought to play a role in fine behaviors like speech vocalizations for the ambiguus (controls the larynx) and facial expressions for the facial motor nucleus (Arriaga et al., 2015; Grinevich et al., 2005a).

Motor neurons in adult mammals typically project to a single muscle (Buchthal and Schmalbruch, 1980). The input to the cranial motor neurons is most dense from the reticular formation of the brainstem (Stanek et al., 2014; Takatoh et al., 2013b). Thus, the premotor level between the cortex and the motor neurons mediates most face and head-related behaviors.

Retrograde tracing of the premotor neurons from the muscles or motor neurons shows a large overlap with anterograde tracing from motor cortex (Hattox et al., 2002). A rather long list of premotor nuclei targeted by motor cortex has been created. Of the identified nuclei, there are well-studied regions like the superior colliculus and periaqueductal grey and many poorly understood subdivisions of the reticular formation.

The reticular formation, sometimes called the reticular activating system, is the middle part of the brainstem that histologically looks like a net (Pfaff et al., 2008). Its subdivisions are largely congruent with the different divisions of the brainstem i.e. midbrain, pontine, and medullary reticular formation. Some of these are further divided based on cell size—the parvicellular, intermediate, and giganticellular reticular formation or on the relative position—the dorsal and ventral medullary reticular formation or the oral and caudal pontine reticular formation. While there are known aspects of each of these parts of the reticular formation, there is a lot of missing pieces to understanding their various roles in motor control as well as other contributions like sleep and breathing. Cell groups in the reticular formation have been less compact than in other nuclei. An example of this is the vibrissa intermediate reticular formation. This region contains the central pattern generator for the vibrissa rhythmic whisking (Moore et al., 2013). When recording

identified these cells, they were in a loose cluster with interspersed cells rather than all bundled together as is often seen in other brain regions. This particular feature of the reticular formation complicates the identification of function within each loosely defined subdivision.

While the reticular formation constitutes most of the premotor neurons in the brainstem, here we chose to study the trigeminal sensory nuclei, another region that receives motor cortex input and also projects to different motoneurons. The advantage of the secondary sensory nuclei was the topography defined by sensory afferents (Jacquin et al., 1993). Additionally, these sensory afferents position the trigeminal sensory neurons to be part of short di- and trisynaptic sensorimotor loops.

In studies comparing projections from different injections that span motor cortex, bouton density for different brainstem nuclei is similar (Alloway et al., 2010). Further, studies examining single cell axonal projections of motor cortex neurons find these cells typically send collaterals to many of these structures (Kita and Kita, 2012). How then does specificity of motor movements arise? While there must be some specific connection between the motor cortex cells and their brainstem targets, it is not simply in which nuclei they target.

1.3 The sensory and motor features of the trigeminal complex

The somatosensory information for the face is directed through the trigeminal ganglion and into the trigeminal complex (Olszewski, 1950; Zucker and Welker, 1969). The trigeminal complex includes the principal sensory nucleus (PrV), the spinal trigeminal nucleus (SpV), and the mesencephalic nucleus (Zucker and Welker, 1969). The mesencephalic nucleus is not discussed here. In rodents, SpV can be further subdivided into oralis (SpVO), rostralis interpolaris (SpVIr), caudalis interpolaris (SpVIc), muralis (SpVM), and caudalis (SpVC) (Furuta et al., 2006b). Each

nucleus has its own sensory map that is related but distinct from its neighbors (Jacquin et al., 1993; Jacquin and Rhoades, 1990; Jacquin et al., 1986; Kerr, 1970). Originally defined in humans, PrV and the subnuclei of SpV show clearly different patterns of cell density and heterogenetiy in rodents (Furuta et al., 2006a; Furuta et al., 2008; Olszewski, 1950).

Rodent PrV is composed of small, densely packed excitatory cells (Furuta et al., 2008). This nucleus is responsible for relaying information up to ventral posterior medial (VPM) thalamus. This sensory pathway is classically called the lemniscal pathway and will be further discussed in section 1.4. The sensory map in PrV dedicates the dorsal part of the nucleus to mechanosensation of the neck and jaw fur and skin as well as the inside of the mouth and teeth. The ventral part of PrV has a rostro-caudal column for each vibrissa (Jacquin et al., 1993). The ventromedial part of PrV has a representation for the nose and area of the face around the eye. The map in PrV is defined by the discrete sensory inputs to cells. This is clearest when examining the vibrissa barrelette region. In coronal sections stained with either SDH or the excitatory neurotransmitter vGluT1, small circles corresponding to each vibrissa can be seen showing the physical representation of the vibrissae (Sakurai et al., 2013b).

Caudal to PrV is SpVO, a region defined in human by small cells but in rodent is a region that begins with small cells with a few scattered larger cells and transitions caudally to an increased density of these larger scattered cells. This transition blends in to the beginning of the SpVIr, a region with a relatively constant pattern of small cells with larger cells mixed in (Jacquin et al., 1989a; Jacquin et al., 1989b; Jacquin and Rhoades, 1990). SpVO and SpVIr are typically divided at the caudal end of the facial motor nucleus due to the less than clear border present in a nissl stain (Furuta et al., 2006a). The border is clearer when looking at excitatory and inhibitory cell distribution. The large cells in SpVO and SpVIr express the excitatory transmitter vGluT2 while

the small cells express the inhibitory transmitter VIAAT. What defined the boundary is vGluT1, which is only found in SpVIr, not SpVO (Furuta et al., 2008).

The sensory maps in SpVO and SpVIr are not discrete but rather cells here receive input for a wider swatch of the face (Furuta et al., 2006b). The sensory maps still follow the same general organization of the jaw fur, inside the mouth, and teeth in the dorsal part of the two nuclei with the vibrissae, nose, and region around the eye at the bottom. The sensory maps in SpVO and SpVIr have much smaller vibrissa representations than the adjacent PrV and SpVIc nuclei (Jacquin and Rhoades, 1990). In the rostral part of SpVO they are very small and gradually increase in size so that the representation in SpVIr is a little larger. In turn, the teeth and inside the mouth representation of SpVO is larger than in SpVIr. SpVIr projects to the Po thalamus as the conduit for the paralemniscal pathway (See 1.4).

SpVO and SpVIr are distinctive for having premotor neurons. Studies have found premotor neurons here for the facial (Erzurumlu and Killackey, 1979; Pinganaud et al., 1999; Takatoh et al., 2013a), trigeminal (Olsson and Westberg, 1991; Stanek et al., 2014; Westberg et al., 1998), and hypoglossal motor nuclei (Borke et al., 1983; Pinganaud et al., 1999; Stanek et al., 2014) as well as the spinal cord (Esposito et al., 2014). Tracing studies using the EnvA-rabies virus for input output tracing have found premotor neurons specifically for the intrinsic (vibrissa protraction) and extrinsic (vibrissa retraction) vibrissa muscles, the masseter (jaw closing), the genioglossus (tongue retraction), and the biceps brachii (elbow flexion).

SpVIc is composed mostly small inhibitory cells expressing VIAAT and GAD67 with a few vGluT1 positive cells (Furuta et al., 2008). This region is relatively taller and wider than its neighbors with a much larger vibrissae representation, spanning most of the dorsoventral length (Sakurai et al., 2013a). Here, the sensory map, like that in PrV, has discrete barrelettes for the

vibrissae. The small inhibitory cells have been found to keep their dendritic arbors within the barrelettes and extend their axons to PrV where they are hypothesized to play a role in modulating incoming sensory information that is destined for the barrel cortex (Furuta et al., 2010). Additionally, a small thalamic projection passes up to VPMvl that forms the extralemniscal pathway.

Caudal to SpVIc is SpVM, a distinctly pale barrier between SpVIc and SpVC in a cytochrome oxidase or SDH stain. SpVM has mostly VIAAT and GAD67 positive inhibitory cells with a few vGluT2 positive cells bordering the trigeminal nerve (Furuta et al., 2008). Past work suggests the sensory map in SpVM is particularly different than the other trigeminal nuclei (Jacquin et al., 1988). Rather than a map of the whole face, the SpVM sensory map depicts touch to the oral and nasal mucosa and the cornea. This type of sensory information is likely to play a role in processing noxious stimuli.

SpVC, the most caudal of the spinal trigeminal nuclei, is known for its processing pain inputs from the face. SpVC is a heterogeneous mix of excitatory and inhibitory cell types (Furuta et al., 2008). The histological feature that marks SpVC are the distinct rostral caudal layers. SpVC projects to VPM thalamus as part of pain processing circuits that mimic the anterior lateral tract that originates from nociceptive secondary neurons in the spinal cord.

PrV and SpV are visibly different from the reticular formation based on the broad swatch of flowing myelinated fibers that course trough in the rostral caudal direction. At the border with the reticular formation, distinctly smaller and more numerous fiber tracts course through the parvicellular reticular formation (PcRt)(Sreenivasan et al., 2015). These fibertracts are where the descending motor cortex fibers most commonly flow, sending collaterals into both the trigeminus and the reticular formation.

1.4 Descending projections to the spinal trigeminal nuclei

The presence of a motor cortex projection to SpV in rodents has been controversial. Part of this controversy arose from the use of traditional tracers, which are less efficient than modern viral tools. As anterograde AAV tracing began to be used, the presence of projections from motor cortex to SpVO and SpVIr emerged in figures and tables in the literature (Grinevich et al., 2005a; Jeong et al., 2016; Sreenivasan et al., 2015). However, in cats, a motor cortex descending pathway to SpVO showed that SpVO is a mediator of different motor cortex induced chewing movements (Olsson and Westberg, 1991). In macaques it has been shown that M1, which projects most heavily lamina VII of the spinal cord, was known to have boutons in the dorsal horn, a parallel pathway from motor cortex to secondary sensory cells in the spinal cord (Morecraft et al., 2013).

SpVO and SpVIr have many projections within SpV, particularly to each other (Jacquin et al., 1989b). Additional inputs are similar: to the posterior medial thalamic, zona incerta, the cerebellar cortex, spinal cord, lateral part of the superior colliculus, periaqueductal gray, nucleus of the solitary tract, and throughout the reticular formation (Bosman et al., 2011). Inputs are most prominent from other SpV subnuclei and PrV. There is a known input from the superior colliculus and midbrain reticular formation and less studied inputs from the amygdala and lateral hypothalamus (Abdallah et al., 2013).

Primary and secondary somatosensory cortices (S1 and S2 respectively) have long been known to project to the entire length of PrV and SpV (Smith et al., 2015). This projection is thought to be involved in sensory feedback. The projection from S1 and S2 to SpVC is particularly well studied for its role in pain modulation (Castro et al., 2017). Given that it is unclear what the precise role of SpVO, SpVIr, and SpVM is, it is difficult to hypothesize as to why S1 and S2 project there however, studies have shown that stimulation of the primary somatosensory cortex vibrissa region,

called the barrel cortex, results in vibrissa movements and the projections down to SpVIr have been suggested as the premotor circuit most likely mediating the movement (Matyas et al., 2010; Sreenivasan et al., 2015).

1.5 Lemniscal and paralemniscal pathways

PrV and SpVIr are the two major relays for trigeminal information ascending to the thalamus. The thalamic projections to the barrel cortex originate in the ventral posteromedial thalamus (VPM) (Bosman et al., 2011). These projections target layer 4 of the barrel corrtex. Cells with vibrissa receptive fields in VPM project to the layer 4 of the barrels. From barrelette in PrV to the barreloids in VPM and up to the barrels in S1 barrel cortex, cells are responsive to a single whisker all along the line. Each whisker has its own barrelette, barreloid, and barrel and all together they can be visualized as a representation of the whisker pad. In contrast to this clean-cut organization, vibrissa receptive field cells project to the septa of L4, between the barrels. POm neurons, like SpVIr, have bigger receptive fields that typically include many vibrissae (Furuta et al., 2006a). This pathway also projects to secondary somatosensory cortex (S2) and motor cortex(Ahissar et al., 2008).

The paralemniscal pathway includes an inhibition from zona incerta (ZI) to POm (Urbain and Deschênes, 2007a). This pathway has been hypothesized to be disinhibited by motor cortex during movement. Given that SpVIr, a premotor trigeminal nucleus, and motor cortex are both involved in the paralemniscal pathway, this pathway has been thought to be involved in reporting the position of the vibrissae in space, called reafferent signaling, while the lemniscal pathway is important for touch signaling.

1.6 Summary

Sensorimotor circuits are the basis for organisms perceiving and moving through their environment. That motor and sensory are tied together and effect the same circuits is often overlooked at the expense of simplicity. Here we will focus on sensory brainstem nuclei that have premotor neurons but also secondary sensory neurons and receive input from both motor and somatosensory cortices. First, we will discuss the descending motor cortex inputs (**Chapter 2**) and then we will address the ascending thalamic pathways (**Chapter 3**).

Chapter 2. Motor cortex drives orofacial behaviors through distinct brainstem networks

Focal activation of motor cortex has been shown to enact behaviorally meaningful motor output. These include defensive behaviors, ethological limb movements, and chewing. Yet the details of how the cortical circuitry interfaces with the brainstem premotor circuits is unknown. We studied the hierarchical nature of this control with respect to orofacial motor acts that involve the vibrissae, jaw, and forelimb. The spinal trigeminal nucleus pars oralis (SpVO) and interpolaris rostralis (SpVIr) contain premotor neurons known to directly synapse on vibrissa, jaw, and forelimb motoneurons. In addition to cortical input, SpVO and SpVIr receive direct sensory signals from the periphery. Their ability to integrate descending motor input and peripheral sensory information positions them as ideal candidates to delimit the specificity of cortex-to-brainstem-to-muscle feed forward networks. Here we show that two distinct clusters of premotor neurons, one in SpVO and a second in SpVIr, control partially overlapping sets of motor actions. We used a transectional virus strategy to encode a red-shifted channelrhodopsin (ChR) in SpVO- and SpVIr-projecting motor cortex neurons. Activation of these two different cortical populations evokes distinct muscle activation during long stimuli. Similar stimulations of localized regions of motor cortex in Thy1-ChR2 mice show patterns of muscle activity and forelimb and jaw movements that correspond to behaviorally meaningful movements. All together, our data illustrates the functional specificity of motor circuits that originate in cortex and descend onto specific premotor populations. We suggest that the specificity of projections from neurons in motor cortex to premotor nuclei is a major determinate in the coordination of motor actions into behavior.

2.1 Introduction

The motor cortex orchestrates voluntary movements through its connections with an array of cortical and subcortical targets (Alloway et al., 2010; Hattox et al., 2002; Jeong et al., 2016;

Mao et al., 2011; Oswald et al., 2013; Sreenivasan et al., 2015). In rodents, the bulk of the motor cortex descending projections transmit through premotor neurons in the brainstem and spinal cord (Alloway et al., 2010; Esposito et al., 2014). While motoneurons in the adult mammal typically target a single muscle (Buchthal and Schmalbruch, 1980), premotor regions target a variety of motoneurons for different muscles (McElvain et al., 2018; Pinganaud et al., 1999; Stanek et al., 2014; Takatoh et al., 2013b). Added to this complexity, motor cortex neurons send broad collaterals to most brainstem premotor nuclei, independent of where the cell body is within motor cortex (Alloway et al., 2010; Jeong et al., 2016; Kita and Kita, 2012). How these hierarchical projections result in discrete voluntary movements is the focus of this study.

An outstanding question is whether projection neurons target independent nuclei for coordination of movements or if coordination utilizes downstream specialized premotor nuclei (**Fig 2.1a**). One hypothesis is that motor cortex projection neurons are specialized for movement of one body part and project only to premotor nuclei for those targets (**Fig 2.1b**, left). A second hypothesis would be that motor cortex neurons target specialized overlapping population of premotor neurons that can in turn be part of the coordination of the movement (**Fig 2.1a**, right).

Motor cortex projects to many downstream targets. One such region is the spinal trigeminal nucleus (SpV). Classic tracing along with modern monosynaptic rabies-envA tracing have found that the oral (SpVO) and rostral interpolar (SpVIr) subregions of the spinal trigeminal nucleus project to motoneurons for the vibrissae (Erzurumlu and Killackey, 1979; Nguyen and Kleinfeld, 2005; Pinganaud et al., 1999; Takatoh et al., 2013b), jaw (Olsson and Westberg, 1991; Stanek et al., 2014; Westberg et al., 1998), tongue (Borke et al., 1983; Pinganaud et al., 1999; Stanek et al., 2014), and forelimb (Esposito et al., 2014). SpVO and SpVIr receive direct somatosensory input from the trigeminal ganglion (Jacquin and Rhoades, 1990; Jacquin et al., 1986). Jaw, mouth, and

teeth somatosensory information inputs to the dorsal part of SpVO and SpVIr while the ventral part receives input from the vibrissae, nose, and the region around the eye. While premotor neurons have been identified in SpVO and SpVIr, no effort has been made to determine the distribution and overlap of different populations.

Here we test the hypothesis that the cortical descending inputs have a specific interface with premotor neurons that coordinate individual motor actions, each involving one or more muscle, for behaviorally relevant movements. First, we ask what is the distribution of premotor neurons for vibrissa, jaw, and forelimb in trigeminal subnuclei SpVO and SpVIr? Second, can we transiently drive different muscles in the vibrissa, jaw, and forelimb by activating spatially congruent SpVO- or SpVIr-projecting motor cortex neurons? Further, can we drive these muscles phasically, through extended activation, to achieve ethologically relevant patterns in movement of the vibrissa, jaw, and forelimb? Lastly, what locations involve the coordinated activation of non-rhythmic versus rhythmic motion? We use anatomical tract tracing and functional labeling, along with optogenetic-driven stimulation and video and electromyographic recording in awake, head-fixed mice to address these questions.

2.2 Materials and Methods

Subjects. 38 female C57BL/6 mice and 9 Thy1-ChR2 mice (JAX strain B6.Cg-Tg (Thy1-COP4/EYFP)18Gfn/J)(Arenkiel et al., 2007) age 5-18 weeks were used. All experimental procedures followed the Guide for the Care and Use of Laboratory Animals and has been approved by the Institutional Animal Care and Use Committee at the University of California, San Diego.

Muscle injections. Nine C57BL/6 mice were anesthetized in a box with 2% isoflurane (v/v) with oxygen until they did respond to a toe pinch. A single injection of 500 nL of pseudorabies was injected into either the whisker pad (Haidarliu et al., 2015), the anterior belly of the digastric

muscle, or the biceps brachii muscle (Tosolini et al., 2013). 80 hours later the mice were deeply anesthetized with pentobarbitol before being transcardially perfused with a 0.01 mM phosphate buffered salt solution (1x PBS) followed by 4% paraformaldehyde (w/v) in 1x PBS.

Brain injections. Each animal was anesthetized with 2% isoflurane (v/v) with oxygen until they did not respond to a toe pinch. Body temperature was maintained at 37^{o}C (no. 40-90-8; FHC Inc.) and isoflurane decreased to 1.5% once placed in the stereotaxic frame (KOPF). The fur above the skull was cleaned with betadine before being cut to open access to the skull. Small holes were drilled over motor cortex and/or the spinal trigeminal nucleus (EXL-M40, Osada, CA, USA). Injections into the spinal trigeminal nucleus were made over a depth of 400-800 µm. Motor cortex injections were made between 400 and 700 µm below the brain surface. Injections were made using a Nanojet (Drummond).

Table 2.1 Virus injection parameters.

Virus(es) injected	# of mice	Injection volume (1)	Injection volume (2)	Delay before perfusion or functional test
Retrograde lenti-cit[1]	11	150-270 nL		5 weeks
AAV-flex-cit[2] (1) and Retrograde lenti-Cre[3] (2)	5	250 nL	180-250 nL	6 weeks
Lenti-synaptophysin-eGFP[4]	7	70-100 nL		5 weeks
AAV-flex-ReaChR[5] (1) and AAV retro-Cre[6] (2)	6	100 nL	125 nL	3 weeks

[1]FuGB pseudotyped lentivirus-synapsin-ReaChR-citrine was also used for preliminary stimulation experiments. [2]AAV-flex-synapsin-citrine. [3]FuGB pseudotyped lentivirus-synapsin-Cre. [4]Lentivirus-CAG(?)-synaptophysin-eGFP. [5]AAV-flex-synapsin-ReaChR-cit. [6]AAV retro-synapsin-Cre.

Headbar placement. 6 C57BL/6 mice and all 9 Thy1-ChR2 mice were anesthetized and placed in a stereotax as previously described. The fur over the skin was cleaned with iodine before a straight anterior posterior cut was opened from the nasal to the intraparietal bone. A 4 mm open cranial window was made over the frontal bone with a centroid over bregma +2 mm, lateral 2 mm. A thin layer of ACSF was applied before a 4 mm glass coverslip (Fisher Brand) was gently placed over the brain surface. A small amount of cyanoacrylate glue was used to seal the bone to the glass. Once the glue was dry, the remaining exposed skull was cleaned and layered with cyanoacrylate glue. Once dry, a metal headbar was attached to the skull via cyanoacrylate glue. Last, a layer of dental cement covered the headbar and skull.

Optogenetic stimulation experiments. The scan maps and specific positions of the laser were made using a scan system of Murphy and colleagues (Lim et al., 2012) (**Fig 2.4a**). Either a blue 446 nm laser (Cube; Coherent Inc.) or a red 637 nm laser (Obis; Coherent Inc.) was run through the scanning system. The scan objective, effective NA of 0.01, was used to create a focused light point of 35 µm.

EMGs electrodes were made of 50 µm diameter insulated tungsten wire (AM systems 795500). The tip of the wire for recoding was stripped 1 mm before being hooked and threaded through a 30-gauge needle. EMGs were inserted at the beginning of each recording session in while the mice were under light (0.5-1.0% isoflurane). Two EMGs electrodes were inserted in each muscle (intrinsic vibrissae, digastric, masseter, right and left biceps brachii, splenius capitis, or

quadriceps). Three to five muscles were recorded per session. EMG recordings were taken using individual amplifiers for each muscle (DAM 80, World Precision Instruments) at 10 kHz. The raw signals were processed for extraction of the EMG envelope by using an 8^{th} order butterworth filter between 250 hz and 2.5 kHz in the forward and reverse direction, then rectified by taking the absolute value, followed by a low pass 2^{nd} order butterworth filter at 50 hz in the forward and reverse directions. Last, a median filter was applied.

Videos were used to track the vibrissa, nose, forelimb, and jaw. Vibrissa and nose videos were taken from above. The forelimb and jaw utilized two mirrors, one in front and one to the side, that reflected the front image of the mouse up to the camera above. A high speed, 1000 by 1000-pixel camera was used with a frame rate of 200 frames per second (no. A504K; Basler Vision Technologies). For vibrissa tracking, one vibrissa was painted (Tulip dimensional fabric paint, 65101) for light contrast imaging with a mask for live tracking. For nose and jaw tracking, a dot of paint was placed on the top of the nose or the center bottom of the jaw. Forelimb tracking focused bright light on the paws.

Histology. After perfusion, brains were left in 4% paraformaldehyde (w/v) in 1x PBS between 4 and 24 hours and then cryoprotected in 30% sucrose (w/v) in 1x PBS. Sections were collected on a sliding microtome maintained between -21 and -24^{o}C. For synapse reconstructions, sections were cut horizontally at 16 µm and mounted on slides. Cell reconstructions were cut at 30 µm and immunostained free floating. The synapse and cell labeling was converted to dark product using rabbit anti GFP (Novus; 1:1000 (v/v) in a 2% goat block solution (v/v) in 1x PBS), biotinylated anti-rabbit secondaries (1:200 (v/v) in goat block), amplified with ABC kit (Vector Labs;) and converted to dark product with the SG kit (Vector Labs;). Slides were processed with increasing ethanol concentrations and xylines before being coverslipped with DPX (Sigma). All slides were

scanned on a Hammamatsu Nanozoomer and loaded into Neurolucida and then MATLAB for 3-D reconstruction. Fluorescent sections were cut between 30 and 50 µm. Citrine containing sections were amplified with rabbit anti GFP (Novus; 1:1000 in goat block) and alexa 488 conjugated goat anti rabbit (Invitrogen; 1:1000 (v/v) in goat block) and coverslipped with Fluoromount (Southern Biotech). 16-bit images were collected on a fluorescent microscope and analyzed in ImageJ.

Data analysis. Code was written in Matlab (The Mathworks). For the spectra we used the chronux package (Mitra and Bokil, 2008).

2.3 Results

Background

The mammalian motor cortex has been defined by three types of maps: a cytoarchitectural map (Brecht et al., 2004; Brodmann and Gary, 2006; Donoghue and Wise, 1982), a muscle twitch map (Ferezou et al., 2007; Fritsch and Hitzig, 2009; Tennant et al., 2011), and a map of coherent movements (Graziano and Aflalo, 2007; Graziano et al., 2002; Hira et al., 2015).

One of the first described features of the motor cortex was that it was agranular, or lacking an identifiable layer 4 (Brodmann and Gary, 2006; Donoghue and Wise, 1982). In rodents, the motor cortex cytoarchitecture map is composed of two distinct regions: the agranular medial (AG_m) and lateral (AG_l) areas (Donoghue and Wise, 1982; Tennant et al., 2011) (**Fig 2.1b**). Agranular medial cortex has a dense layer 2 with a pale layer 3 (Donoghue and Wise, 1982; Tennant et al., 2011). In contrast, AG_l cortex has homogeneous appearing layers 2 and 3 (Donoghue and Wise, 1982; Tennant et al., 2011).

The muscle twitch map is a result of lowering the electrical current applied to the cortex until only a single muscle twitches. As these low threshold stimulations are made across motor

cortex, a mousunculus appears: twitches of the vibrissa, jaw, and neck are rostral with the body and trunk caudal (Ferezou et al., 2007; Hollis et al., 2016; Tennant et al., 2011) (**Fig 2.1b**). The maps based on muscle twitch overlay AG_m cortex with vibrissa, neck, and nose movements (Barthas and Kwan, 2017; Brecht et al., 2004; Ferezou et al., 2007; Hollis et al., 2016; Tennant et al., 2011). Agranular medial cortex also receives sensory information from visual, somatosensory, olfactory, and auditory cortices (Barthas and Kwan, 2017; Donoghue and Parham, 1983; McNamara et al., 2004; Mori et al., 2013; Reep et al., 1987; Yamawaki et al., 2016). Thus AG_m cortex has been described as a transformer of sensory information into purposeful exploratory movements (Barthas and Kwan, 2017; Brecht et al., 2004). In contrast, Agranular lateral cortex receives inputs from the dysgranular region of primary somatosensory cortex as well as secondary somatosensory cortex and broadly evokes forelimb movements (Donoghue and Parham, 1983; Hira et al., 2015). The AG_l cortex is often considered the equivalent of the primate M1 because it evokes movement at lower stimulus thresholds than AG_m cortex (Donoghue and Parham, 1983; Reep et al., 1987).

While short pulses of electrical stimulation can evoke muscle twitches, excitatory neurons in motor cortex tend to be active throughout a movement (Georgopoulos et al., 1982; Graziano et al., 2002; Peters et al., 2014). When electrical or channelrhodopsin stimulations mimic these longer durations of activity in primates (Graziano and Aflalo, 2007; Graziano et al., 2002; Overduin et al., 2012) and rodents (Bonazzi et al., 2013; Harrison et al., 2012; Hira et al., 2015), complete motor acts, e.g., forelimb to mouth, were observed. In mice it has been shown that the forelimb movements evoked using long stimuli from rostral of bregma, results in abduction or elevation of the forelimb (Harrison et al., 2012), orienting the limb within the space of the head and near the mouth.

Tying together the muscle twitch and movement maps is the mousunculus. Where there are forelimb twitches, forelimb movements can be evoked. The muscle twitch map itself is a consequence of the lowest possible electrical stimulus required to evoke a twitch. At normal activity levels in awake, behaving animals, the representative region for a muscle would be larger and overlap with other muscles. The movement map is likely an expression of overlap of many muscles required for movements. The synergy of muscle and movement maps has begun to be elucidated by electrophysiological recordings of motor cortex neurons (Kakei et al., 1999) and electromyographic recordings during intercranial microstimulation (Kakei et al., 1999; Overduin et al., 2012). These past results motivate the present project to determine the relation of maps in motor cortex with premotor maps in SpVO and SpVIr, brainstem structures with sensory maps in addition to motor output.

Premotor distribution in the spinal trigeminal nucleus pars oralis (SpVO) and rostralis interpolaris (SpVIr)

While it has been previously shown that diverse premotor neurons are present in SpVO and SpVIr (Esposito et al., 2014; Pinganaud et al., 1999; Stanek et al., 2014; Takatoh et al., 2013b), the distribution and overlap of different populations were unknown. To map the premotor neuron input from muscles of the face and forelimb we use the transsynaptic retrograde virus pseudorabies. To explore coordination of different muscle groups, we chose to use one muscle for each muscle group of interest: the intrinsic vibrissae muscle, the digastric jaw muscle, and the biceps brachii forelimb muscle (three mice per muscle) (**Fig 2.1c**). The border between the spinal trigeminal nucleus and the parvicellular reticular formation is determined from the intensity of cytochrome oxidase staining (Furuta et al., 2006b). The pattern of projections shows that -trigeminal premotor neurons are found in SpVO and SpVIr across all nine mice; example sections

for each muscle are shown in **Figure 2.1d-e**. Premotor neurons are also found in the adjacent reticular formation (**Fig 2.1e**). No labeled neurons are found in the principal sensory nucleus (PrV) or the caudal aspect of the spinal trigeminal nucleus pars interpolaris (SpVIc) (**Fig 2.1e-f**), regions well-studied for the sensory properties. These data indicate that SpVO and SpVIr are distinctly sensorimotor.

We reconstructed the labeled neurons in three-dimensions and projected them onto the sagittal plane (**Fig 2.1f**, left). We determined that the top 70% densest labeled neurons (**Fig 2.1f**, right) formed two clusters of premotor neurons. The first is in the dorsal part of SpVO and the second is in the ventral part of SpVIr. The dorsal aspect of SpVO receives somatosensory information for the jaw, inside the mouth, and the teeth (Jacquin and Rhoades, 1990) and has a cluster of premotor neurons for all three muscles: the intrinsic vibrissae, digastric, and biceps brachii muscle. The ventral part of SpVIr receives sensory input from the vibrissae, nose, and face around the eye (Jacquin and Rhoades, 1990) and has a more selective premotor neuron population for only the intrinsic vibrissae and the biceps brachii. The distinction between the premotor clusters and the known sensory topography indicate that these clusters are part of separate circuits, potentially one that requires jaw movements for feeding and grooming behaviors and a second that excludes jaw movements and is used for exploration related behaviors.

Density analysis of motor cortex inputs

To further examine the division between these the two premotor clusters in subnuclei SpVO and SpVIr, we asked if there were distinctions in motor cortex afferents to these two populations. To quantify the density of projections, we used an anterograde lentivirus-synaptophysin-GFP virus that specifically labeled the presynaptic endings (**Fig 2.2a-c**). We first injected in three locations across the mediolateral axis of motor cortex (**Fig 2.2d**) in a line that

nominally passes through the region of greatest overlap of projections to the different motor actions (gray area in **Fig 2.2.1a**). Boutons were recognized, reconstructed and projected in the sagittal plane (**Fig 2.2e**). The medial injections projected most densely to ventral SpVO and SpVIr (**Fig 2.2f**). As the injections progressed towards the AG_l motor cortex, the density shifted to the dorsal region of SpVO and to SpVIr (**Fig 2.2e-f**). This distinction in density suggests that the motor cortex differentially targets dorsal and ventral SpVO and SpVIr depending on the mediolateral location in motor cortex.

The caudal part of the AG_m cortex is known to be innervated by visual and retrosplenial cortex (Barthas and Kwan, 2017; Wang and Burkhalter, 2007), whereas the more rostral region is innervated by the ventral orbital cortex, associated with olfactory information (Mori et al., 2013), and by auditory cortex (Donoghue and Parham, 1983; Reep et al., 1987). We next asked if there was a bias in density from these different parts of AG_m cortex through a series of injections that roughly paralleled the AG_m/AG_l border (**Fig 2.2g**). Here we found that injections into rostral AG_m cortex projected most densely to SpVIr and, as the injections were more caudal, the projections shift toward sSpVO (**Fig 2.2h,i**). Together, we observe two distinct gradients formed from MCtx inputs to subnuclei SpVO and SpVIr. Medial-lateral injections shift the inputs dorsal-ventrally while rostral-caudal injections shift the inputs caudal-rostrally in PrV and SpV (**Fig 2.2j**).

To further define the motor cortex inputs to subnuclei SpVO and SpVIr, we used a retrograde lentivirus to identify the range of cortical neurons projecting to either subnucleus SpVO (**Fig 2.3a,c-d**) or SpVIr (**Fig 2.3b,d**). A three-dimensional reconstruction (**Fig 2.3d**) illustrates the range of virus labeled neurons in motor (Mx) cortex and primary somatosensory (S1) cortex for two example animals. For both SpVO and SpVIr, cells in motor cortex were broadly labeled from

the rostral pole to bregma and the entire mediolateral extent of AG_m and AG_l cortex (**Fig 2.3d**). Similar results were found in all retrogradely labeled animals (11 mice).

Motor cortex corticofugal neurons are known to have broad collateralization across the brainstem (Kita and Kita, 2012). We next asked if subnuclei SpVO and SpVIr were collaterals of the same neurons in motor cortex. We injected a Cre-dependent AAV into motor cortex (**Fig 2.3e**) and a retrograde lentivirus-Cre into SpVIr (**Fig 2.3f**). We observed boutons in SpVO (**Fig 2.3f**) in all animals (five mice). Additional collaterals were seen in the superior colliculus, pontine nucleus, spinal cord, and sparsely to a variety of subdivisions of the reticular formation (data not shown).

Taken together, the data from these anatomical studies (**Figs 2-3**) confirm that SpVO and SpVIr receive input broadly from motor cortex, further show that both areas receive collaterals from the same descending cortical neurons, and that gradients of inputs from cortex can be identified in at least two dimensions (**Fig 2.3g**).

Phasic activation of motor output by optogenetic activation of SpVO- and SpVIr-projecting motor cortex neurons

Despite broad patterns of connectivity downstream (Alloway et al., 2010; Kita and Kita, 2012), motor cortex can evoke clearly defined movements (Harrison et al., 2012; Hira et al., 2015). Given that subnuclei SpVO and SpVIr have distinct premotor clusters, we determined if prolonged stimulation of SpVO- or SpVIr-projecting motor cortex neurons activated distinct sets of muscles that reflected their pattern of premotor drive. Long stimulus trains engage entire networks, including feedback and inhibitory circuits (Caggiano et al., 2018). To measure long-term dynamics, we stimulated a discrete region of neurons labeled with a red-shifted channelrhodopsin {Lin, 2013 #7620} **(Fig 2.4a-b,e**) with a 10 s, 5 Hz train of light with a 50 s intertrial intervals (**Fig 2.4e**). To target SpVO- or SpVIr-projecting motor cortex neurons, we used a transectional

virus strategy in which we injected AAV retro-Cre into either SpVO (**Fig 2.4d,f**) or SpVIr (**Fig 2.4i**) and AAV-flex-ReaChR-Cit in the jaw region of motor cortex (**Fig 2.4b-c**). After the viruses expressed, mice were headfixed and a scanning laser system used to selectively target the location of the laser to the injection site of the virus in motor cortex (**Fig 2.4a-c**) while recording EMGs from the intrinsic vibrissae, digastric, biceps brachii, masseter, and splenius capitis muscles (**Fig 2.4a,e**). We observe robust single-trial responses of the intrinsic vibrissae, digastric, and biceps brachii muscles (**Fig 2.4e**).

Prolonged stimulation of SpVO-projecting motor cortex neurons shows significant activation of the intrinsic vibrissae, digastric, biceps brachii, and masseter, shown as stimulus triggered averages of the EMG envelopes (**Fig 2.4g**) and average amplitude across three mice (**Fig 2.4h**). In contrast, stimulating SpVIr-projecting motor cortex neurons only significantly activates the intrinsic vibrissae and biceps brachii muscles consistently (**Fig 2.4i-k**) with a lack of evoked activity in the jaw muscles (**Fig 2.4j-k**). All told, our data (**Figs 2.1 and 2.4)** illustrate that there are two distinct premotor clusters in SpVO and SpVIr. Further, during persistent activation of projection-specific motor cortex neurons, distinct network activity could be evoked that reflected the premotor neuron clusters found in the retrograde targeted region (**Fig 2.4l**).

Transient activation of orofacial muscles by optogenetic stimulation of discrete regions of layer 5 motor cortex

We next wanted to address the relationship between descending network activation and motor output. We used Thy1-ChR2 mice to stimulate small regions of motor cortex with a one second train of blue light while recording movements of the jaw, forelimb, vibrissae, and nose and EMGs of the intrinsic vibrissae, digastric, biceps brachii, masseter, splenius capitis, and quadriceps

muscles (**Fig 2.5a-d**). 15 locations in rostral motor cortex were targeted with blue light (**Fig 2.5a,c**).

To determine the light intensity for mapping, we targeted two of the original fifteen stimulation sites (**Fig 2.5b**), we modulated the laser intensity while recording EMGs. We found that from both vibrissa motor cortex and jaw motor cortex, muscle activation tended to increase monotonically with light intensity (**Fig 2.5e**). The jaw motor cortex showed a dominance of the digastric muscle but still all recorded muscles increasing together (**Fig 2.5e**).

Composite maps of amplitude were made for each muscle as well as for the nose movement across all stimulation sites (N=4) (**Fig 2.5f**). Significant activation or modulation (i.e. suppression) of all EMG channels was found at all locations (k-s test, $p<0.001$). However, some muscles, like the digastric and splenius capitis, had strong activation from specific regions of motor cortex with smaller, yet still significant evoked movements from all other stimulation locations (**Fig 2.5f**). The activation of the quadriceps muscle far from the hindlimb representation in motor cortex and of broadly strong activation of the biceps brachii muscles suggest that motor cortex might be controlling posture in addition to orchestrating actions (Amundsen Huffmaster et al., 2017; Overduin et al., 2012).

Taken together, we show that motor cortex has broad activation of muscles during one second stimulations. Close examination of the composite maps in **Figure 2.5f** show a division between the medial and lateral sides that may reflect the underlying cytoarchitecture. The medial elicits strong activation of the nose, splenius capitis, and the intrinsic vibrissae, while the lateral division can generate activation of the digastric, masseter, and biceps brachii (**Fig 2.5f-g**). Two additional, small regions were detected on the edges of the explored region (**Fig 2.5g**).

To classify motor cortex evoked movements, we next mapped movement of the jaw, nose, and forelimb (**Figs 2.6a & 2.7a**). Consistent with the broad activation of the digastric and masseter muscles (**Fig 2.5f**), jaw movements were evoked from most stimulus sites (filled blue circles in **Fig 2.6b**). Jaw trajectories were down and contralateral as shown by example traces with corresponding projected trajectories (**Fig 2.6c**). Small movements could be detected corresponding to low amplitude movements of the digastric (**Fig 2.5f & 6c top row,** location 8) For a subset of locations, rhythmic activity was detected (**Fig 2.6b**, location 12 and 7). Subtle differences could sometimes be detected between location sites. One subtly was observed rhythmic protrusion of the tongue in location 8 (**Fig 2.6b**). This location is close in location and description the previously identified cortical licking region (Komiyama et al., 2010). The rostral-lateral region of motor cortex consistently evoked rhythmic jaw movements (**Fig 2.6f**).

Consistent with previous work, nose movements were found in the medial region of motor cortex (Brecht et al., 2004) (**Fig 2.6d**). Examples of trajectory over time and projected trajectory are shown for two locations (**Fig 2.6e**). Nose movements were found predominantly in both the anterior-posterior axis (**Fig 2.6e**, top) and medial-lateral axis (**Fig 2.6e**, bottom) but could move in all radial directions. Only one stimulation site in each mouse (N=4) evoked rhythmic activity, confining the rhythmic nose region to a small part of rostral-medial motor cortex (**Fig 2.6h**). The rhythmic activity from the jaw and nose were at distinct frequencies (**Fig 2.6f**) consist with previous literature on chewing and sniffing (Kobayashi et al., 2002; Kurnikova et al., 2017).

Consistent with previous studies in mice (Ferezou et al., 2007), we found only a small region of motor cortex evoked vibrissa retraction (**Supp Fig 2.1a-b**). These stimulation sites also correspond with strong activation of the splenius capitis neck muscle, a muscle most strongly active in deep (90-130^{o}) head turns (**Fig 2.6f, 5e**)(Richmond et al., 1992; Roucoux et al., 1989)

and corresponds with the location where head movements have been evoked in freely moving animals (Barthas and Kwan, 2017). Together, this evidence suggests that this localized region is specialized for head turning exploratory movements (**Supp Fig 2.1c**).

To further examine motor cortex evoked network activity, we quantified forelimb movements from across the rostral part of motor cortex (**Fig 2.7a-b**). While biceps brachii muscle modulation was found from all stimulation locations (**Fig 2.5f**), trackable forelimb movements were found from only a subset of locations (**Fig 2.7b**). Typically, the contralateral forelimb would directly move to a spatial target and stay there throughout the duration of the light train (**Fig 2.7c**). Example images of the forelimb during the stimulation are shown for four of the seven sites: forelimb supinating and coming to the mouth (**Fig 2.7c**, location 5), forelimb grasping below its jaw (**Fig 2.7c**, location 7), holding the forelimb ventral lateral of the body (**Fig 2.7c**, location 11), and holding the forelimb dorsal lateral (**Fig 2.7c,** location 1). Corresponding 2d traces are shown over time (**Fig 2.7 c**, middle) and corresponding projected trajectories (**Fig 2.7c**, right) All trials are shown in color with the average in black. The trajectories are darker where the forelimb spent more time.

Forelimb target locations (**Fig c-d**) were mapped to stimulation location in motor cortex (**Fig 2.7d**). At least two distinct subdivisions were found: one with forelimb movements oriented below the mouth near the midline and a second, inverted map of the forelimb targeted lateral regions of space (**Fig 2.7d-e**). The former subdivision corresponds to the lateral division shown with the jaw dominant lateral division found in **Figure 5f** and supports the hypothesis that this division is involved in feeding-related movements. With data from **Figures 5 and 6**, this lateral region has a gradient of prominent jaw activity in the rostral part (**Fig 2.7e**, right**, Fig 5f-g, Fig 6g**)

which is reflected by the forelimb targeted nearer the jaw in the rostral-lateral region and then transitioning to close to the ground caudally (**Fig 2.7d-e**).

The medial division evoked targeted movements up to the level of the eye and vibrissae (**Fig 2.7c-e**). The elevation or abduction of the forelimb evoked here is inverted from displacements seen in the lateral division (**Fig 2.7e**), indicating these areas function as separate modules. Further, the sensory inputs provide important context for the forelimb targets evoked from the medial division. The caudal-medial region receives distinct visual and somatosensory cortex inputs (Barthas and Kwan, 2017; Smith et al., 2015) and results in evoked movements closer to the level of the eyes and vibrissae (**Fig 2.7d-e**). In contrast, the rostral medial division receives input from the olfactory and auditory systems and is also where we found rhythmic nose movements (**Fig 2.6h**). Stimulation of this rostral-medial region resulted in forelimb movements closer to the ground (**Fig 2.7d-e**).

Taken together, this data shows that motor cortex broadly activates many muscles that synergize into a coherent movement and that motor cortex activates specific patterns of activity in the jaw, nose, and forelimb. Likely, subsets of some of the motor cortex descending projections are contributing to the action movement and others to controlling or stabilizing posture of other muscles. That coherent movements can be evoked and sustained throughout the stimulation indicates that motor circuits are wired in such a way that only specific networks are activated which enact and sustain specific movements.

2.4 DISCUSSION

Here we addressed the question of how the motor cortex interfaces with downstream targets to drive specific networks. We found two distinct networks that were enacted from the same location in motor cortex but projected to two distinct brainstem premotor neuron clusters (**Figs**

2.1,3-4). We further showed that as the location within motor cortex changes, that the density of boutons to these two brainstem regions shifts **(Fig 2.2**) and that stimulation across these different locations of all layer 5 motor cortex neurons results in broad muscle activation and behaviorally relevant motor actions that persist for the duration of the stimulation (**Figs 2.5-7**). All told, this data describes the ethological movements motor cortex can orchestrate, details the anatomical substrate for two such pathways, and shows two different networks driven by such projections despite broad targeting and collateralization from motor cortex.

Breaking down the movement map into smaller projection networks

The three historical types of motor maps created an important groundwork for disentangling the role of the motor cortex in voluntary movements. One missing piece has been to connect these maps directly with known premotor populations to create one larger picture. Here we found that differentially targeted projection neurons within the same location of motor cortex can evoke different patterns of muscle activity (**Fig 2.1,4**). Then we showed that when stimulating all L5 projection neurons in that same location, many muscles are engaged (**Fig 2.5**). This leads to the question of why brainstem areas have specific premotor clusters (**Fig 2.1**) but are broadly targeted from across motor cortex (**Fig 2.3**)?

One possibility is that these two described pathways (**Fig 2.2-4**) are specifically for postural adjustments that incorporate incoming sensory information, rather than for driving the action component of the movement. Another possibility is that there is another layer of specificity in what types of cells are being targeted (i.e. inhibitory or excitatory) and whether they are directly premotor to a subset of muscles. An important point is that these projection neurons send collaterals to many targets (Kita and Kita, 2012). What each target does for a movement has been difficult to parse due to backfiring of cells when their target boutons are stimulated. Using methods

of anterograde transynaptic tracing of Cre or Flp coupled with Cre- or Flp-dependent opsins would allow for selective activation of cells that directly receive input cells at the original injection site. With these new methods, we can finally parse the targets of motor cortex alongside experiments stimulating projection-specific motor cortex neurons and begin to understand the role of these different hierarchical layers within the motor system.

Synthesizing a map of EMG data from broad muscles groups with tracked movements

Here we focus on the rostral part of motor cortex that evokes head and face related movements (Ferezou et al., 2007; Tennant et al., 2011) as well as the rostral forelimb area (Brown and Teskey, 2014; Hira et al., 2013; Tennant et al., 2011). While this area has been historically divided based on its cytoarchitecture into a medial division with a diversity of sensory inputs and a lateral division that is more devoted to forelimb movements (Barthas and Kwan, 2017), a separate set of studies have found that in the anterior lateral part of motor cortex (ALM, Bregma +2.4, 2.0 lateral (Komiyama et al., 2010)) rhythmic licking can be induced. The ALM region falls within the spatial location of where we evoked rhythmic jaw movements (**Fig 2.6g**) and found large amplitude responses of the digastric and masseter muscles (**Fig 2.5f**). These findings are consistent with previous work showing that jaw and tongue muscles are rhythmically active together during licking.

We also found that muscles more often involved in exploratory movements (e.g. the splenius capitis and the intrinsic vibrissae) are found more medially (**Fig 2.5f, Supp fig 2.1a-c**)(Barthas and Kwan, 2017; Saiki et al., 2014). We found activation of the nose and intrinsic vibrissae most rostrally within this division followed caudally by the splenius capitis. As has been seen previously (Tennant et al., 2011), forelimb movements and biceps brachii activation are also

found in this medial division (**Fib 2.5f, Fig 2.7e**). Here we see that jaw movements are modulated to low levels of activity (**Fig 2.5f**), potentially as a posture control.

The rostral part of the lateral division evokes strong activation of the digastric, masseter, and biceps brachii muscles. We propose this as the cortical masticatory area of the mouse which includes evoked incision, chewing, and licking. This region evoked elevated forelimb movements (**Fig 2.7c-e**) and activation of the biceps brachii muscle (**Fig 2.5f**). Evoked forelimb movement targeted space below the mouse and, most laterally (**Fig 2.7d-e**) forelimb to mouth with supinated hand position. These movements support a role of this region of cortex for feeding behaviors. The coordinates of the digastric high amplitude responses (**Fig 2.5f**) are mostly within the coordinates of the AG_l (Tennant et al., 2011). The lateral division has a gradient of strong jaw activity and elevated forelimb movement rostrally that transitions to low jaw activity and forelimb positioned nearer the ground (**Fig 2.7d-e**).

On the medial side of the division (**Fig 2.5g**) at about 2.5 mm rostral from bregma and 1.5 mm lateral from the midline, is a region with distinct activation of the splenius capitis, nose, biceps brachii, and quadriceps (**Fig 2.5f**) along with rhythmic jaw movements (**Fig 2.6g**). This region has the potential to be specifically involved in grooming behaviors. Given the mouse is headfixed and the stimulations are only one second, it is unlikely we would evoke full grooming. However, this region has a distinct pattern of activity that includes the initiation of rhythmic jaw activity alongside strong activation of the splenius capitis muscle, a muscle used for deep neck turns like seen in phase II of grooming (Berridge et al., 2005). Additionally, activation of the hindlimb potentially corresponds to the sitting upright mice take throughout grooming (Berridge et al., 2005).

Conclusion

All together we show that motor cortex evoked broad patterns of muscle activity that are part of a broader movement pattern. The hierarchical control of movements involved coordination at the level of the cortex through the brainstem. We show specific movements by EMG and video analysis that illustrate ethological movements and further show that activating specific projection neurons within one location activate specific muscles that reflect the target's premotor neurons.

2.5 Acknowledgements

We thank Fan Wang and Daniel Gibbs for generously making viruses for us and Laura McElvain, Celine Mateo, Amalia Callado Perez, and Anastacia Kurnikova for discussions.

This work is a manuscript in preparation: Mercer Lindsay N, Knutsen, Per M, and Kleinfeld D. "Motor cortex drives orofacial behaviors through distinct brainstem networks." Under final preparation. The dissertation author is the primary author of this work.

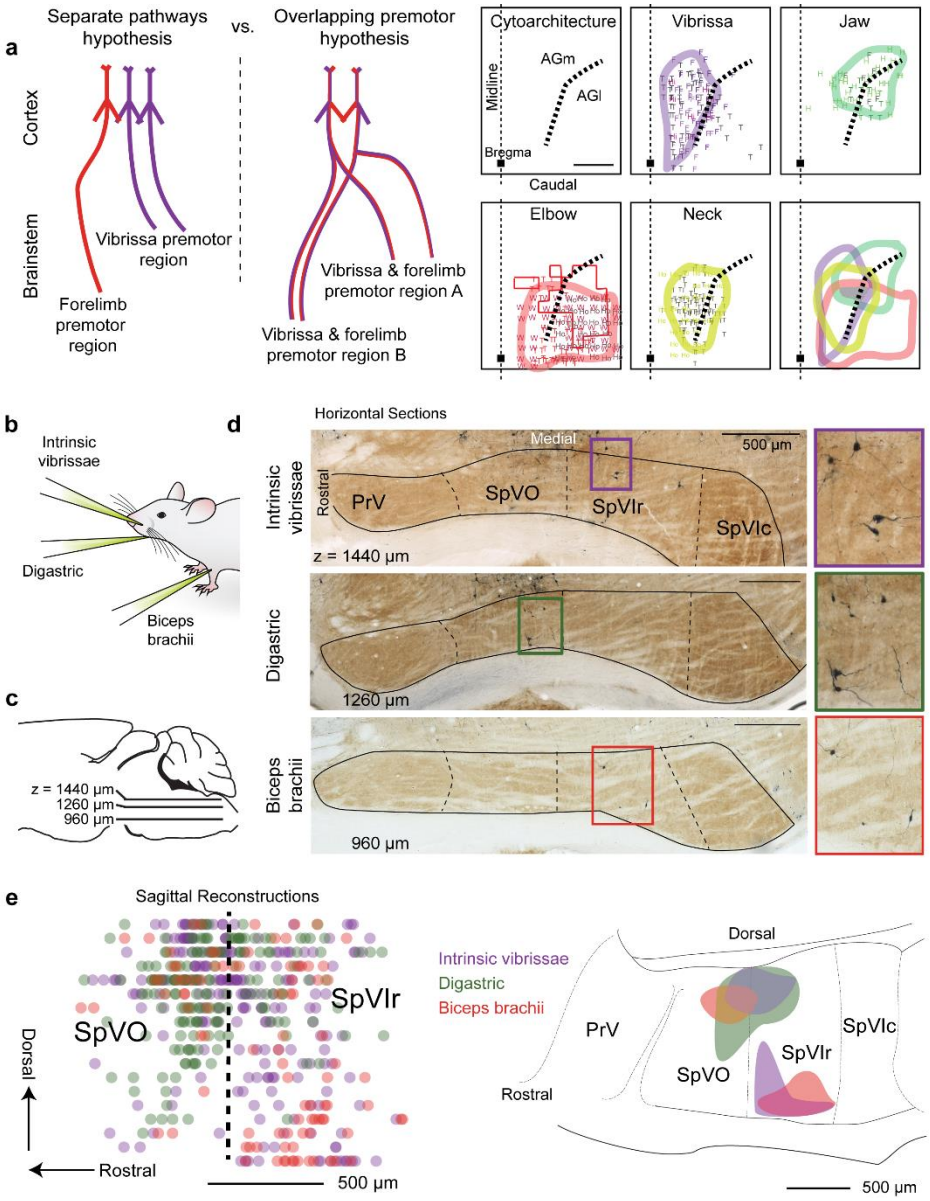

Figure 2.1 Premotor neuron clustering using pseudorabies virus in SpVO and SpVIr. (a) Two hypotheses of how the motor cortex evokes motor acts. Coordination could occur solely at the cortex; in this case, motor cortex contacts discrete populations of premotor neurons (left). A second hypothesis is that coordination occurs at both the cortex and premotor levels by the motor cortex contacting overlapping premotor populations (right). **(b)** Schematic illustrating locations of pseudorabies injections. **(c)** Example sagittal section illustrating the depths of the sections shown in **(d)**. **(d)** Example horizontal sections from an injection in the intrinsic vibrissae, digastric, and biceps brachii muscles. GFP from the pseudorabies was converted to dark product and sections were counterstained with cytochrome oxidase to label the boundaries of SpV. **(e)** Sagittal reconstruction of all premotor labeled neurons in SpVO and SpVIr from 3 mice/muscle (left, N=9). Two clusters found using the 70% densest labeling of premotor neurons in SpV are overlaid on a sagittal atlas section (right).

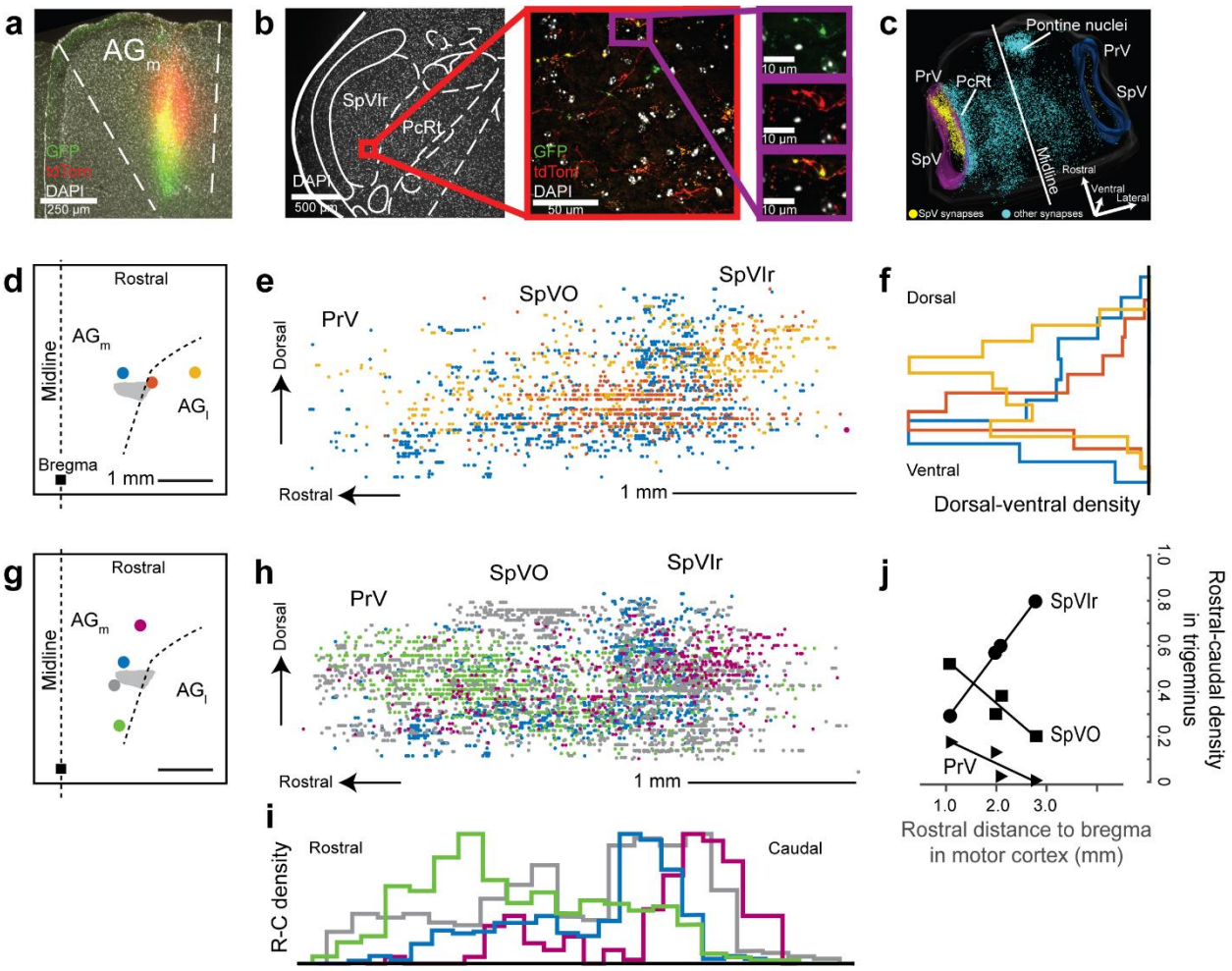

Figure 2.2 Density of inputs from motor cortex biases towards different regions of SpVO and SpVIr based on cortex location. (a) Example injection of Lentivirus-CAG-synaptophysin-eGFP coinjected with AAV-synapsin-tdtomato in the AG_m region of motor cortex. **(b-c)** Synapses (green and red) and axons (red only) labeled in SpVIr from **(a)**. **(d)** 3-D reconstruction of GFP-labeled boutons of the hindbrain viewed from above. SpV boutons are labeled in yellow while all others are in cyan. **(e)** Schematic of motor cortex injections in AG_m and lateral to AG_l, the square represents bregma, the scale bar is 1 mm. **(f)** Sagittal projection of synapses labeled rostrally from PrV through SpVIc caudally color coded by injection site in **(e)**. **(g)** Overlaid histograms of dorsal – ventral density in PrV through SpVIc for injections in AG_m and AG_l. **(h)** Schematic of motor cortex injections in AG_m that run along the rostral – caudal axis and their corresponding sagittal projected synapses **(i)**. **(j)** Plot of synaptic density PrV (black), SpVO (red), and SpVIr (blue) out of all trigeminal synapses as the injections move rostral from bregma. **(k)** Histogram of rostral – caudal density from color coded injection sites in **(h)**. AG_m/AG_l border is drawn from paxinos coordinates and verified with mouse nissl sections from Tennant et al. 2011.

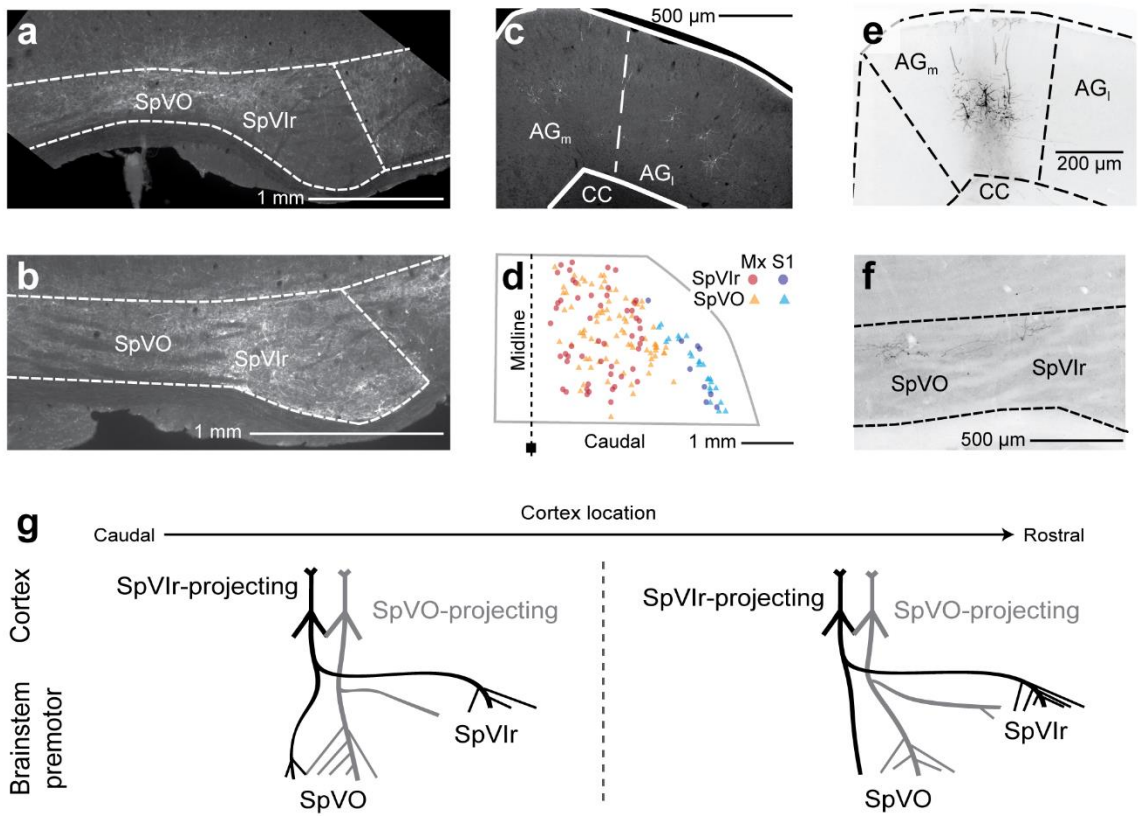

Figure 2.3 Motor cortex broadly targets SpVO and SpVIr. Retrograde lentivirus-cit injected into SpVO **(a)** and SpVIr **(b)** and corresponding cells labeled in AG_m and AG_l **(c)**. **(d)** 3-D reconstruction of GFP labeled cells in motor and primary somatosensory cortex, viewed from above. The square represents bregma. **(e)** Pyramidal neurons labeled at the injection site in AG_m of AAV-flex-Cit and the corresponding retrograde lentivirus-Cre in SpVIr **(f)** and collateral boutons in neighboring SpVO. **(g)** Model from **Fig 2-3** illustrating that 1) a broad swath of motor cortex projects to SpVO and SpVIr (**Fig 3a-d**), 2) that SpVO and SpVIr are targets of the same pyramidal neurons in motor cortex (**Fig 3e-f**), and 3) that the bouton density in SpVO is higher in caudal motor cortex and in turn, SpVIr density is higher in rostral motor cortex (**Fig 2 h-k**).

Figure 2.4. SpVO- and SpVIr-projecting motor cortex neurons drive different networks that activate muscles reflecting their respective premotor clusters. (a) Schematic illustrating the injection scheme as well as the later used red laser and recorded EMGs in the intrinsic vibrissae, digastric, bicep brachii, masseter, and splenius capitis muscles. **(b)** Schematic of injection site and corresponding laser size, the square represents bregma. **(c)** Pyramidal neurons labeled in a coronal section of motor cortex and corresponding fibers in SpVO **(d)**. Note that pyramidal neurons in rostral most frontal cortex send their apical dendrites forward rather than just straight up. **(e)** EMG envelopes for the intrinsic vibrissae, digastric, biceps brachii, masseter and splenius capitis muscles for one trial. **(f-h)** AAV retro-Cre targeted to the SpVO premotor cluster **(f)**. Responses when long stimuli were applied to motor cortex show consistent activation of the intrinsic vibrissae, digastric, biceps brachii, and masseter. First shown using stimulus-triggered averages **(g)** and then averaged responses from throughout the stimulus are compared across animals **(h)**. **(i-k)** AAV retro-Cre targeted to the SpVIr premotor cluster show consistent activation of only the intrinsic vibrissae and biceps brachii muscles. Shown with stimulus triggered averages from one animal **(j)** and then averaged through the duration of the stimulus and compared across animals **(k)**. **(l)** Model of data from **Fig 2.1** and **2.4** that shows that 1) there are two distinct premotor clusters, one in SpVO and the second in SpVIr and 2) that by using prolonged laser stimulations on specific motor cortex projection neurons, you evoke muscle activity that reflects the premotor clusters.

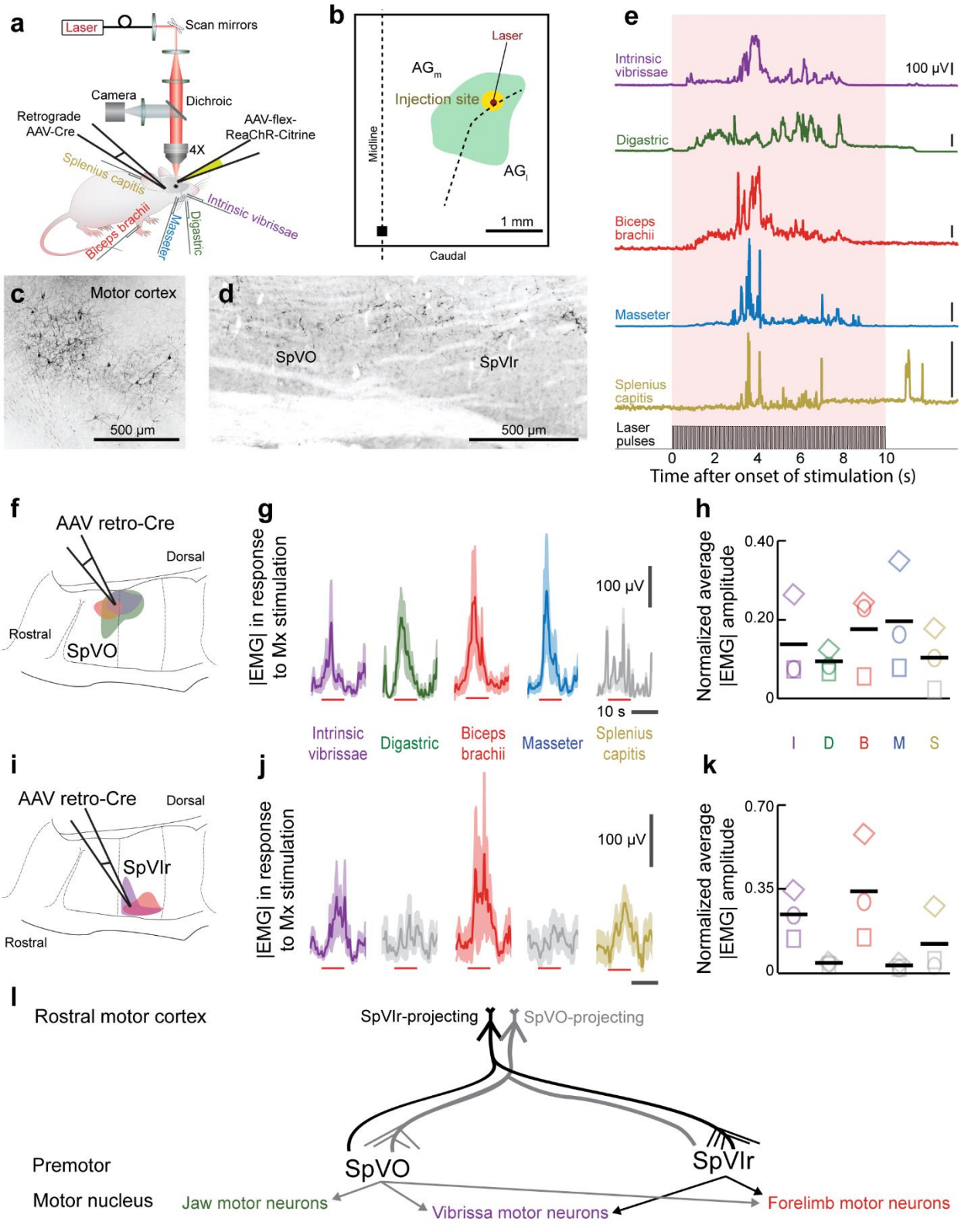
a
Laser
Scan mirrors
Camera
Dichroic
Retrograde AAV-Cre
AAV-flex-ReaChR-Citrine
4X
Splenius capitis
Intrinsic vibrissae
Biceps brachii
Masseter
Digastric
b
Laser
AG$_m$
Injection site
AG$_l$
Midline
1 mm
Caudal
e
Intrinsic vibrissae
100 µV
Digastric
Biceps brachii
Masseter
Splenius capitis
Laser pulses
0 2 4 6 8 10
Time after onset of stimulation (s)
c
Motor cortex
500 µm
d
SpVO
SpVIr
500 µm
f
AAV retro-Cre
Dorsal
Rostral
SpVO
g
|EMG| in response to Mx stimulation
100 µV
10 s
Intrinsic vibrissae
Digastric
Biceps brachii
Masseter
Splenius capitis
h
Normalized average |EMG| amplitude
0.40
0.20
0
I D B M S
i
AAV retro-Cre
Dorsal
SpVIr
Rostral
j
|EMG| in response to Mx stimulation
100 µV
k
Normalized average |EMG| amplitude
0.70
0.35
0
l
Rostral motor cortex
SpVIr-projecting
SpVO-projecting
Premotor
Motor nucleus
SpVO
SpVIr
Jaw motor neurons
Vibrissa motor neurons
Forelimb motor neurons

Figure 2.5. Light activation of Thy1-ChR2 mice across motor cortex shows broad activation of muscles. (a) Schematic of laser activation of Thy1-ChR2-YFP mice with EMG recordings and high-speed video from above for the vibrissa and nose movements and using two mirrors reflecting up the forelimb and jaw movements. **(b)** Coronal section of Thy1-ChR2 mouse through motor cortex with dense yfp labeling in L5. **(c)** Schematic of positions targeted by a blue laser in motor cortex for trials including one second of blue light. **(d)** Single trial examples of jaw, forelimb, vibrissa, and nose movements and intrinsic vibrissae, digastric, biceps brachii, masseter, splenius capitis, and quadriceps EMG envelopes. The blue box indicates the time the light train is ongoing. Single trials are not all from the same location in cortex. **(e)** EMG amplitude for the intrinsic vibrissae, digastric, and splenius capitis muscles from classic vibrissa motor cortex (Bregma + 1.5, 1.5 lateral) compared with jaw motor cortex (Bregma + 3, 2 lateral). From a second mouse, EMG amplitude for the intrinsic vibrissae, digastric, masseter, and biceps brachii muscles as a function of light intensity from digastric motor cortex. **(f)** Composite amplitude maps (N=3, interpolated between light points) for the digastric, masseter, splenius capitis, intrinsic vibrissae, biceps brachii, and quadriceps EMG envelope recordings and anterior-posterior nose movements. **(g)** Model of rostral motor cortex shows four distinct quadrants. One major division separates the medial and lateral aspects. The medial region has strong representation of the nose and splenius capitis muscle while the lateral region has a strong representation of the digastric, biceps brachii, and masseter muscles. A small quadrant from the ventromedial region showed strong activation of the biceps brachii and masseter muscles while another small quadrant off the lateral most edge had strong activation of the biceps brachii, intrinsic, masseter, and digastric muscles.

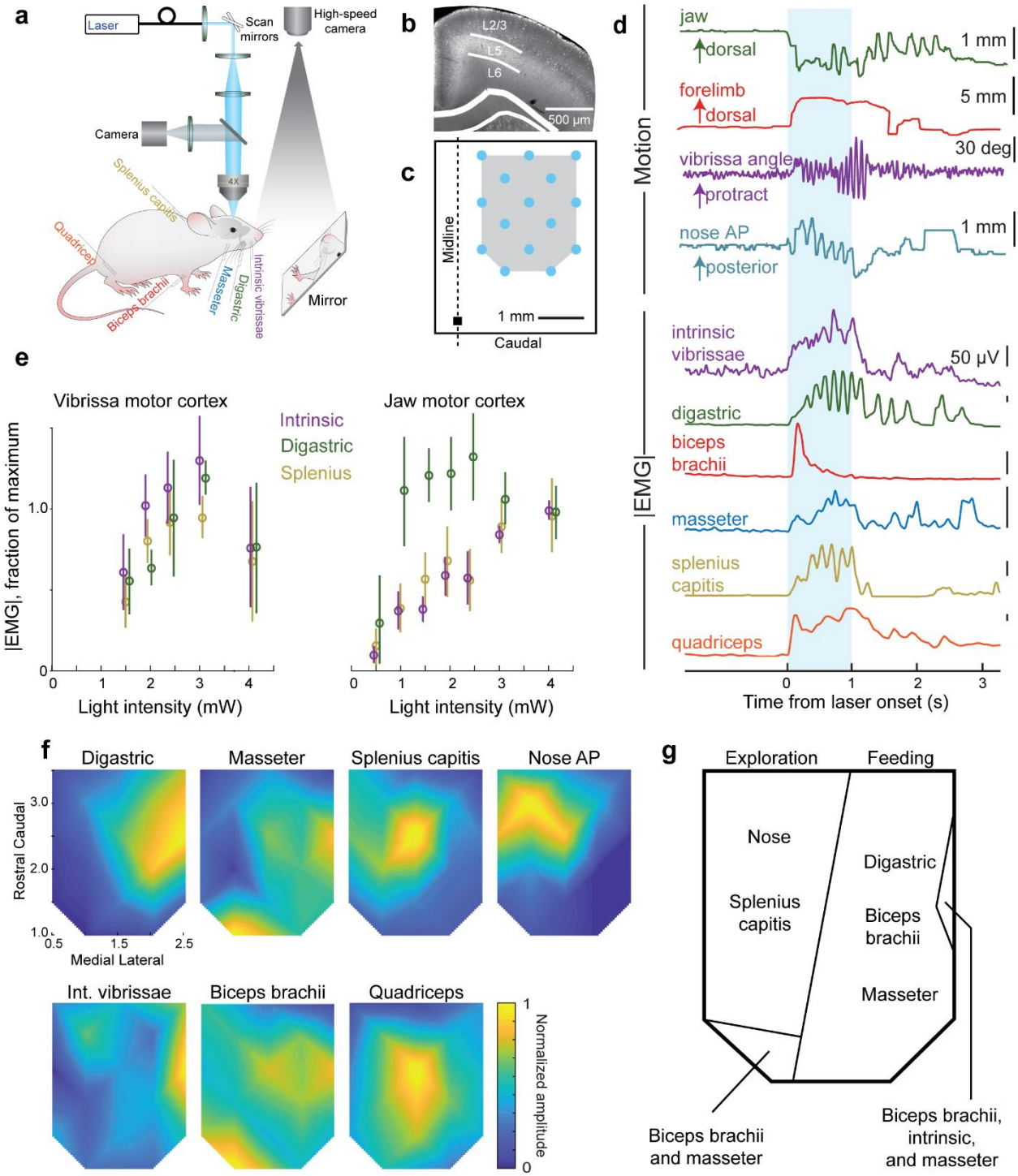
a
Laser
Scan mirrors
High-speed camera
Camera
4X
Splenius capitis
Quadriceps
Biceps brachii
Masseter
Digastric
Intrinsic vibrissae
Mirror
b
L2/3
L5
L6
500 µm
c
Midline
1 mm
Caudal
d
Motion
jaw
dorsal
1 mm
forelimb
dorsal
5 mm
vibrissa angle
protract
30 deg
nose AP
posterior
1 mm
|EMG|
intrinsic vibrissae
50 µV
digastric
biceps brachii
masseter
splenius capitis
quadriceps
Time from laser onset (s)
e
Vibrissa motor cortex
Jaw motor cortex
Intrinsic
Digastric
Splenius
|EMG|, fraction of maximum
Light intensity (mW)
Light intensity (mW)
f
Digastric
Masseter
Splenius capitis
Nose AP
Rostral Caudal
Medial Lateral
Int. vibrissae
Biceps brachii
Quadriceps
Normalized amplitude
g
Exploration
Feeding
Nose
Splenius capitis
Digastric
Biceps brachii
Masseter
Biceps brachii and masseter
Biceps brachii, intrinsic, and masseter

Figure 2.6. Patterns of activity in the jaw and nose show behavioral domains within motor cortex. (a) Motor cortex stimulation points as seen in **Fig 2.5c.** Filled blue circles indicate locations where significant jaw movements were found. **(b)** Jaw movements in 2d over time (middle) with projected trajectory (right). Black indicates the average, colors all trials. Darker lines indicate locations where more time was spent. The blue bar represents the time during the stimulation. Examples of rhythmic activity shown from locations 7 and 12, pictures show tongue protrusion from location 7 but not 12 (left). **(c)** Same as **(a**) but here filled blue circles indicate locations where significant nose movements were seen. **(d)** Nose movements in 2d over time (left) and projected trajectory (right), as seen in **(b)** for the jaw. **(e)** Spectral power of the digastric EMG and nose motion. Composite maps of rhythmic jaw **(f)** and **(g)** nose movements.

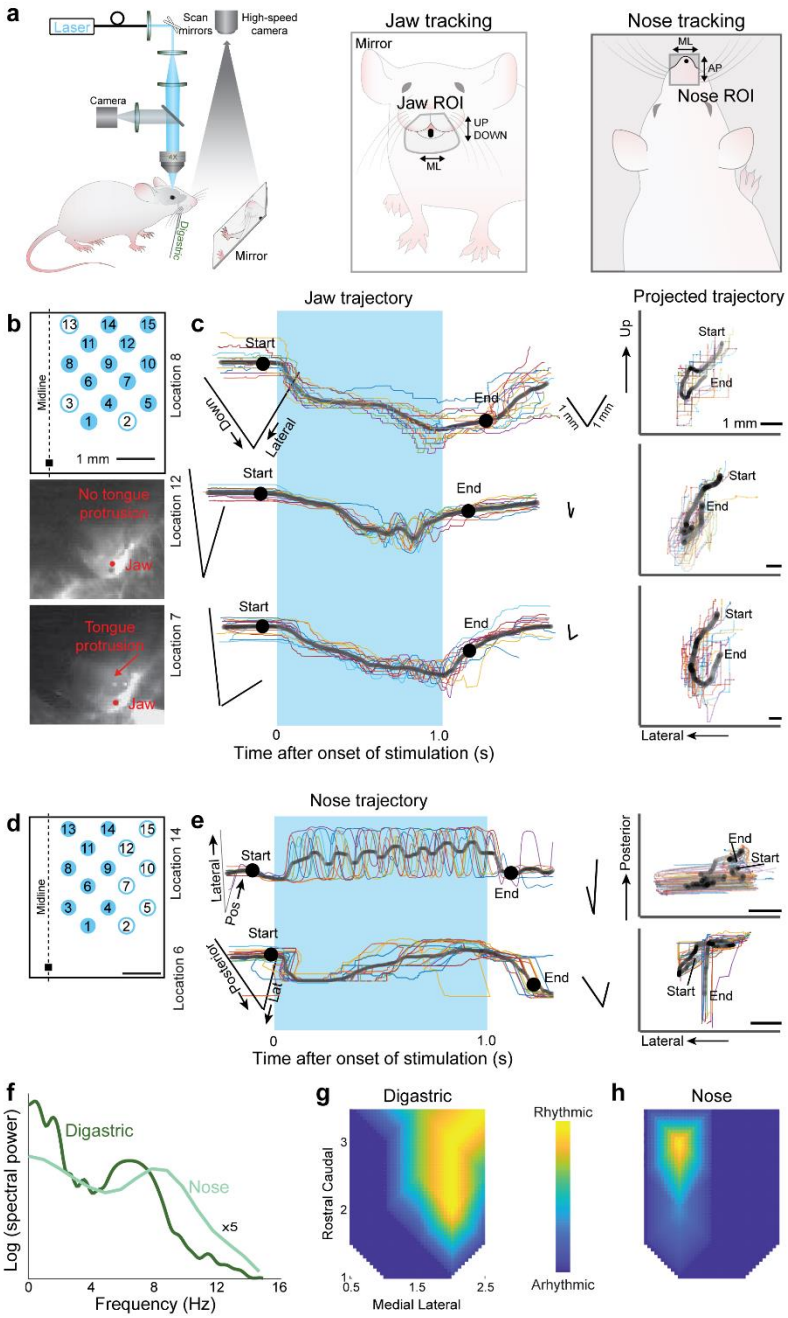
a
Laser
Scan mirrors
High-speed camera
Camera
Digastric
Mirror
Jaw tracking
Mirror
Jaw ROI
UP
DOWN
ML
Nose tracking
ML
AP
Nose ROI
b
Midline
1 mm
No tongue protrusion
Jaw
Tongue protrusion
Jaw
Location 8
Location 12
Location 7
c
Jaw trajectory
Start
End
Down
Lateral
1 mm
Time after onset of stimulation (s)
Projected trajectory
Up
Lateral
d
Midline
Location 14
Location 6
e
Nose trajectory
Lateral
Pos
Posterior
Lat
Time after onset of stimulation (s)
Posterior
f
Digastric
Nose
x5
Log (spectral power)
Frequency (Hz)
g
Digastric
Rostral Caudal
Medial Lateral
Rhythmic
Arhythmic
h
Nose

Figure 2.7. Forelimb tracking shows motor cortex targets the forelimb in the mouses's external space. **(a)** Schematic showing the setup for recording video from the front via two mirrors to a camera above. **(b)** Schematic of motor cortex sites as shown in **Fig 2.5c**. Filled in circles indicate locations where distinct forelimb movements were observed. **(c)** Example images of the mouse target in space (left) for laser positions 1, 5, 7, and 11 as shown in **(b)** and corresponding forelimb tracking (middle) and projected trajectory (right). The blue bar indicates the time duration of the light train. All trials are shown (colors) with the average (black). Darker traces in the projected trajectory indicate more time spent in that location. **(d)** All forelimb targets shown overlaid on an example mouse. **(e)** Model of forelimb targets evoked from motor cortex. Two major divisions were found, one in medial motor cortex where caudal stimulation sites evoked more elevated forelimb positions and the positions evoked became less elevated as the stimulation sites moved rostral (left). The more caudal part of this region receives visual and vibrissa sensory input whereas the more rostral receives olfactory inputs. The second division had more rostral stimulation sites evoking more elevated movements. The more elevated movements positioned the forelimb closer to the jaw as seen in **(d)** and coincide with where strong jaw muscle and movements were evoked (**Fig 2.5f-g, Fig 2.6a-b,f**) The exception to this gradient was position 5 where stimulation evoked forelimb supination to the mouth, a distinctly different movement than was seen in other stimulation locations.

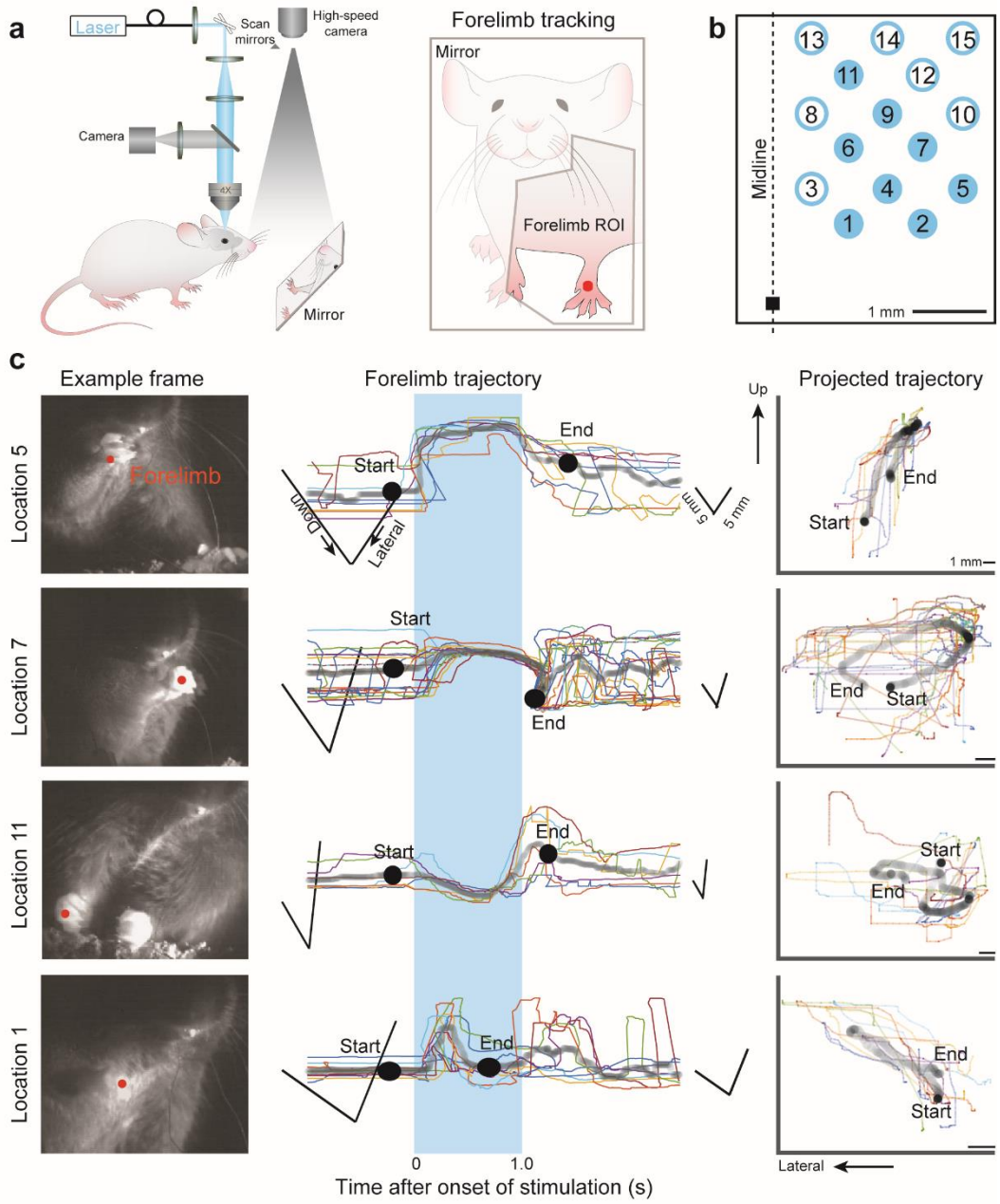
a
Laser
Scan mirrors
High-speed camera
Camera
4X
Mirror
Forelimb tracking
Mirror
Forelimb ROI
b
Midline
1 mm
c
Example frame
Forelimb trajectory
Projected trajectory
Location 5
Location 7
Location 11
Location 1
Forelimb
Start
End
Down
Lateral
5 mm
Up
1 mm
Lateral
0
1.0
Time after onset of stimulation (s)
d
5 Forelimb to mouth
2,4,7,9 Forelimb below mouth
1,6,11 Forelimb moves lateral
Jaw
Location 5
e
Midline
Olfactory & auditory inputs
Visual & vibrissa inputs
Jaw dominant
Forelimb dominant
Forelimb elevation

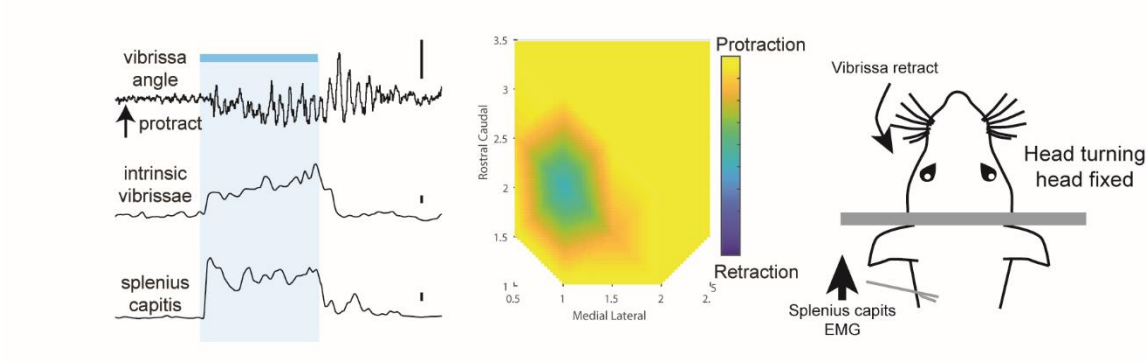

Figure S2.1. Motor cortex evoked head turning (a) Vibrissa retraction during stimulus (blue) along with intrinsic vibrissae and splenius capitis EMG envelopes. **(b)** Map of protraction and retraction of the vibrissae. **(c)** Model showing two aspects of head turning found during stimulation of this region of motor cortex.

Chapter 3. Vibrissa self-motion and touch are reliably encoded along the same somatosensory pathway from brainstem through thalamus

Active sensing involves the fusion of internally-generated motor events with external sensation. For rodents, active somatosensation includes scanning the immediate environment with the mystacial vibrissae. In doing so, the vibrissae may touch an object at any angle in the whisk cycle. The representation of touch and vibrissa self-motion may in principle be encoded along separate pathways, or share a single pathway, from the periphery to cortex. Past studies established that the spike rates in neurons along the lemniscal pathway from receptors to cortex, which includes the principal trigeminal and ventral-posterior-medial thalamic nuclei, are substantially modulated by touch. In contrast, spike rates along the paralemniscal pathway, which includes the rostral spinal trigeminal interpolaris, posteromedial thalamic, and ventral zona incerta nuclei, are only weakly modulated by touch. Here we find that neurons along the lemniscal pathway robustly code rhythmic whisking on a cycle-by-cycle basis, while coding along the paralemniscal pathway is relatively poor. Thus the representations of both touch and self-motion share one pathway. In fact, some individual neurons carry both signals so that upstream neurons with a supralinear gain function could, in principle, demodulate these signals to recover the known decoding of touch as a function of vibrissa position in the whisk cycle.

3.1 Introduction

Animals interrogate the world around them with actively moving sensory organs (Gibson, 1962). This process results in a blend of sensory input from the presence of two underlying sensory signals. One input is from the environment or object under study, while the second is from self-generated movement of the sensor (Cullen, 2004). The detection of an external stimulus with confidence, as well as the ability to confirm the position and trajectory of the sensor, depend on the ability of the animal to distinguish among internally versus externally generated sensations.

Ambiguity among these sources leads to unpleasant outcomes, such as vertigo (Dieterich, 2007) and motion sickness (Oman and Cullen, 2014) for the case of vestibular control.

To resolve this ambiguity, nervous systems use three complementary signaling mechanisms to reference input from a sensory organ relative to the position of the sensors (von Holst, 1954). One is to encode self-generated sensor movement by the exo-receptors that also code changes in the external environment; this is denoted peripheral re-afference. A second mechanism is to use muscular endo-receptors to encode elongation and contraction force, as performed by spindle fibers and Golgi tendons, respectively; this is denoted proprioception. A third mechanism is to generate a central copy of the motor commands for the intended sensor position; this is denoted corollary discharge. These three mechanisms report complementary, but not necessarily complete (Berryman et al., 2006), information on sensor position.

While movement of a limb involves proprioceptive and corollary discharge reference signals, current evidence suggests that facial muscles, which bridge attachment points across soft tissue as opposed to bone, contain neither spindle fibers nor Golgi tendons (Bowden and Mahran, 1956; Hines, 1927; Semba and Egger, 1986; Stål et al., 1990; Welt and Abbs, 1990). Additional evidence demonstrates that despite the presumed lack of proprioceptors in the vibrissa musculature, neuronal signals related to rhythmic self-generated vibrissa motion, *i.e.* whisking, are encoded predominantly through peripheral sensory mechanisms (Crochet and Petersen, 2006; Fee et al., 1997; Khatri et al., 2009). Together these observations lead to the hypothesis that self-generated vibrissa motion is encoded through re-afferent activation of mechanoreceptors. Specifically, activation of lanceolate- and/or Merkel-ending trigeminal neurons could presumably code both re-afferent and ex-afferent input. These primary sensory neurons have identical, broad axonal arborizations across nuclei in the trigeminal brainstem (Sakurai et al., 2013a; Shortland et

al., 1995). Vibrissa self-motion signals are thought to inform the rodent about the position of its vibrissae upon tactile contact with an object (Curtis and Kleinfeld, 2009; Kleinfeld and Deschênes, 2011; Mehta et al., 2007; O'Connor et al., 2010), though an alternative possibility based on contact forces been proposed (O'Connor et al., 2013) and critiqued (Kleinfeld et al., 2014).

How might the animal determine the location of objects that it contacts with its moving vibrissae? Past work shows that the strength of vibrissal ex-afferent touch responses, as measured in cortex, are strongly modulated by the phase in the whisk cycle at the moment of contact (Curtis and Kleinfeld, 2009). The responses of these units therefore contain the information necessary to determine object location through self-motion, but the underlying neuronal architecture required to achieve this cortical representation of object location remains unknown. Elements of signal detection theory (Skolnick, 1962) suggest two scenarios to demodulate touch relative to phase in the whisk cycle. One scenario is that the whisking and touch signals are encoded by different populations of peripheral receptors and are maintained as separate whisking and touch pathways to somatosensory cortex. A plausible scheme for demodulation involves gating of the touch signal by the separate whisking signal (Curtis and Kleinfeld, 2009). A second scenario is that both whisking and touch signals are encoded by the same sensory receptors and central neurons to cortex. In this case a gain function with an accelerating nonlinearity (Finn et al., 2007) can serve to demodulate the touch signal.

As a means to gain insight into the particular scenario used by rodents to merge touch and self-motion of the vibrissae, we examine the response of neurons along the two dominant ascending somatosensory pathways (Bosman et al., 2011; Kleinfeld et al., 1999). Our investigation is motivated by the pioneering work of Ahissar and colleagues (Yu et al., 2006), who addressed the issue of pathways at the level of thalamus. These investigators made use of anesthetized

animals, in which whisking was induced by electrical stimulation of the buccal motor branch of the facial nerve **(Waite, 1973)**. Under these conditions, the neuronal spikes rates are much reduced by the effects of anesthesia and the concurrent loss of neuromodulation. Further, the process of electrical stimulation leads to the preferential activation of motoneurons with large caliper axons, as opposed to physiological recruitment that begins with of fibers of small caliper and progresses to those of larger caliper (Henneman, 1957). Thus there is a need for a thorough reexamination of the signaling of vibrissa input along ascending somatosensory pathways.

The lemniscal somatosensory pathway includes trigeminal nucleus principalis (PrV) and the upstream dorso-medial division of ventroposterior lateral (VPMdm) thalamic nucleus (**Fig. 1**). Neurons along this pathway spike vigorously in response to stimulus-induced deflection of one or multiple vibrissa (Chapin and Nicolelis, 1994; Pierret et al., 2000; Simons and Kyriazi, 1993; Veinante and Deschênes, 1999). Yet there is limited information on the nature of the response to vibrissa self-motion (Khatri et al., 2010). The paralemniscal pathway encompasses the rostral aspect of spinal trigeminal nucleus interpolaris (SpVIr), the upstream posterior medial (PO) thalamic nucleus, and includes collaterals to the ventral aspect of zona incerta (ZIv), a region that further provides feedforward inhibition to PO thalamus (Lavallee et al., 2005; Trageser et al., 2006) (**Fig 3.1**). Neurons along this pathway in PO thalamus spike, albeit less prominently, in response to deflection of the vibrissae (Diamond et al., 1992b; Pierret et al., 2000), yet there is apparently contradictory data on the nature of the self-motion response (Masri et al., 2008a; Yu et al., 2006). Lastly, we consider an alternate origin for whisking-related re-afference and ask if whisking is coded by mechanoreceptors in the mystacial pad, which moves in phase with the vibrissae during whisking (Hill et al., 2008). Coding of self-motion in these receptors would represent re-afferent signals that are in principle independent of vibrissa touch. The result of these

measurements define the utilization of different pathways for sensorimotor signaling and constrain computational models of vibrissa-based object location (Kleinfeld and Deschênes, 2011; Mitchinson et al., 2011).

3.2 Materials and methods

This study was performed in strict accordance with the recommendations in the Guide for the Care and Use of Laboratory Animals of the National Institutes of Health. The protocol was approved by the Committee on the Ethics of Animal Experiments of the University of California at San Diego (Protocol numbers: S02173 and S02174R).

Animals

Fifty four female Long Evans rats, 250 to 350 g in mass (Charles River), were used for combined anatomical, behavioral, and electrophysiological experiments. All behavior and electrophysiological data were obtained from head-restrained rats (Kleinfeld et al., 2002; Ono et al., 1986).

Staining for spindles and fibers

Rats were transcardially perfused with 0.1 M phosphate buffered saline (PBS) followed by 4 % (w/v) paraformaldehyde in PBS. Whole rat heads were post fixed for 4 to 12 hours at 4^{o} C. Muscles were dissected off of the fixed heads and cryoprotected in 30 % (w/v) sucrose in PBS for 8 to 12 hours at 4^{o} C.

Both mystacial pad and masseter muscles were sectioned tangentially at a thickness of 60 μm with a sliding microtome. Sections were incubated in 2 % (w/v) goat serum (S-1000, Vector) block for 30 minutes and then the primary antibody rabbit anti Neurofilament H 1:500 (Ab 1991, Millipore) overnight at room temperature. For fluorescent staining, secondary antibodies raised in goat were

used (rabbit anti-594, A-11012, Life technologies). For dark product staining, sections were incubated in biotinylated rabbit secondary antibody (BA-1000, Vector) for 90 minutes followed by processing with an ABC kit (PK-6100, Vector) and the SG peroxidase kit (SK-4705, Vector). Sections were either initially counterstained with cytochrome oxidase or a solution of 0.25% (w/v) Eosin Y in 79 % ethanol and 21 % water.

Mystacial pad and masseter muscles were frozen in blocks of OCT (25608-930, Tissue-Tek) and sectioned transversely at a thickness of 10 μm with a cryostat. Sections were directly mounted on slides to maintain the integrity and orientation of the muscle fibers. They were left to dry for a minimum of one hour. Slides were rehydrated and, sequentially, incubated in Mayer's Hematoxylin Solution (MHS15-500, Sigma-Aldrich) for 8 minutes, washed with running tap water for five minutes, differentiated in a 1 % (v/v) hydrochloric acid in distilled water for 30 s, further washed with running tap water for two minutes, "blued" in a saturated lithium carbonate solution (1.4 % (w/v) lithium carbonate in distilled water) for 30 to 60 s, washed for five minutes in running tap water, rinsed by dipping 5 to 7 times in 95 % (v/v) ethanol in water, counterstained with a 0.25 % (w/v) Eosin Y solution in 79 % ethanol and 21 % tap water for 2 minutes, finally dried in air, and covered using mounting media (ProLong Gold, Life Technologies).

Confocal stacks of images of spindle fibers were obtained with a Leica Sp5. Dark product, hematoyxlin, and eosin stained slides were imaged with a slide scanning microscope (Nanozoomer 2.0 HT, Hamamatsu). Fibers were counted using Photoshop (CS4, Adobe).

Staining for motoneurons

Rats were perfused and fixed and the brains were extracted and sectioned at a thickness of 30 μm, as above. Sections containing trigeminal and facial motor nuclei were incubated overnight in anti-

ChAT (1:100 AB144P, Millipore) and anti-NeuN (either 1:100 MAB377, Millipore, or 10μg/mL of a custom anti-NeuN directly conjugated to Alexa 594Chemicon (Tsai et al., 2009)). Sections were then rinsed and incubated for 90 minutes in anti-goat Alexa 488 (1:200 A11055, Invitrogen) and anti-mouse Alexa 647 (1:200 A31571, Invitrogen), rinsed again, mounted, and coverslipped.

Slides were scanned as described above. Motoneurons in the trigeminal and facial motor nuclei that contained a DAPI-stained nucleus were manually outlined based only on the anti-ChAT label (green channel) using Neurolucida™ software. The area and average intensity of the anti-NeuN label (red channel) within the outlined perimeter was then calculated.

Recording

Brainstem. We recorded single- and multi-unit neuronal signaling in the trigeminal complex of the head-fixed awake and alert rat using quartz micropipets as extracellular electrodes. A craniotomy was made based on stereotaxic coordinates, centered at 9 mm posterior and 3 mm lateral to Bregma for PrV and 12 mm posterior / 3 mm lateral to Bregma for SpVir. Trigeminal PrV and SpVIr nuclei were identified based on their stereotaxic coordinates and their multi-unit spiking responses to deflections of the macro-vibrissae, micro-vibrissae, and peri-mystacial fur with the use of 20 to 50 ms air puffs delivered at 0.1 to 0.2 Hz. As the position of the vibrissae were continually shifting in the awake animal, we used broad puffs that essentially stimulated all of the vibrissae (Ganguly and Kleinfeld, 2004). After a set of recordings were complete, we briefly anesthetized the rat with isoflurane, while maintaining the micropipet in the same location, so that the topology of the receptive field could be mapped. We manually deflected small patches, *i.e.*, approximately 1 to 5 mm, of peri-mystacial fur as well as individual macro- and micro-vibrissae with a hand-held probe and listened for spiking activity on an audio monitor. Lastly, we marked the location of the neighborhood of units by iontophoretic injections of Chicago sky blue dye and

determined the anatomical location in *post-hoc* histology (Moore* et al., 2013). Animals underwent 1-3 days of recording, in which 3-14 units were recorded per day. We used previously described *post-hoc* spike sorting procedures (Fee et al., 1996; Hill et al., 2011b).

Thalamus. We used neuronal recording procedures similar to those reported for brainstem recordings to examine spiking in head-fixed alert rats within VPM and PO thalamus and ZIv, except that recordings were made in the juxtacellular configuration (Moore et al., 2015b; Pinault, 1996) using micropipettes with 1 to 3 μm tip diameters. Briefly, a craniotomy was made based on stereotaxic coordinates, centered 3 mm posterior and 3 mm lateral to Bregma. We first identified these regions based on stereotaxic coordinates and spiking responses to broad air-puffs that simultaneously deflected the macro-vibrissae, micro-vibrissae, and peri-mystacial fur. Air-puffs were 5 to 20 ms delivered at 1 to 3 Hz. The somatosensory region of ZIv is located ventrally to the portion of VPM that corresponds to the A and B rows of vibrissae. We identified units in PO thalamus based on a 400 μm proximity to the border to the functionally identified VPM region. Once a unit was located we continued to move the micropipette in 1 μm increments until the spike waveform displayed an initial positive voltage deflection, which was usually accompanied by a 1.5-times or greater increase in resistance of the pipet. Recordings sites were labeled, as above. After a subset of the VPM thalamic recordings, we anesthetized the rat with isoflurane to determine the approximate receptive field of the recorded unit, as described above.

Anatomy. Recording sites were localized by concurrent dye injections from the recording pipet in all animals. Animals were perfused and fixed and the brains were extracted and sectioned at 60 μm-thick (Moore* et al., 2013). Sections were stained for cytochrome oxidase reactivity (Bourassa et al., 1995) and scanned at a resolution of 0.5 μm/pixel on a slide scanner (Nanozoomer™, Hamamatsu). Standard anatomical features were traced for the sections that

contained the dye labels with the use of Illustrator™ software (Adobe). A reference atlas was prepared from a single, un-injected brain that was sectioned and prepared in the same manner.

Sections that contained a dye label were manually assigned to the nearest plane in the reference atlas. The sections were then manually rotated and scaled to approximately match the corresponding anatomical borders and standard anatomical features in the reference atlas. A subset of the following structures were used for alignment: ventrobasal thalamus, VPM thalamus, VPL thalamus, thalamic reticular nucleus, habenula, dorsal lateral geniculate nucleus, ventral lateral geniculate nucleus, dorsal zona incerta, ventral zona incerta, subthalamic nucleus, external medullary lamina, mammilothalamic tract, fornix bundle, and the third ventricle. The mapped locations of the recording sites on the reference atlas, along with nearby anatomical borders, were traced and reconstructed in three dimensions using Neurolucida™ software (Microbrightfield).

Behavior

Vibrissae were clipped to approximately 2/3 of their original length and vibrissa position was monitored simultaneously with neuronal spiking activity under two behavioral conditions. First, as the rats were coaxed to whisk in air by presenting food or bedding from their home cage (Ganguly and Kleinfeld, 2004; Premack and Shanab, 1968). Second, as vibrissae were deflected externally by brief puffs of air applied to the face (Ganguly and Kleinfeld, 2004; Kleinfeld et al., 2002). We monitored vibrissa position with a Basler A602f camera and a white light emitting diode backlight (Moore* et al., 2013). We chose a spatial resolution of 120 μm/pixel, a field of 360x250 pixels, a frame rate of 250 Hz, and a trial time of 10 s. The pixel intensity in the image was thresholded and the mean position of the full set of vibrissae was tracked by computing the center of mass of the thresholded pixels in each frame. The data were then converted into whisking angle versus time, denoted $\theta(t)$. Lastly, a Hilbert transform was used to decompose the whisking

angle, $\theta(t)$, into the phase within the whisk cycle, $\phi(t)$, with $\theta(t) = \theta_{Amplitude}\, cos[\phi(t)] + \theta_{Midpoint}$, where $\theta_{Amplitude}$ and $\theta_{Midpoint}$ are slowly varying parameters and the whisking frequency, f_{whisk}, is given by (Hill et al., 2011a):

(1) $$\mathbf{f_{Whisk}} = \frac{\mathbf{1}}{\mathbf{2\pi}} \frac{\mathbf{d\phi(t)}}{\mathbf{dt}}.$$

Lastly, we recall that the vibrissae tend to move in phase with one another during free-air whisking (Hill et al., 2011a); thus the phase, but not the amplitude or midpoint, of all vibrissae may be taken as identical.

Analysis

Free-whisking. The range of possible phases, *i.e.*, 0 to 2π radians, was divided into 32 bins, each spanning $\pi/16$ radians. Thus phase is now labeled by an index k with $1 \leq k \leq 32$. Each spike that occurred during a detected whisk, at time t_S, was assigned an instantaneous phase $\phi(t_S)$ and thus assigned to one of the phase bins. We define $N(\phi_k|spike)$ as the number of spikes in phase bin k across all detected whisks and $P(\phi_k|spike) = N(\phi_k|spike)/N_{spikes}$, where N_{spikes} is the total number of spikes, as the probability density function of phase for spiking events. Since the distribution of phases is not uniform across time, we similarly computed the number of phases observed for each bin, denoted $N(\phi_k)$, along with the probability density function of the number of whisking events for each phase bin, denoted $P(\phi_k)$. These two distributions used to compute the mean spike rate for each phase bin, ϕ_k, which we denote $\lambda[\phi_k]$ and define as:

(2) $$\boldsymbol{\lambda[\phi_k]} = \mathbf{r} \cdot \frac{\mathbf{N(\phi_k|spike)}}{\mathbf{N(\phi_k)}}$$

where *r* is the video frame rate.

We characterized the modulation of each unit by fitting a sine wave with a period 2π to the rate versus phase in the whisk cycle with standard linear least-squares regression techniques. The fit, defined by:

(3) $$\hat{\boldsymbol{\lambda}}(\mathbf{t}) = \langle\boldsymbol{\lambda}\rangle + \boldsymbol{\lambda}_{\mathbf{Amplitude}}\,\mathbf{cos}[\boldsymbol{\phi}(\mathbf{t}) - \boldsymbol{\phi}_{\mathbf{Preferred}}],$$

is completely described by its mean, $<\lambda>$, amplitude, $\lambda_{Amplitude}$, and phase, $\phi(t)$. A preferred phase of $\phi_{Preferred} = 0$ corresponds to fully retracted while $\phi_{Preferred} = \pm\,\pi$ corresponds to fully protracted.

The modulation depth of the averaged whisking response is defined as:

(4) $$\mathbf{M}_{\mathbf{Whisk}} \equiv 2\,\frac{\boldsymbol{\lambda}_{\mathbf{Amplitude}}}{\langle\boldsymbol{\lambda}\rangle}$$

and the signal-to-noise ratio for a point process with Poisson distributed arrival times and a temporal window of T, denoted SNR_{Whisk}, is:

(5) $$\mathbf{SNR}_{\mathbf{Whisk}} = \mathbf{M}_{\mathbf{Whisk}}\sqrt{\langle\boldsymbol{\lambda}\rangle\mathbf{T}} = 2\boldsymbol{\lambda}_{\mathbf{Amplitude}}\sqrt{\frac{\mathbf{T}}{\boldsymbol{\lambda}}}$$

.

The statistical significance of the modulation was determined by comparing the distributions of all spike phases, $N(\phi_k|spike)$ with all whisk phases, $N(\phi_k)$, using a Kuiper test (Batschelet, 1981; Berens, 2009), *i.e.*, a modification of the Kolmogorov-Smirnov test that accounts for periodic variables.

Air-puff. We characterized the modulation in spike rate of each unit in response to air-puff deflections based on a peri-stimulus time histogram of spiking activity aligned to the onset of the stimulus. The histograms were computed by counting the number of spikes in 5 ms bins that were averaged by a 2 ms sliding window. We denote the maximum and the minimum binned spike rates in the first 100 ms after the onset of the stimulus as $\lambda_{maximum}$ and $\lambda_{minimum}$, respectively. We

computed the background rate, denoted $\lambda_{background}$ as the mean rate for the 100 ms period that was 150 to 250 ms after the onset of the stimulus. As the response to air-puff typically was observed to be fully contained within the first 100ms, the statistical significance of the modulation upon air-puff was determined by comparing the distribution of spike times in the first 100 ms post-stimulus to a uniform distribution (Kolmogorov-Smirnov test).

3.3 Results

Assessment of potential proprioceptive input in the vibrissa system

Although current evidence suggests a lack of proprioceptive innervation of most facial muscles in a number of species, data specific to the innervation of the rodent vibrissa musculature are more limited (Semba and Egger, 1986). We therefore used three complementary anatomical techniques to determine whether vibrissa muscles contain endo-receptors:

First, a classic measure to observe endo-receptors is via the labeling of spindle-like proprioceptive afferent endings (Granit, 1970). Spindles appear as helical-shaped fine processes that surround intrafusal muscle fibers. Spindles are well known to be prominent in the masseter muscle (Rokx et al., 1984), as confirmed by immunostaining of neurofilament proteins from tangential sections of the muscle (**Fig 3.2a**). We thus searched for spindle-like endings in the mystacial pad, in both intrinsic and extrinsic muscles, as compared to sections of masseter muscle from the same animals. The number of motoneuron endplate claws in the same sections serves to normalize our counts. We observed spindles in the vibrissa musculature in only one of three animals (2,480 endplates across 23 sections) (**Fig 3.2b**), which correspond to 0.0012 ± 0.0007 (mean ± SD) spindles/plate compared to 0.0279 ± 0.0054 for the masseter muscle (970 endplates

across 36 sections) (**Fig 3.2c**). Thus the vibrissa muscles contain over 20-fold less spindles than a muscle with known proprioceptive control (**Fig 3.2d**).

As a second measure, we prepared transverse sections of both the mystacial pad and the masseter muscles and directly stained both the intrafusal and extrafusal fibers. The intrafusal fibers are identified by their small size and bundling of multiple fibers within a capsule (**arrows in Fig 3.2e,f**). Here the total number of extrafusal fibers in a section serves as the normalization. We observed intrafusal fibers in the vibrissa musculature in two of three animals (53,800 extrafusal fibers across 13 sections) (**Fig 3.2e**), which corresponds 0.00011 ± 0.00005 intrafusal to extrafusal fibers compared to 0.00160 ± 0.00017 for the masseter muscle (56,960 extrafusal fibers across 13 sections) (**Fig 3.2f**). Thus the vibrissa muscles contain 15-fold less intrafusal fibers than a muscle with known proprioceptive control (**Fig 3.2d**).

A final measure we asked if γ-motoneurons, which innervate intrafusal fibers, are present in the lateral facial nucleus. This nucleus contains the motoneurons for the vibrissa musculature (Klein and Rhoades, 1985; Takatoh et al., 2013b). As a positive control, we compared staining in the lateral facial nucleus to the trigeminal motor nucleus, which innervates the masseter and other jaw muscles and, consistent with the presence of spindles in the masseter muscle (**Fig 3.2a**), is known to contain γ-motoneuron efferents (Sessle, 1977a, b). Recently, it has been demonstrated that γ-motoneurons can be distinguished from α-motoneurons based on their size and the relative intensity of anti-ChAT and anti-NeuN staining. Specifically, both α- and γ-motoneurons are labeled intensely with anti-ChAT, but α-motoneurons have larger somata and are labeled by anti-NeuN, whereas γ-motoneurons are smaller and are not labeled by anti-NeuN (Friese et al., 2009).

We analyzed immunohistochemical labeling on rat brainstem sections for ChAT and NeuN **(Fig 3.3)** and considered only neurons whose nucleus was contained in the section as indicated by

a DAPI counterstain (**Fig 3.3a,b**). Qualitatively, the trigeminal motor nucleus contained two populations of motoneurons. Larger motoneurons were labeled both by anti-ChAT and anti-NeuN, whereas smaller motoneurons were labeled only by anti-ChAT (**Fig 3.3c-e**). In the facial nucleus, we observed only one population of medium-sized motoneurons, presumably α-motoneurons, that were labeled both by anti-ChAT and anti-NeuN (**Fig 3.3f-h**). To quantify these observations, we calculated the area of each motoneuron and the average intensity of anti□ChAT and anti-NeuN labeling within the labeled area. We observed two clusters of neurons in the trigeminal motor nucleus, putatively corresponding to α- and γ-motoneurons (**Fig 3.3i,k**). Approximately one-third of the motoneurons fell into the putative γ-motoneuron cluster, consistent with spinal motoneuron pools that innervate muscles with spindles (Friese et al., 2009). In the facial motor nucleus we observed a unimodal distribution of motoneuron sizes and anti-NeuN intensities, putatively corresponding to α-motoneurons (**Fig 3.3j,l**). These results imply that the innervation of intrafusal fibers by the lateral facial motor nucleus represents at most a small fraction of its total output, and are consistent with past reports that most facial muscles lack proprioceptive signaling (Bowden and Mahran, 1956; Hines, 1927; Semba and Egger, 1986; Stål et al., 1990; Welt and Abbs, 1990). Together, these anatomical analyses of neuronal endings, muscle fibers, and motoneuron types imply that classic propriception makes a negligible contribution to the coding of vibrissa self-motion.

Spiking activity in trigeminal brainstem nuclei during free whisking

Given the relatively poor proprioceptive innervation of the vibrissa musculature, re-afferent activation of trigeminal mechanosensory afferents, including lanceolate and Merkel ending neuron types, is a likely source of the sensory signal of whisking phase. We thus monitored neuronal activity in two of the target nuclei in the brainstem for these neuron types (Sakurai et al.,

2013a; Shortland et al., 1995), nuclei PrV and SpVIr, that provide the majority of the ascending projections to thalamus (**Fig 3.1**). These nuclei anchor the lemniscal and paralemniscal pathways, respectively, and the literature is unequivocal about the presence of vibrissa touch responses in both nuclei. We recorded single and multi-unit activity in nucleus PrV (25 putative single unit and 31 multi-unit spiking signals) and nucleus SpVIr (14 putative single unit and 10 multi-unit spiking signals) (**Methods**). As illustrated by the example of **Figure 3.4,** the spike rates of units in nucleus PrV are substantially modulated on a cycle-by-cycle basis during rhythmic whisking in air (**Fig 3.4a,b**). To quantify this modulation of the spike rate, we isolated individual whisk cycles (**Eqn. 1**) and aligned spike events relative to the instantaneous phase in the whisk cycle (Hill et al., 2011a) (**Fig 3.4c).** We next computed the distributions of whisking phases and of whisking phases at which spikes occurred (**Fig 3.4d**). From these distributions, we estimated the spike rate as a function of phase in the whisk cycle, (**black line in Fig 3.4e**) and fit a sinusoid rate function (**Eq. 4**) to the data as a means to parameterize the modulation depth (**Eq. 4**) and preferred phase. For the unit in **Figure 4**, the majority of spikes, *i.e.*, 373/404 (92 %) of spikes across 303 whisks, occurred during the retraction phase of the whisk cycle, when the vibrissae were moving in the caudal direction (**Fig 3.4f**).

Tactile receptive fields were established for a subset of the recorded units by briefly anesthetizing the rat with isoflurane and manually stimulating different vibrissae **(Methods)**. The unit in the example of **Figure 3.4** was located among many units that responded to vibrissa E3. The firing rates of additional example units as a function of. phase in the whisk cycle, along with their local receptive fields, are shown in **Figure 3.5.** These include units in the sub-region of nucleus PrV that corresponds to the macro-vibrissae (**Fig 3.5a**) and units in sub-regions that correspond to the skin and fur around the mouth and nose (**Fig 3.5b**). Further, we observed units

in nucleus SpVIr that were significantly, albeit modestly, modulated by whisking (**Fig 3.5c).** As a population, 49/56 PrV units (88 %) and 16/24 SpVIr units (67 %) were significantly modulated by whisking (Kuiper test, $p < 0.05$). Units in nucleus PrV tended to fire more spikes when the animal was whisking as opposed to not whisking (Wilcoxon signed rank test, $p = 1.0 \times 10^{-5}$), whereas spike rates were not significantly different between whisking and not whisking in nucleus SpVIr (Wilcoxon signed rank test, $p = 0.39$; **Fig 3.5d**)

We characterized the sinusoidal fits of spike rates across all units (**Fig 2.4f & 2.5a-c**) by two measures. The first measure is the modulation depth, M_{Whisk} (**Eq. 4**), which reports the fraction of the unit's response that is locked to whisking**.** The second measure is the signal-to-noise ratio, SNR_{Whisk}, over a time interval (T) chosen to be the average period between whisks for head-fixed rats, *i.e.*, T = 165 ms (Hill et al., 2008; Moore* et al., 2013) (**Eq. 5**). We observe a greater modulation depth for lower mean spike rates, with a SNR_{Whisk} that peaks at a mean rate of $<\lambda> \sim$ 20 Hz (**Fig 3.6a**)**.** As a population, units in brainstem nucleus PrV were more strongly modulated than those in nucleus SpVIr (Wilcoxon ranked sum test, $p = 0.03$), with median M_{Whisk} values of 1.0 versus 0.6 for nucleus PrV versus SpVIr, respectively. Further, units in nucleus PrV had a greater SNR_{Whisk} than those in nucleus SpVIr (Wilcoxon ranked sum test, $p = 0.0016$, with median values of $SNR_{Whisk} = 1.6$ versus 0.8 for nucleus PrV versus SpVIr, respectively (**Eq. 5**).

Different units preferentially spiked at different phases of the whisk cycle, denoted $\phi_{Preferred}$ (**Eq. 3**). All phases are represented for units in both nuclei PrV and SpVIr (**Fig 3.6b**). There is a significant bias in the preferred phase across all units in nucleus PrV, with a vector average $<SNR_{Whisk}> = 0.6$ and $<\phi_{Preferred}> = 4.9$ radians (Hotelling's one-sample test; $p = 0.02$); this phase corresponds to retraction from the fully retracted position. There was no bias for units in SpVIr (Hotelling's one-sample test; $p = 0.3$) (Batschelet, 1981). *In toto*, these data show that self-motion

is represented along the primary nuclei of the lemniscal and paralemniscal pathways, but more robustly along the lemniscal pathway.

Spiking activity in thalamic nuclei and zona incerta during whisking

To determine the encoding of self-generated whisking in the thalamic nuclei that receive inputs from PrV and SpVIr (**Fig 3.1**), we recorded spiking activity of individual neurons using the juxtacellular configuration in VPM and PO thalamus (74 neurons). Occasionally, extracellular recordings of nearby units were obtained on the same micropipette; these units had negative initial deflections, as opposed to the initial positive spike deflections of the juxtacellularly recorded neurons (3 of 71 records). Similarly, we recorded spiking activity of individual neurons using the extracellular or juxtacellular configuration in ZIv (15 neurons). We next consider the spiking dynamics of individual neurons in VPM and PO thalamus, as well as in ZIv, in response to self-generated whisks (**Fig 3.7-9**) and external vibrissa deflections with air puffs (**Fig 3.10**).

As illustrated by the example of **Figure 3.7**, in which the neuron was located among units that responded to vibrissa C4, neurons in VPM thalamus are substantially modulated on a cycle-by-cycle basis during whisking (**Fig 3.7a,b**). The analysis of the spike rate as a function of phase in the whisk cycle for thalamic neurons (**Fig 3.7c-f**) proceeded similarly to that for units in the brainstem (**Fig 3.4,3.5**). For the neuron in **Figure 3.7,** the majority of spikes occurred during the protraction phase of the whisk cycle. The spike rate from this neuron was particularly well described by a sinusoidal modulation as a function of phase (**Fig 3.7f**).

Additional example neurons from VPM thalamus, the adjacent sub-region in PO thalamus, and ZIv, along with their anatomical locations of the recording sites, are shown in **Fig 3.7, Supp fig 3.1, Supp fig 3.2, and Supp fig 33.** Qualitatively, neurons in the sub-region of VPM thalamus

that corresponds to the macro-vibrissae (**Fig 3.8a**), as well as units in sub-regions that correspond to the skin or fur around the mouth and nose (**Fig 3.8b**), were modulated. PO thalamus also contained a minority of neurons that were modulated (**Fig 3.7c**), while modulation appeared absent in neurons in ZIv (**Fig 3.8d**). As a population, neurons in VPM and PO thalamus tended to fire more spikes when the animal was whisking as opposed to not whisking (Wilcoxon signed rank test, $p = 10^{-9}$ and $p = 0.04$, respectively (**Fig 3.8e)**. This is consistent with past results (Poulet et al., 2012). Neurons in ZIv tended to fire fewer spikes when the animal was whisking (Wilcoxon signed rank test, $p = 0.02$) (**Fig 3.8e**). Overall, neurons in VPM thalamus tended to have significantly higher spike rates than in those PO thalamus during whisking epochs (Wilcoxon ranked sum text, $p = 0.0057$), but not during non-whisking epochs (Wilcoxon ranked sum text, $p = 0.15$).

Similarly to the analysis for units in nuclei PrV and SpVIr, we characterized the population response for neurons in VPM and PO thalamus and ZIv in terms of the modulation depth, M_{Whisk} (**Eq. 4**), and the signal-to-noise ratio, SNR_{Whisk} with T = 165 ms (**Eq. 5**). The majority of neurons in VPM thalamus were significantly modulated by whisking phase (49/57; Kuiper test $p < 0.05$). (**Fig 3.9a**), whereas only a minority of PO neurons were significantly modulated (4/17; Kuiper test $p < 0.05$) (**Fig 3.9a**) and no neurons in ZIv were significantly modulated (0/15; Kuiper test $p < 0.05$). Of the VPM neurons located among units that had receptive fields corresponding to the micro-vibrissae or peri-mystacial fur, 12/15 of these neurons were significantly modulated. As in the case for brainstem (**Fig 3.6b**), different VPM neurons preferentially spiked at different phases of the whisk cycle. All phases are represented for neurons in VPM thalamus (**Fig 3.9b**), but with no significant bias in the preferred phase (Hotelling's one-sample test; $p = 0.72$). *In toto*, these data

show that self-motion is represented in thalamic nuclei of the lemniscal and paralemniscal pathways but, as with the case of brainstem, only robustly along the lemniscal pathway.

We computed the perpendicular distance between the Chicago sky blue spot and the VPM/PO border for each labeled recording site, based on cytochrome-oxidase stained sections. The location of the VPM/PO border, determined by visual inspection, was estimated to be accurate to approximately 80 μm (**Supp fig 3.4**). There does not appear to be a clear systematic relationship between the signal-to-noise ratio for whisking and the distance to the border between VPM and PO thalamus at this spatial resolution. Neurons with high values of SNR_{Whisk} occur in VPM thalamus both close to the border as well as deeper in the nucleus (**Fig 3.9c**). To further clarify whether there is a potential segregation of function within VPM thalamus, we reconstructed the locations of the labelled recording sites in three dimensions (**Fig 3.9d,e**). Again, there is no clear spatial relationship between the location of a neuron within VPM and its SNR_{Whisk}. The lack of topography would imply that self-generated motion and touch are signaled within the same anatomical pathway.

Stimulus-induced spiking in thalamic nuclei and zona incerta

To determine whether the same neurons respond to ex-afferent and re-afferent stimuli, we next consider how the same neurons along the lemniscal and paralemniscal pathways respond to external deflections of the vibrissae. The case for touch-based responses in the VPM thalamus, along the lemniscal pathway, is unequivocal. However, the case for touch-based responses in PO thalamus, along the paralemniscal pathway, is the subject of conflicting reports as to whether external stimuli can drive neurons in PO thalamus independent of feedback activation from deep layers in cortex. As past work involved anesthetized animals (Ahissar et al., 2000; Diamond et al., 1992a; Diamond et al., 1992b; Masri et al., 2008a; Sosnik et al., 2001), we undertook a re-analysis

of the response of neurons in VPM and PO thalamus along with the somatosensory region of ZIv (**Fig. 1**).

As illustrated by the examples of **Figure 3.10a-c**, neurons in all three areas were modulated by air-puff deflections to multiple vibrissae and peri-mystacial fur, with neurons in VPM thalamus responding vigorously, those in PO thalamus the least responsive (**Fig 3.10b**), and those in ZIv responding with short latency, precisely timed spikes (**Fig 3.10c**). Across the population, 49/54 VPM neurons (91 %), 11/17 PO neurons (65 %), and 12/15 (80 %) ZIv neurons were significantly modulated by air-puffs ($p < 0.05$) (**Fig 3.10d**). These data imply that nucleus SpVIr indeed drives ascending targets and that neurons in PO thalamus are responsive to stimulation in alert rats.

We next consider the responses of these same neurons to self-motion of the vibrissae (**inserts in Fig 3.10a-c**). Consistent with the notion of a single anatomical pathway for re-afferent whisking and ex-afferent touch, the majority of VPM units that were modulated by self-generated whisking tended to also be modulated by air-puff deflections. Of the neurons in VPM thalamus, 42/54 (78 %) were significantly modulated by both air-puffs and whisking, five were modulated by whisking only, and seven were modulated by air-puffs only. Yet there does not appear to be a relationship between the fidelity of modulation for VPM neurons that are significantly modulated by both whisking and air-puffs, as measured by the correlation between signal-to-noise ratio for whisking and the peak modulation upon air puff (**Fig 3.10e)**, ($r = 0.05$ with $p = 0.76$ for VPM units).

3.4 Discussion

We report the representation of self-generated whisking in subcortical somatosensory brain regions (**Fig 3.1**). First, we assess the potential contribution of proprioceptive endings in the facial

musculature to somatosensation. We find a small number of previously unreported spindle-like endings and intrafusal fibers within the vibrissa musculature. However, these endings fibers are relatively scarce in comparison with the nearby masseter muscle (**Fig 3.2**). Furthermore, using a recently developed immunohistochemical strategy (Friese et al., 2009), we find that the lateral facial motor nucleus contains few, if any, intrafusal fiber-innervating γ-motoneurons (**Fig 3.3)**. While we cannot rule out the possibility that intrafusal fibers are instead innervated by the hypoglossal (Mameli et al., 2008) and trigeminal mesencephalic nuclei (Mameli et al., 2010), this finding together with comparatively low density of spindles and intrafusal fibers would suggest that vibrissa position is unlikely to be sensed by proprioception (Rice, 1993). Nonetheless we find a robust representation of self-generated vibrissa motion, *i.e.* whisking, in nucleus PrV (**Fig 3.4**), which receives primary afferent input from mechanoreceptors in the vibrissa follicles and the face. These results, together with previous findings that the representation of rhythmic vibrissa motion in somatosensory afferents are derived from peripheral sensors (Leiser and Moxon, 2007; Szwed et al., 2003); (Khatri et al., 2009), suggest that vibrissa position during whisking is encoded through re-afferent activation of mechanical exo-receptors (**Fig 3.4-6**).

We next established the modulation of spiking activity of neurons in the lemniscal and paralemniscal pathways by the phase in the whisk cycle. At the level of the trigeminal brainstem, lemniscal neurons in nucleus PrV are substantially more reliable encoders of phase than paralemniscal neurons in spinal trigeminal nucleus SpVIr (**Fig 3.5-6**). At the level of the thalamus, lemniscal neurons in VPM thalamus are again substantially more reliable encoders of phase than paralemniscal neurons in PO thalamus (**Figs 3.7-9**). In particular, the majority of PO thalamic neurons do not significantly encode phase (**Figs. 7-9**). Consistent with the lack of whisking-related modulation in PO thalamus, neurons in ZIv, which receive inputs from axon collaterals of cells in

SpVIr that primarily project to PO-thalamus (**Fig 3.1**), are also not modulated by whisking (**Fig 3.8-9**). Together these data indicate that the lemniscal pathway from brainstem to cortex contains both neurons with the highest acuity for passive vibrissa deflections and neurons with the greatest reliability for coding phase in the whisk cycle. Some single units are reliable encoders of both signals (**Fig 3.10a,e**), as proposed by studies that utilized electrically-induced whisking in anesthetized animals (Brown and Waite, 1974); (Yu et al., 2006).

The lemniscal pathway in encoding self-motion and touch

Whisking-phase responses observed in VPM thalamic neurons in the present study substantially extend the results of past studies performed with both alert (Khatri et al., 2010) and anesthetized (Brown and Waite, 1974; Yu et al., 2006) rats. We observe phase-dependent spiking modulation throughout the depth of VPMdm thalamus, which presumably comprises units in both the "head" and "core" regions of the barreloids (Urbain and Deschênes, 2007b). This finding is consistent with results in which artificial whisking was induced by electrical stimulation of the facial nerve in anesthetized rats (Yu et al., 2006); however, we find that units are tuned to all phases of the whisk cycle rather than to protraction onset. These broader distributions of preferred phases, which are observed in both PrV and VPM thalamus (**Fig 3.6b,9b**), are consistent with the range of phase preferences observed somatosensory cortex during natural whisking (Fee et al., 1997); (Curtis and Kleinfeld, 2009);(Crochet and Petersen, 2006; Gentet et al., 2010); (de Kock and Sakmann, 2009). We were unable to assess whether there is finer a systematic map of the encoding of self-motion on the scale of individual barreloids (Timofeeva et al., 2003; Urbain and Deschênes, 2007b). Interestingly, in addition to the barreloids, we observe modulation in phase with whisking in some units that encode distortions to the skin or fur outside of the vibrissa follicle in both PrV and VPM thalamus (**Fig. 35b, 3.6a, 3.8b,e, 3.9**).

The observation that the majority of whisking responses are encoded within the lemniscal pathway raises the question of how phase-dependent touch signals, which were previously observed in somatosensory cortex (Curtis and Kleinfeld, 2009), arise from the observed thalamic inputs. There are at least two potential schemes that could produce these cortical phase-dependent touch signals (**Fig 3.11**). One scheme is that whisking and touch are encoded by different populations of peripheral mechanoreceptors and central neurons. In this scheme, thalamic neurons that predominantly encode the whisking signal could change the slope of the gain function of cortical neurons, *i.e.*, the proportionality of spike rate to input current (Curtis and Kleinfeld, 2009), in a phase-dependent manner (**Fig 3.11a**), analogous to heterodyne detection (Skolnick, 1962). Contrary to previously proposed hypotheses (Curtis and Kleinfeld, 2009; Yu et al., 2006), our data indicate that paralemniscal inputs are unlikely to be the source of this cortical gain modulation. However, lemniscal units that encode skin or fur distortions during whisking, which we observed in nucleus PrV and VPM thalamus, could in principle contribute to a re-afferent signal of vibrissa position that is independent of vibrissa touch (**Figs. 3.5b, 3.8b**). It remains to be determined whether such signals can influence phase-dependent touch responses in the barrels of somatosensory cortex.

A more parsimonious scheme is that the same mechanoreceptors, PrV neurons, and VPM thalamic neurons encode both whisking and touch signals. In this scheme a gain function with an accelerating nonlinearity (Finn et al., 2007) could enhance the spike rate at the peak of the whisking signal relative to other positions (**Fig 3.11b**), in analogy to homodyne detection (Skolnick, 1962) and the effect of a threshold nonlinearity (Ahrens et al., 2002). Based on the present results, units that encode both whisking and external vibrissa deflections could provide the relevant inputs to somatosensory cortex (**Fig 3.10a,e**). According to this scheme, if touch occurs at preferred phase

of the whisk cycle the response is enhanced, while touch at the non-preferred phase leads to a diminished response. Such non-linear gain functions could be present at multiple stages along the sensory processing stream, including at the mechanoreceptors themselves. Successive stages of accelerating non-linear gain functions can enhance the response to touch at the preferred versus the non-preferred phase. In fact, modulation of touch by self-motion can occur even if self-motion signal alone is sub-threshold, and the resulting threshold nonlinearity can further enhance the difference between touches at different phases.

Is there a role for the paralemniscal pathway in encoding self-motion and touch?

The potential role of the paralemniscal pathway in sensing vibrissa motion is controversial (Ahissar et al., 2008; Ahissar et al., 2000 ; Golomb et al., 2005; Masri et al., 2008a, b; Urbain and Deschênes, 2007a; Yu et al., 2006). The majority of neurons in nucleus SpVIr are similarly tuned to upward vibrissa deflections of many vibrissae in anesthetized rats (Furuta et al., 2006a), but are only weakly tuned to phase during whisking relative to neurons in nucleus PrV (**Fig 3.5-6**). Neurons in PO thalamus respond only weakly to external vibrissa deflections due to feed-forward inhibition from the output of ZIv neurons in ketamine-anesthetized rats (Lavallee et al., 2005). Electrical stimulation of vibrissa motor cortex inhibits activity in ZIv, which disinhibits neurons in PO thalamus and thereby increases its responsiveness to deflections (Urbain and Deschênes, 2007a). This observation led to the hypothesis that whisking-related activity in primary motor cortex (Carvell et al., 1996; Hill et al., 2011a) might gate PO thalamus so that it is sensitive to whisking. Our data suggest that while the overall firing rates of ZIv neurons decrease slightly during whisking, this decrease is not sufficient to elicit whisking-phase dependent responses in PO thalamus. The lack of phase-dependent responses in the majority of PO units in our study is consistent with a past report (Masri et al., 2008a), but inconsistent with results obtained with

electrically-induced whisking in urethane anesthetized rats (Yu et al., 2006). Nonetheless it is interesting that PO thalamic neurons have been shown to respond to vibrissa movements in the latter condition. In this respect, it remains possible that PO thalamic neurons are able to respond in a similar manner to SpVIr during some currently unknown behavioral context.

Why encode self-motion through peripheral reafference?

In the absence of proprioception (**Fig 3.3**) and corollary discharge (Fee et al., 1997), encoding of self-generated vibrissa movement through re-afferent activation of mechanoreceptors is a means for the animal to compute the position of its vibrissae (Mehta et al., 2007), which can be used to modulate the sensory response to touch depending on phase in the whisk cycle (**Fig 3.11**). Why does self-generated movement appear to be represented differently in the vibrissa system than in the limbs, which involves proprioceptive and cutaneous signals encoded in separate thalamocortical pathways (Francis et al., 2008; Friedman and Jones, 1981)? One possible explanation is that the limbs, which support the body, are likely to carry a variable load. Accurate positioning therefore requires sensory information related to muscle length and force that is independent of tactile sensation. This may also be true for jaw muscles, which are innervated by muscle spindle fibers (Rokx et al., 1984) and corresponding γ-motoneurons (Bae et al., 2002; Sessle, 1977b) (**Fig 3.3**). The vibrissa muscles, on the other hand, support only a small, relatively constant load consisting of the vibrissae themselves and will readily flex under a load (Hires et al., 2013; Huet et al., 2015). While proprioception appears to exist in the extraocular muscles (Daunicht, 1983; Porter et al., 1983), other facial muscles that carry a small, relatively constant load are thought to be devoid of proprioceptive innervation (Bowden and Mahran, 1956; Hines, 1927; Semba and Egger, 1986; Stål et al., 1990; Welt and Abbs, 1990). We can only conjecture that facial expression control may follow similar mechanisms. In the case of other facial

movements in which self-motion is coded by exo- as opposed to endo-receptors, any position-dependent signal may serve as a reference signal for computing sensation in terms of sensor position.

3.5 Author contributions

This chapter is a reprint of the material as it appears in Moore JD, Mercer Lindsay N, Deschénes M, and Kleinfeld D. “Vibrissa Self-Motion and Touch Are Reliably Encoded along the Same Somatosensory Pathway from Brainstem through Thalamus.” PLoS Biology, 13(9):e1002253, 2015. The dissertation author was the second author and contributed Figure 2.

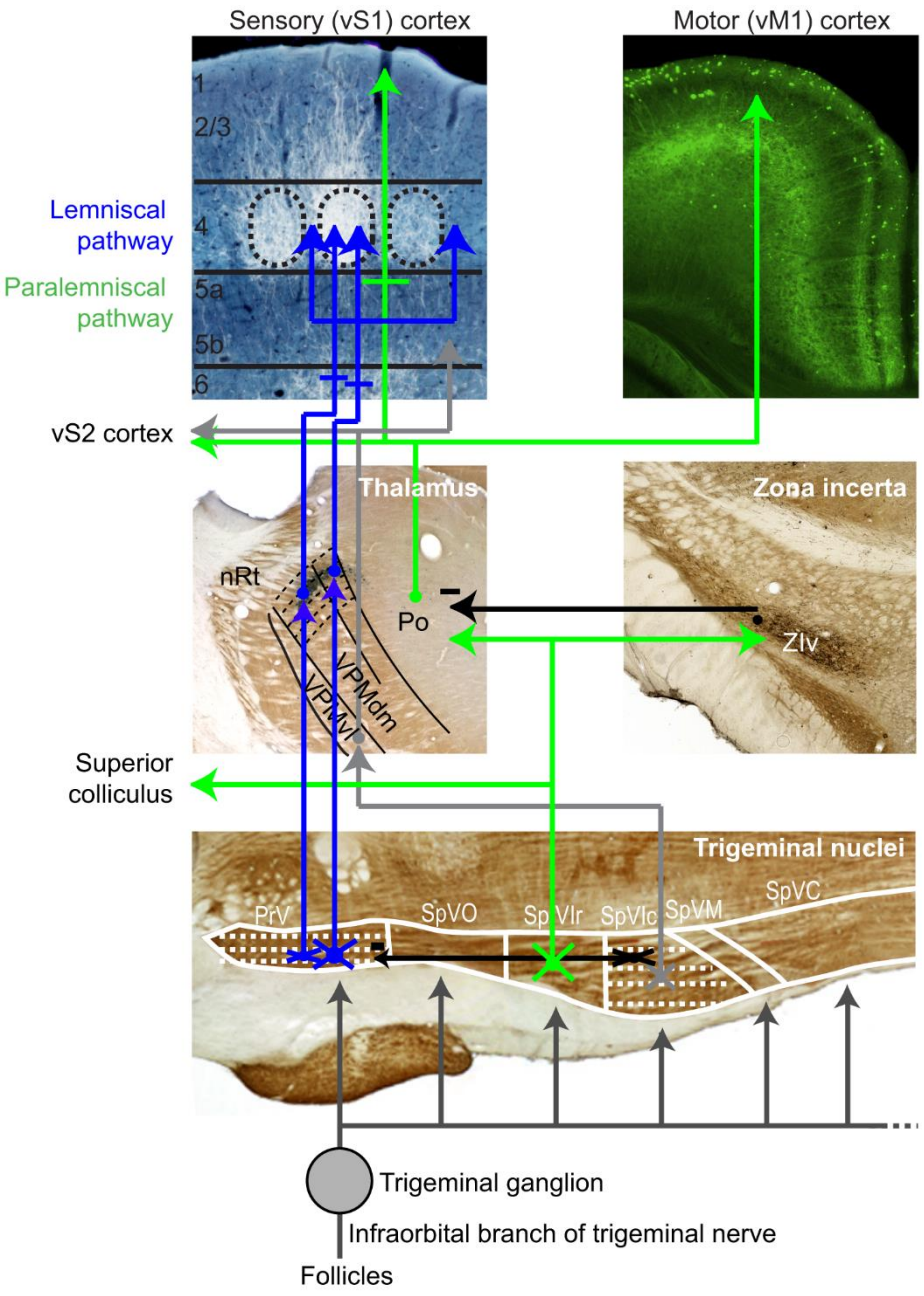

Figure 3.1 Map of vibrissa ascending pathways from the periphery to cortex. Dashed arrows represent individual barrelettes, barreloids, and barrels. The classical lemniscal pathway, including neurons with single- and multi-vibrissae receptive fields through the head and core of the barreloids, respectively, is shown in blue. The paralemniscal pathway is shown in green, and a third, extralemniscal pathway in grey. Inhibitory interactions are shown in black. Abbreviations: PrV, principal trigeminal nucleus; SpVIr and SpVIc, rostral and caudal divisions of spinal nucleus interpolaris, respectively; SpVImu, spinal nucleus muralis; SpVC, spinal nucleus caudalis; VPMdm, dorsomedial aspect of the ventral posterior medial nucleus of dorsal thalamus; PO, medial division of the posterior group nucleus; nRt, nucleus reticularis; ZIv, and ventral aspect of the zona incerta. Adapted from (Kleinfeld and Deschênes, 2011; Matthews et al., 2015).

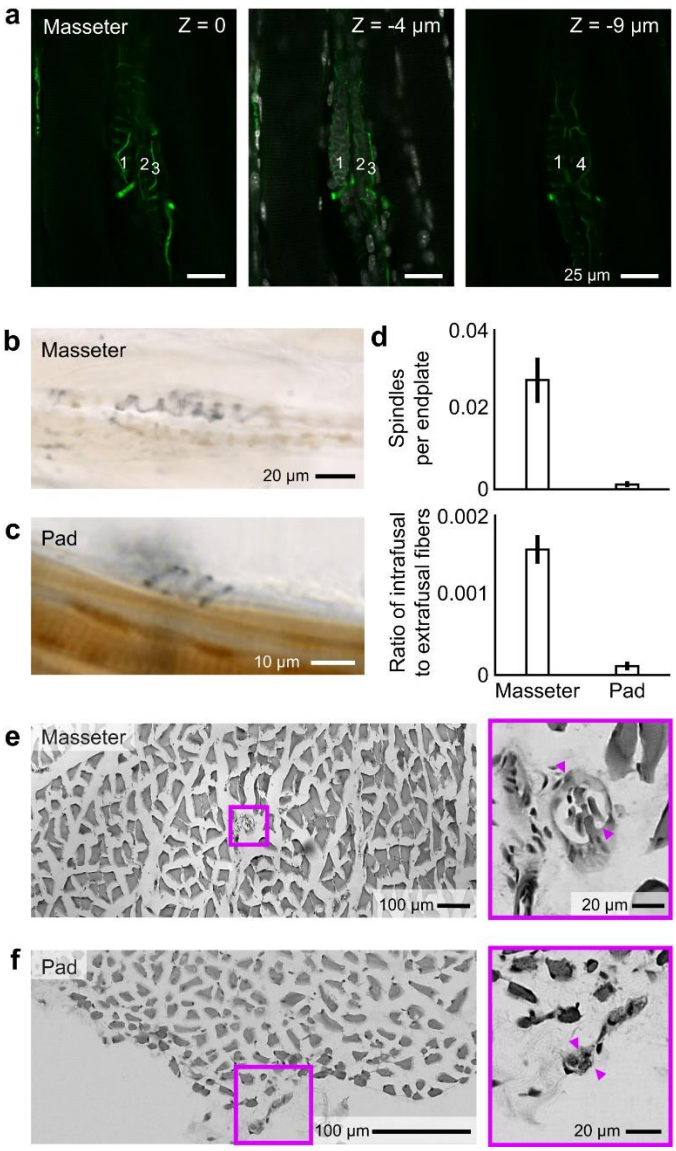

Figure 3.2 Identification of spindle complexes in the cranial muscles. (a) A spindle complex located in the masseter that is labeled by anti-Neurofilament H (green) with the nuclei in the underlying muscle labeled with DAPI (grey) at three imaging depths. Two nuclear bag fibers, labeled 1 and 4, and two chain fibers, labeled 2,3, form this complex. **(b,c)** Spindle sensory afferent fibers labeled by anti-Neurofilament H in the masseter (panel b) and the mystacial pad muscles (panel c). The muscle is stained with cytochrome oxidase (brown). **(d, e)** Fraction of labeled spindles relative to the number of labeled endplates in the same section, together with the fraction of observed intrafusal fibers per extrafusal fiber in the same section. **(f, g)**. Transverse sections of masseter (panel f) and mystacial pad (panel g), stained with hematoxylin and eosin stain to highlight all muscle fibers, together with higher magnification images that highlight intrafusal fibers (arrows).

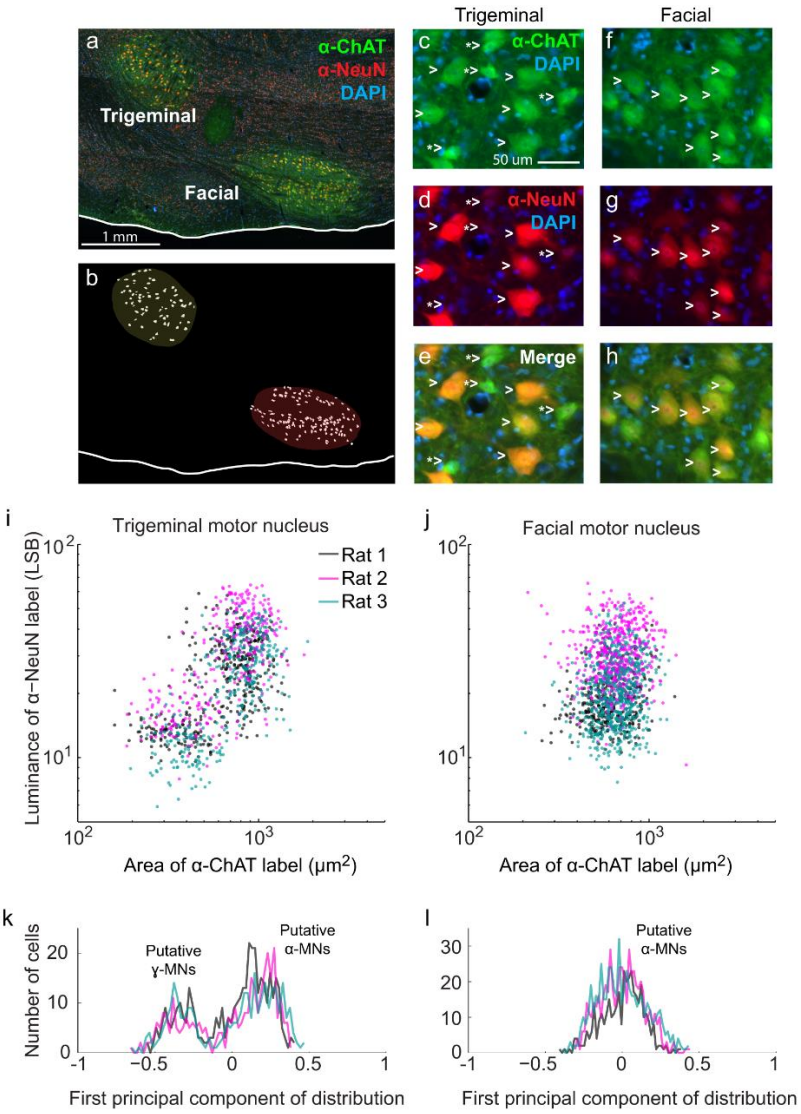

Figure 3.3 Identification of alpha and gamma motoneurons that innervate cranial muscles. (a) Rat brainstem section containing trigeminal and lateral facial motor nuclei. The section is labeled with anti-ChAT (green) anti-NeuN (red) and DAPI (blue). **(b)** Sample outlines of motoneurons in the trigeminal and lateral facial motor nuclei based on anti-ChAT labeling. **(c)** anti-ChAT labeling of motoneurons in the trigeminal motor nucleus. **(d)** anti-NeuN labeling of the neurons in **panel c**. **(e)** anti-ChAT and anti-NeuN labeling of the neurons in **panel c. (f)** anti-ChAT labeling of motoneurons in the facial motor nucleus. **(g)** anti-NeuN labeling of the neurons in **panel f**. **(h)** anti-ChAT and anti-NeuN labeling of the neurons in **panel f. (i)** Luminance of anti-NeuN label versus area of anti-ChAT label for trigeminal motoneurons in 3 rats. **(j)** Luminance of anti-NeuN label versus area of anti-ChAT label for facial motoneurons in 3 rats. **(k)** Histograms of the first principal component of log(Luminance) and log(Area) for the trigeminal motoneurons in **panel i. (l)** Histograms of the first principal component of log(Luminance) and log(Area) for the facial motoneurons in **panel j.**

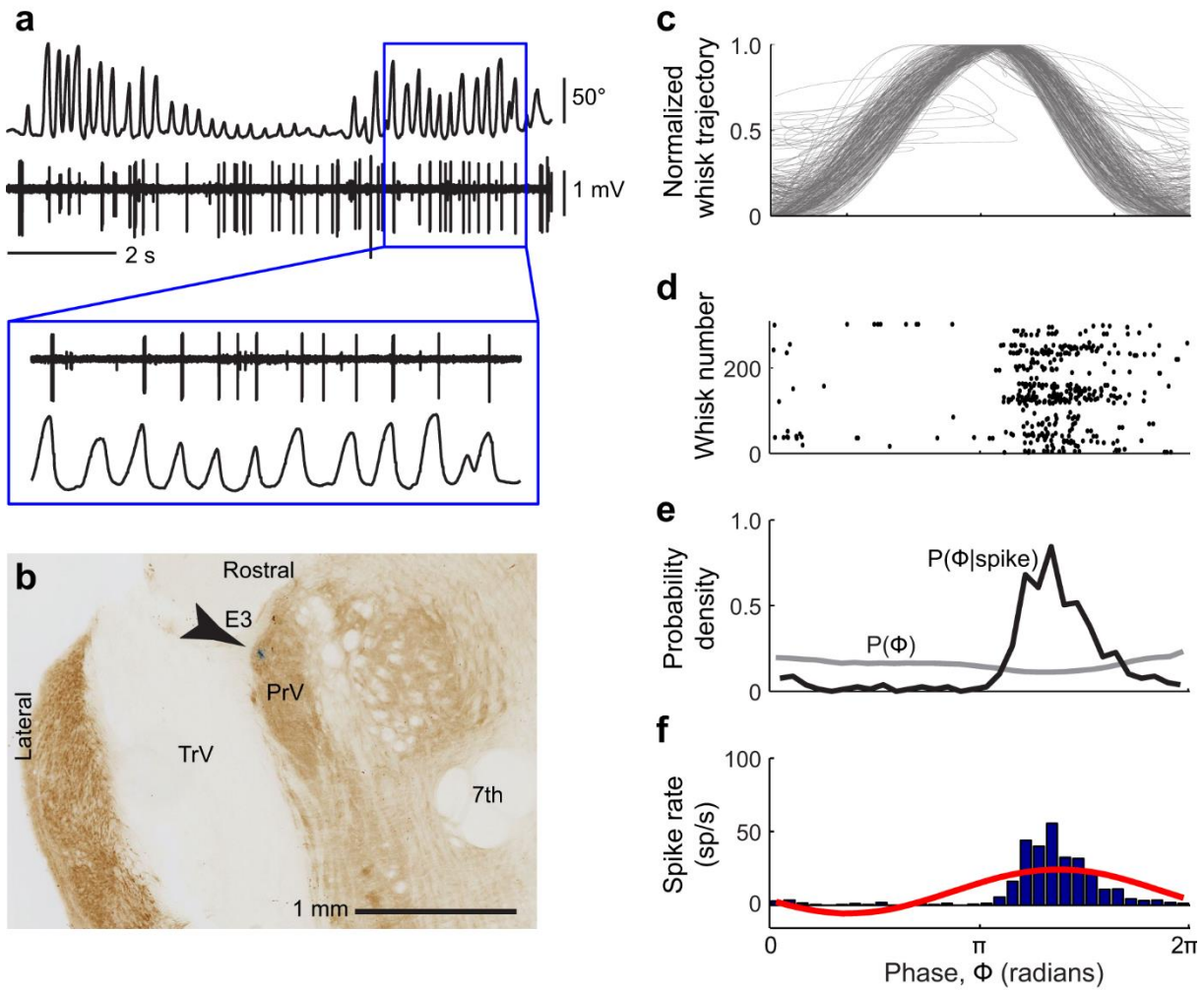

Figure 3.4 Spiking activity of a unit in nucleus PrV during free-air whisking. (a) Simultaneously recorded vibrissa motion and spiking activity during free-air whisking. **(b)** Location of the recorded unit in **panel a** in a horizontal brainstem section counterstained for cytochrome oxidase activity. Multi-unit activity at this recording site was detected in response to manual deflections of vibrissa E3. **(c)** Normalized vibrissa position as a function of phase in the whisk cycle, $\phi(\tau)$. All whisks during the record are superimposed. **(d)** Raster of phases in the whisk cycle at which spikes occurred. Each line on the y-axis represents one whisk. **(e)** Probability density function of all observed instantaneous phases (gray) and phases conditioned on a spike (black). **(f)** Spike rate as a function of phase in the whisk cycle (blue) and a sinusoidal fit to the data (red).

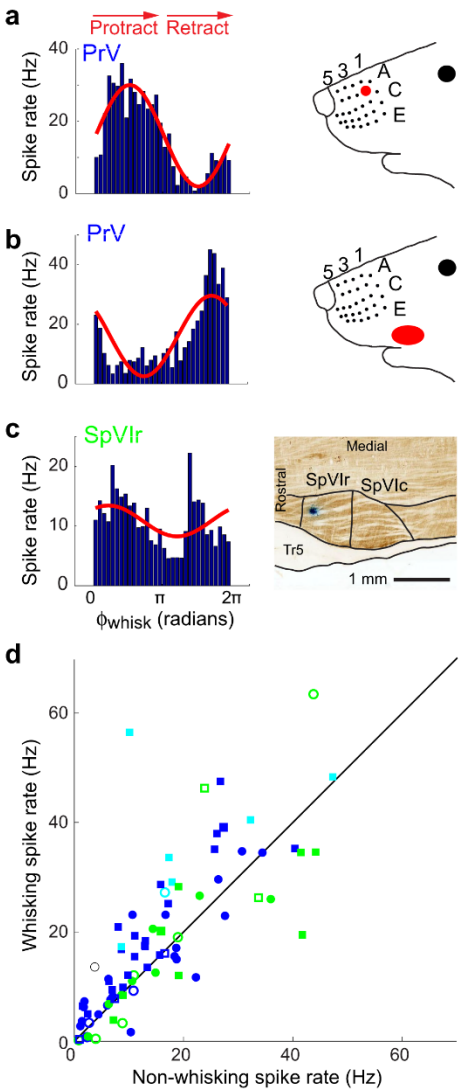

Figure 3.5 Spiking responses of units in nucleus PrV and SpVIr to free-air whisking. (a) Spike rate versus phase in the whisk cycle (blue histogram, left) and sinusoidal fit (red, left). of a unit in nucleus PrV. Multi-unit activity at the same recording site was elicited in response to deflections of vibrissa B1 (right). **(b)** Same as **panel a**, but for a unit in nucleus PrV that is located among units that responded to brushing the fur on the upper lip. **(c)** Spike rate versus phase in the whisk cycle (blue histogram, left) and sinusoidal fit (red, left) for a unit in nucleus SpVIr. Location of the recording site in a horizontal brainstem section (right). **(d)** Mean spike rates during whisking and non-whisking epochs for all putative single-unit (circles) and multi-unit (squares) recordings in nuclei SpVIr (green) and PrV (blue and cyan). PrV units that have macrovibrissa receptive fields (blue), as well as those that have facial skin, fur, or micro-vibrissa receptive fields (cyan) are shown. Of all of these trigeminal units, 49/56 units across 3 rats in nucleus PrV and 16/24 units across three rats in nucleus SpVIr were significantly modulated (Kuiper test, $p < 0.05$); solid symbols correspond to statistically significant modulation and open symbols to non-significant modulation.

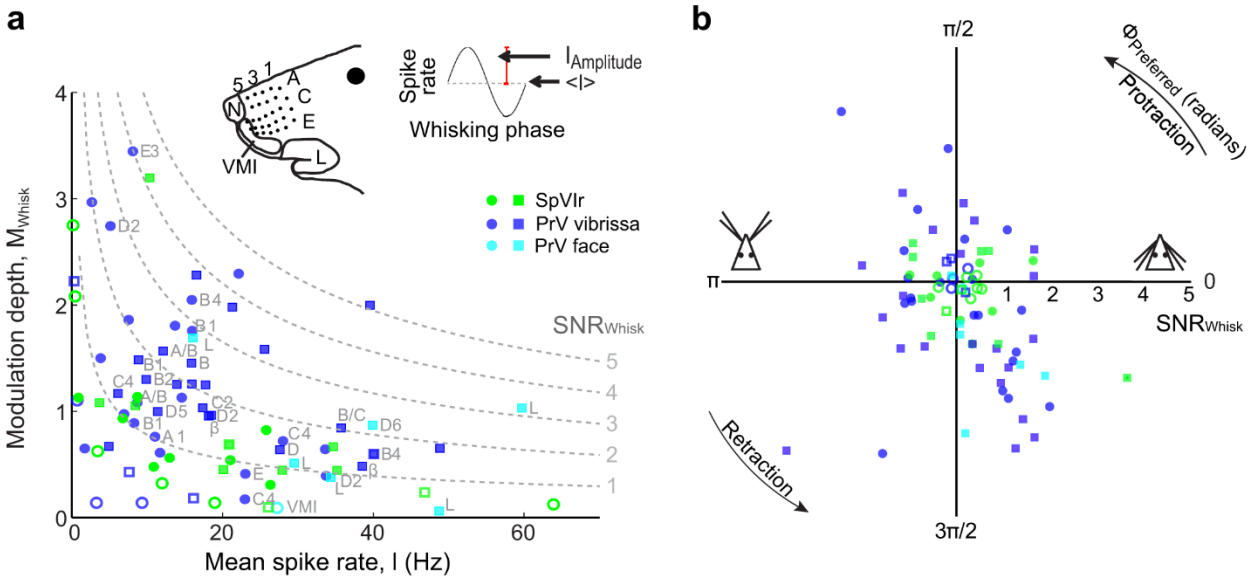

Figure 3.6 Modulation of spiking activity with free-air whisking in the trigeminal nuclei. (a) Whisking modulation, M_{Whisk}, versus mean spike rate for all units, using the notation of **Figure 5d**. Contours with constant value of SNR_{Whisk} are shown as dashed lines for a temporal window of 165 ms. Approximate receptive fields at the recording sites are labeled. **(b)** Plot of the preferred phase (polar axis) versus SNR_{Whisk} (radial axis) for all trigeminal units**.**

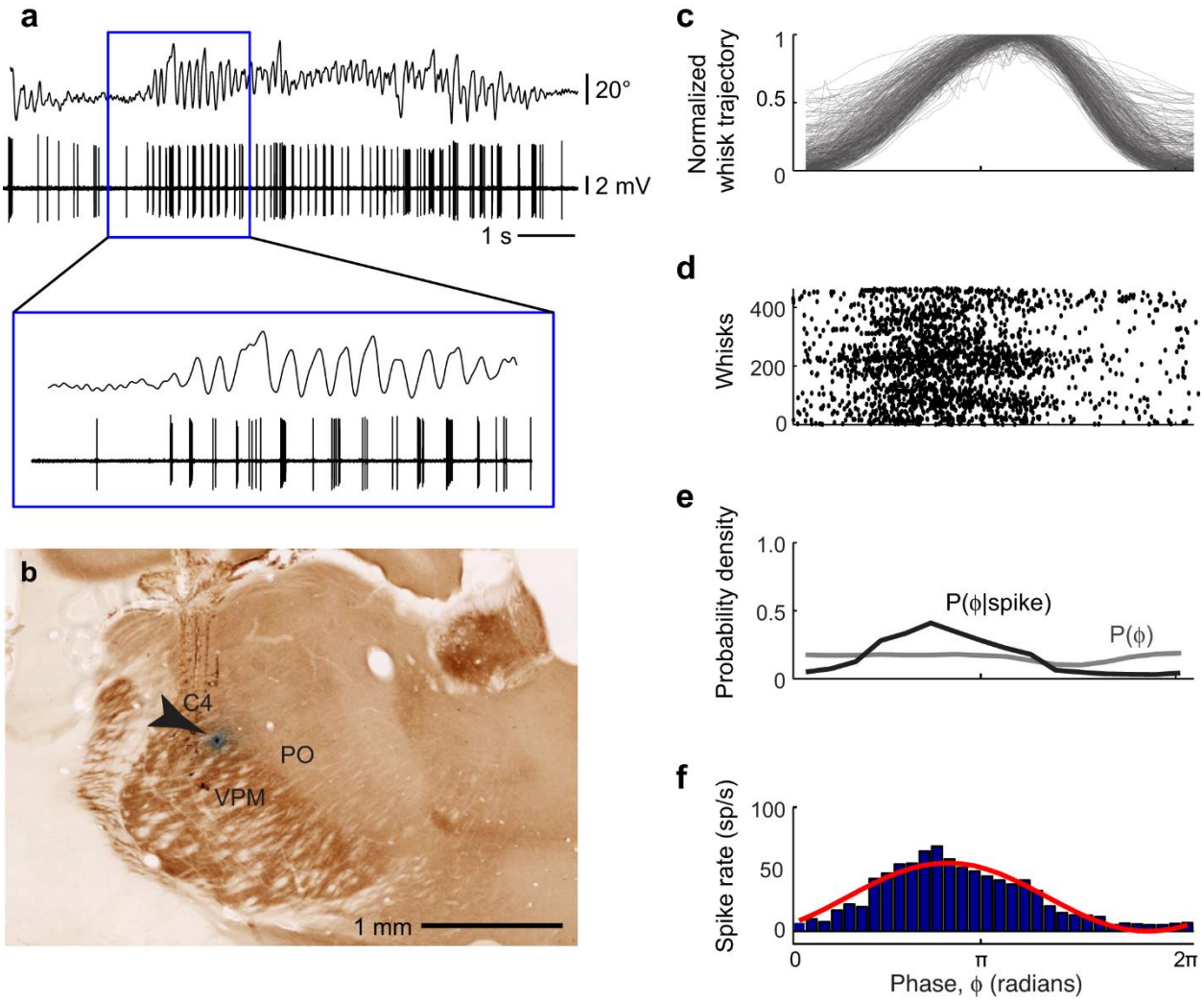

Figure 3.7 Spiking activity of a VPM neuron during free-air whisking (a) Simultaneously recorded vibrissa motion and spiking activity during free-air whisking. **(b)** Location of the recorded unit in a coronal section. Multi-unit activity at this recording site was detected in response to manual deflections of vibrissa C4. **(c)** Normalized vibrissa position as a function of phase in the whisk cycle. All whisks during the record are superimposed. **(d)** Raster of phases in the whisk cycle at which spikes occurred. Each line on the y-axis represents one whisk. **(e)** Probability density function of all observed instantaneous phases (gray) and phases conditioned on a spike (black). **(f)** Spike rate as a function of phase in the whisk cycle (blue) and a sinusoidal fit to the data (red).

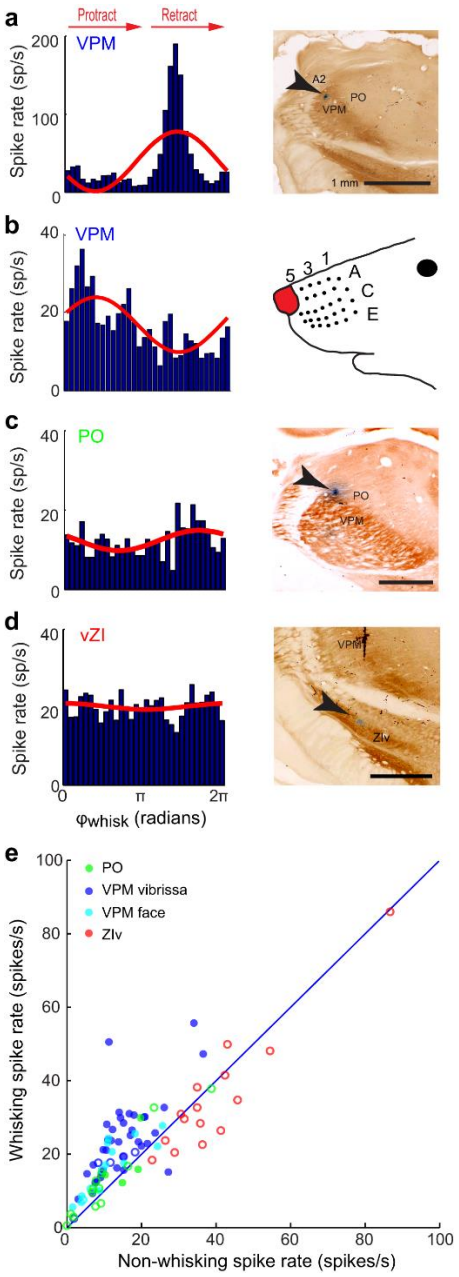

Figure 3.8 Spiking responses of additional VPM and PO thalamic and ZIv neurons to whisking in air. (a) Spike rate versus phase in the whisk cycle (blue histogram, left) and sinusoidal fit (red, right). Multi-unit activity at the same recording site was elicited in response to deflections vibrissa A2. The recording site was identified in VPM thalamus in post-hoc histology (right). **(b)** Spike rate versus phase in the whisk cycle and sinusoidal fit for a unit located in VPM thalamus. The unit was located among units that responded to brushing the naris (right). **(c)** Spike rate versus phase in the whisk cycle and sinusoidal fit for a unit located in PO thalamus. **(d)** Spike rate versus phase in the whisk cycle and sinusoidal fit for a unit located in ZIv. **(e)** Mean spike rates during whisking and non-whisking epochs for all VPM thalamic (blue and cyan), PO thalamic (green) and ZIv (red) neurons in this study. VPM neurons that have macrovibrissa receptive fields (blue), as well as those that have facial skin, fur, or micro-vibrissa receptive fields (cyan) are shown. Solid symbols correspond to statistically significant modulation and open symbols to non-significant modulation (Kuiper test, $p < 0.05$).

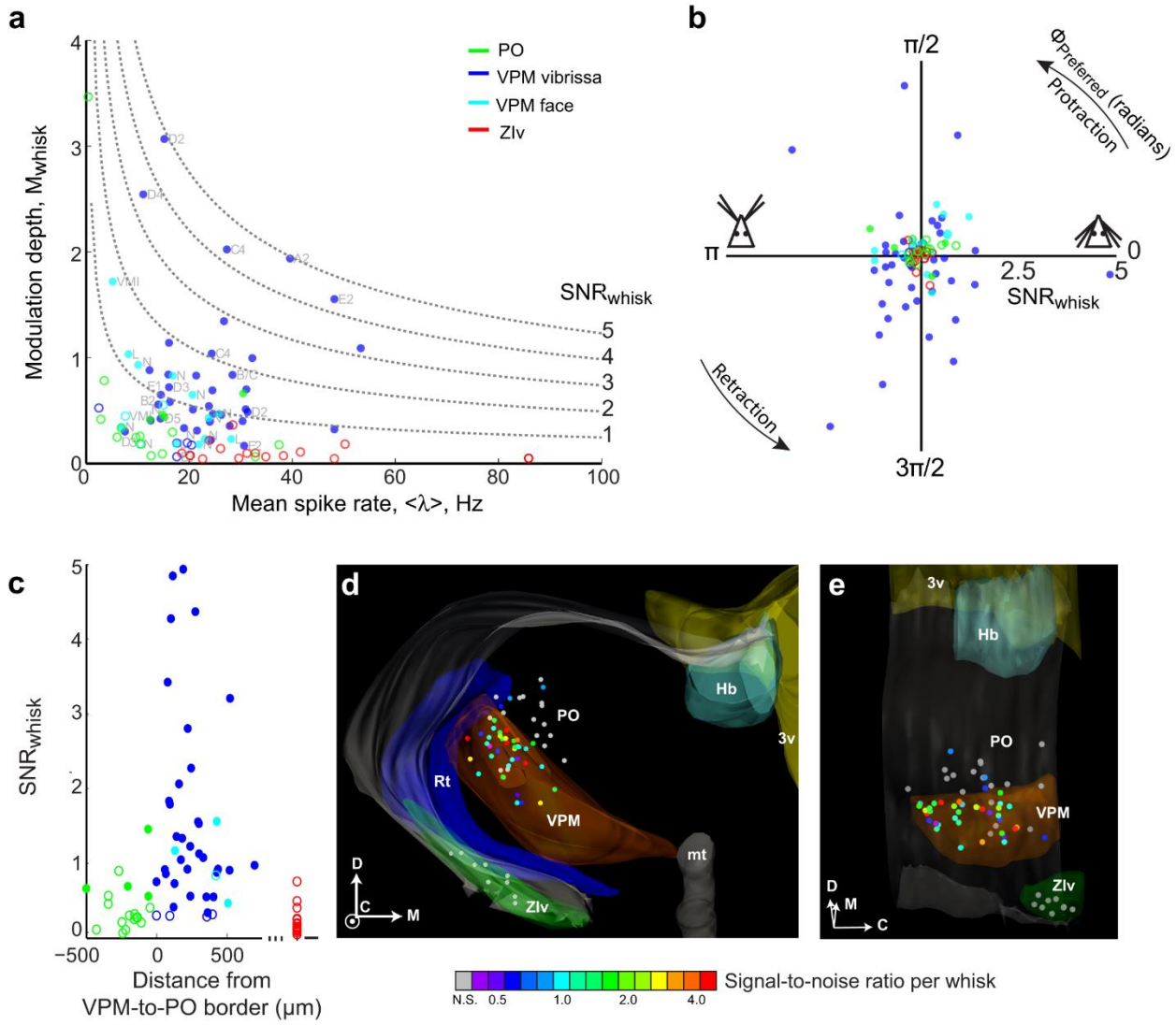

Figure 3.9 Compendium on modulation of spiking by free-air whisking by units in the thalamus and zona incerta. Modulation depth, M_{Whisk}, versus mean spike rate for individual neurons in VPM, PO, and ZIv. Conventions are as in **Figure 8e**. Contours with constant values of SNR_{Whisk} are shown as dashed lines, and approximate receptive fields at the recording sites are labeled. **(b)** Plot of the preferred phase (polar axis) versus SNR_{Whisk} (radial axis) for the units in panel a. **(c)** The value of SNR_{Whisk} versus perpendicular distance to the VPM/PO border for the labeled VPM and PO recording sites in panel a. The values of SNR_{Whisk} for neurons in ZIv are shown at the right end (red). **(d)** Rostral view of the reconstructed locations of recording sites (circles) and select anatomical borders in three dimensions. The colors of the circles represent the SNR_{Whisk} for each recorded neuron; gray corresponds to neurons that were not significantly modulated by whisking phase. Labeled structures correspond to the third ventricle (3v, yellow), habenula (Hb, teal), mammothalamic tract (mt, gray), thalamic reticular nucleus (Rt, blue), and ventral division of zona incerta (ZIv, green). The anatomical axes are shown in the lower right hand corner: dorsal (D), medial (M), and caudal (C). **(e)** An oblique view of the reconstruction in panel d.

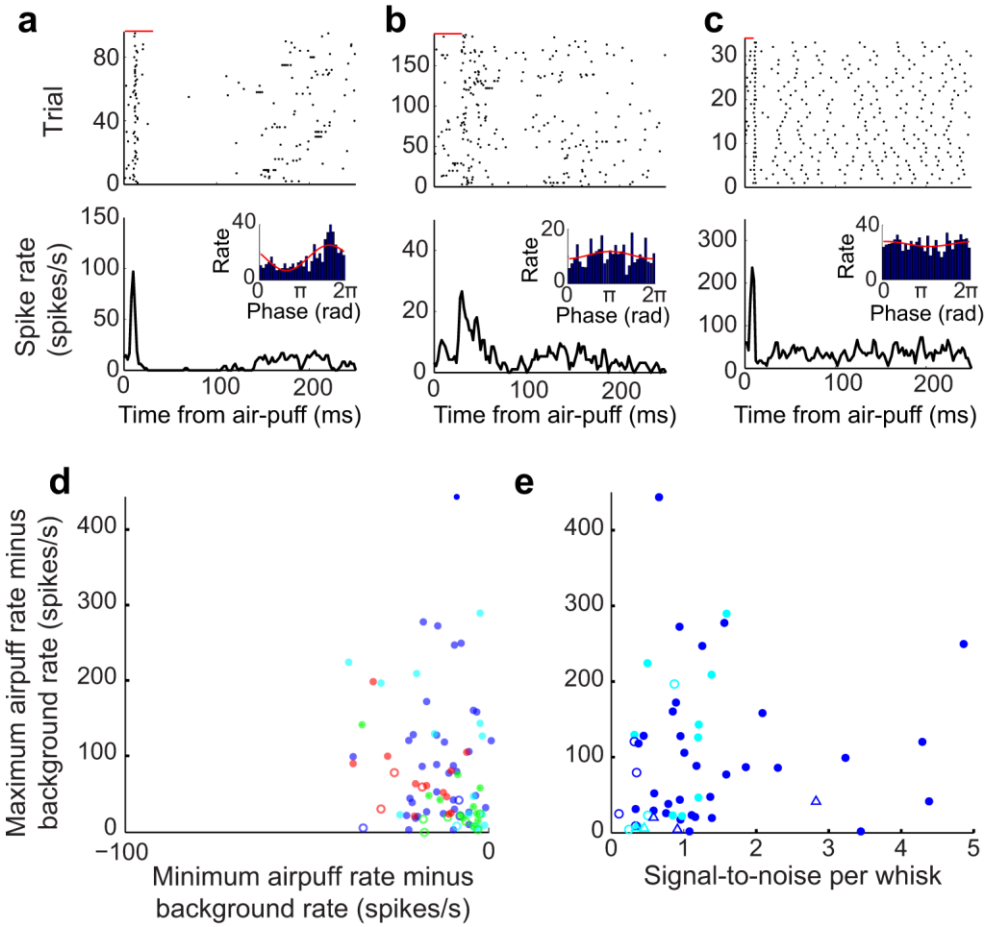

Figure 3.10 Modulation of spiking activity in response to vibrissa deflections induced by brief air-puffs for neurons in thalamus and zona incerta. (a) Raster of spike times relative to air-puff onset for a neuron in VPM thalamus (black ticks); the duration of the air-puff is shown by the red bar. A corresponding peri-stimulus time histogram (PSTH) is shown. The insert is the response of the same neuron to whisking in air, as in **Figure 6a-c**. **(b)** Raster of spike times relative to air-puff onset for a neuron in PO thalamus. Conventions are as in panel a. **(c)** Raster of spike times relative to air-puff onset for a neuron in ZIv. Conventions are as in panel a. **(d)** Modulation of spike rates upon response to air-puff deflections for neurons in VPM thalamus (blue), PO thalamus (green) and ZIv (red) versus the baseline spike rate. Modulation is calculated both as the difference between the maximum spike rate in the first 100 ms in the PSTH **(panels a-c)** and the background rate (y-axis), and as the difference between the minimum spike rate and the background rate (x-axis). Units with both statistically significant (solid circles) and non-significant modulation (open circles) are shown (KS test, $p < 0.05$). **(e)** Modulation of spike rates upon air-puff calculated as the difference between the maximum and background rates, as in **panel d**, versus SNR_{Whisk} for VPM units. Solid circles represent units with statistically significant modulation during both air puffs (KS test, $p < 0.05$) and whisking (Kuiper test, $p < 0.05$). Open circles represent units with statistically significant modulation during air-puffs only, and open triangles represent units with statistically significant modulation during whisking only.

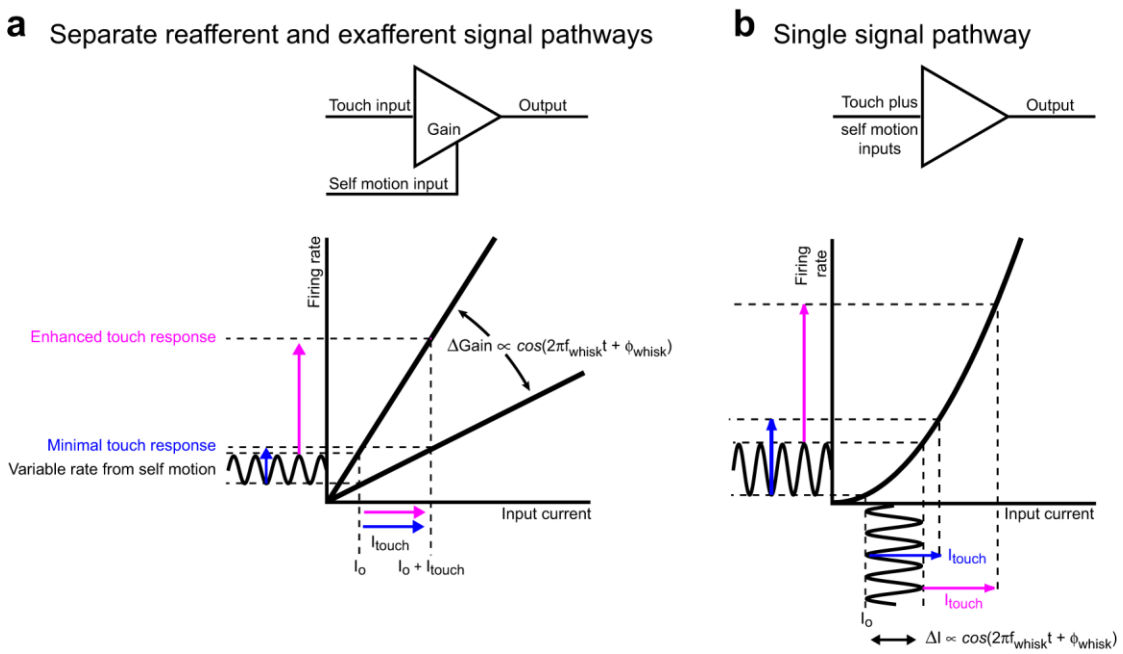

Figure 3.11 Schemes for demodulation of touch signals by vibrissa whisking signals. (a) A scheme for a single pathway for both the ex-afferent signal, which codes touch to the vibrissa, and re-afferent signal that codes phase in the whisk cycle, measured in terms of free whisking in air. The signals are mixed by a spike rate versus input current (*f*-I) function that has an accelerating slope. This scheme is relevant if both the ex-afferent and re-afferent input share the same ascending lemniscal input from VPM to layer 4 cortical neurons. **(b)** A scheme for a parallel pathways for the ex-afferent signal and an re-afferent signal that codes phase in the whisk cycle independent of touch to the vibrissae. The slope of the *f*-I curve is assumed to be modulated by the re-afferent signal, as can occur if re-afference drives shunting inhibition. This scheme is relevant if the coding of whisking by the skin and fur serves as the re-afferent signal.

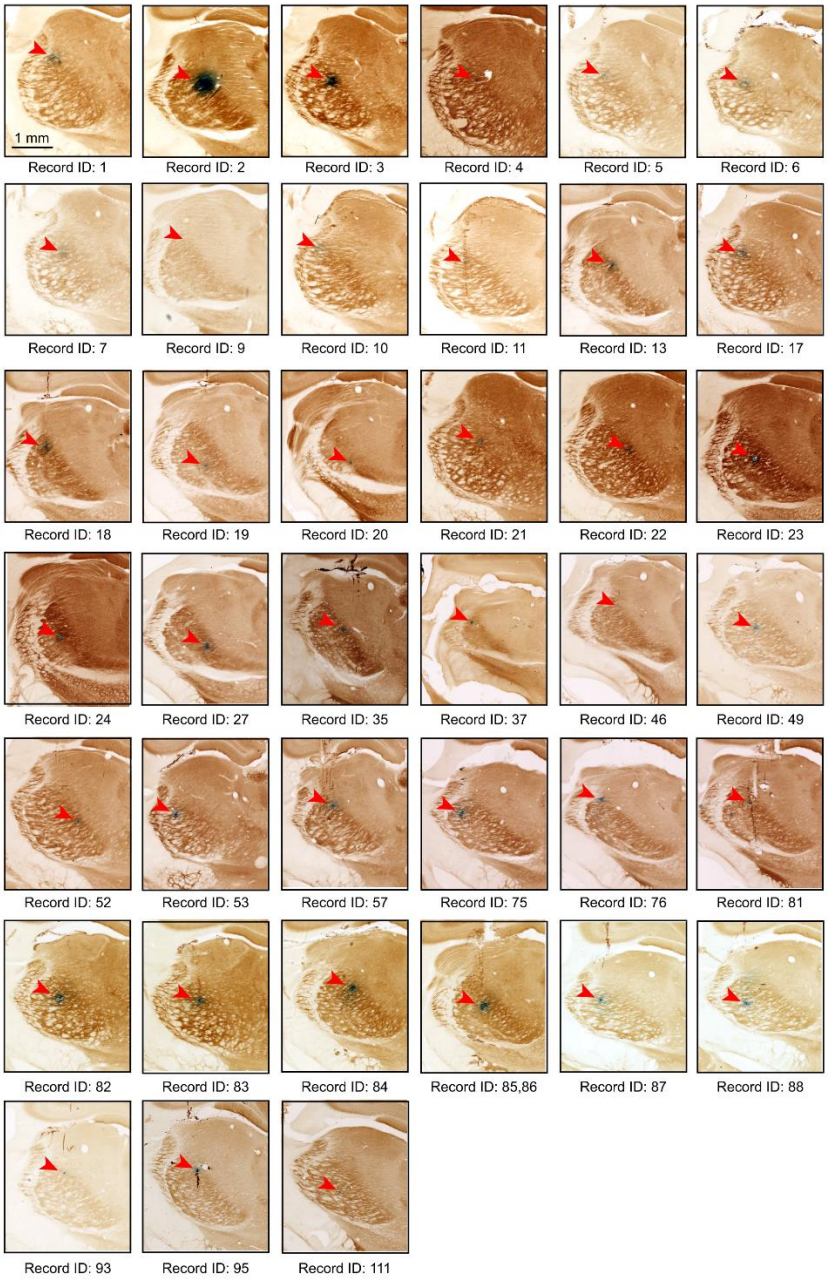

Figure S3.1 Locations of all identified recording sites in VPM thalamus.
The recording sites (blue) were demarked by depositing Chicago Sky Blue dye through the recording pipette at the conclusion of each unit recording (**Methods**). The red arrowheads point to the detected dye spots. The borders of different thalamic nuclei, including VPM and PO thalamus, as well as ZIv were identified by counterstaining the tissue for cytochrome oxidase activity (brown). These locations and borders are summarized in the 3-dimensional reconstruction shown in **Fig 3.9d,e.** Each labeled site is associated with an individual "Record ID" that links it to the electrophysiological parameters included as Supplemental Data and plotted in **Figs. 8e, 9a-c, & 10d,e.**

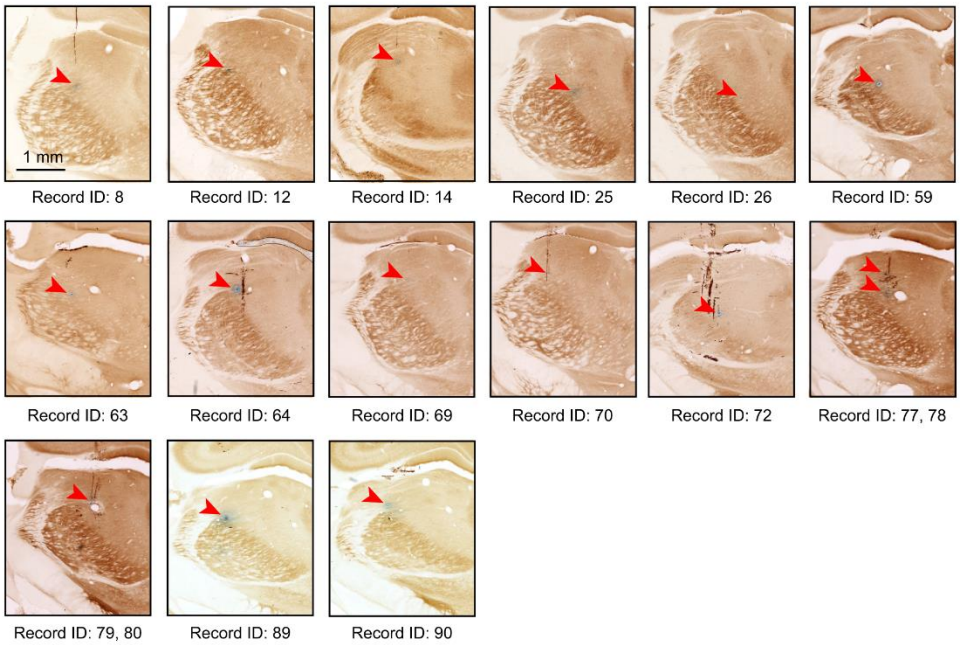

Figure S3.2 Locations of all identified recording sites in PO thalamus.
Conventions are as in **S1 Fig.**

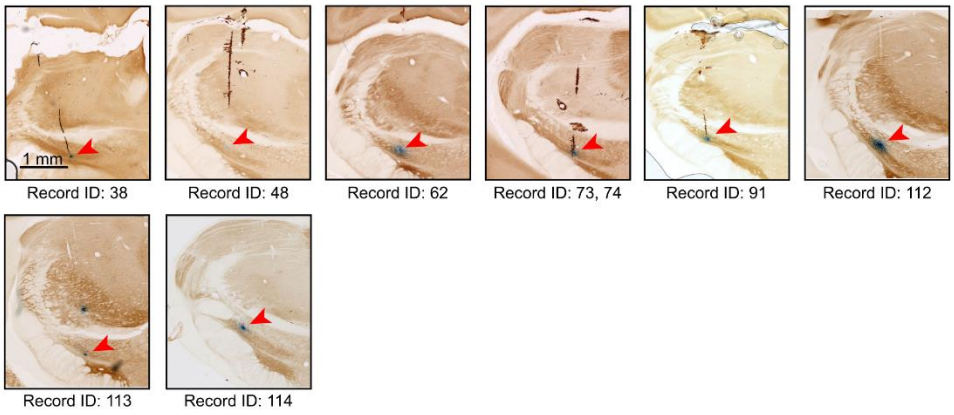

Figure S3.3 Locations of all identified recording sites in ZIv.
Conventions are as in **S1 Fig.**

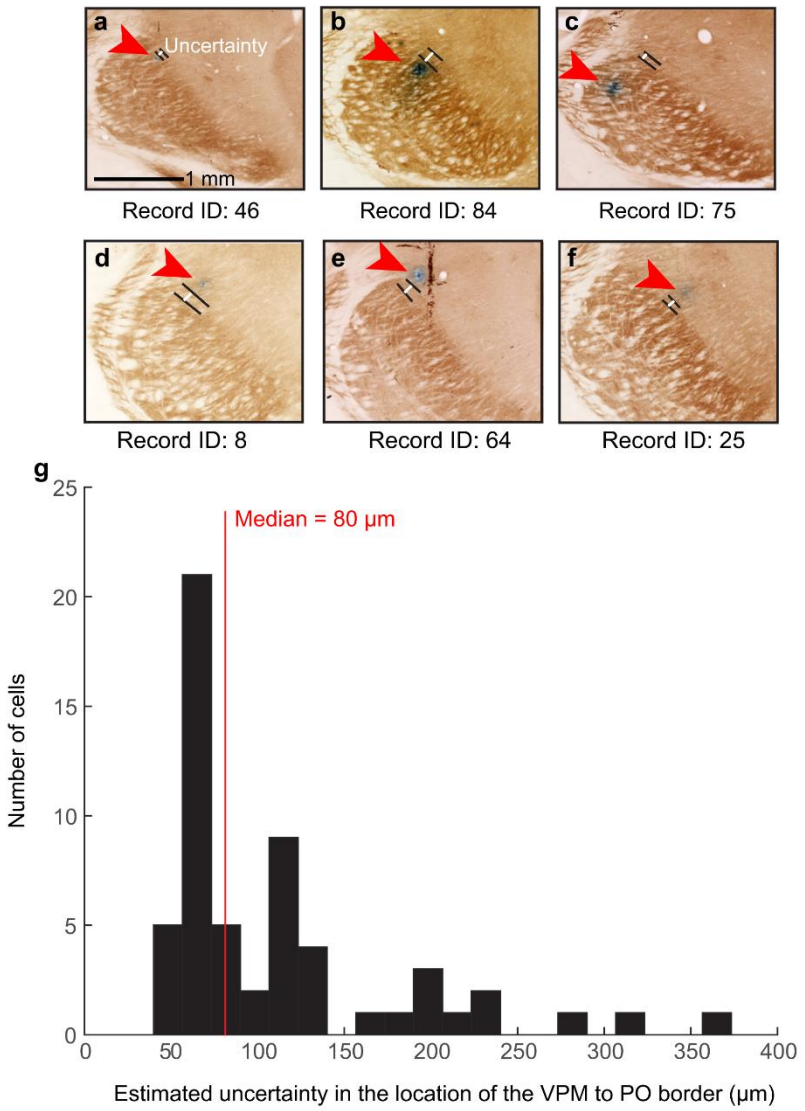

Figure S3.4 Estimate of uncertainty in defining distance to VPM/PO border

The uncertainty in the locations of recording sites relative to the VPM/PO border (**Fig 3.9c**) in our study is dominated by the inability to precisely identify the border in cytochrome-oxidase sections. This uncertainty varies with the rostro-caudal location of the cell, as the border is less clear rostrally, as well as the quality of the cytochrome-oxidase stain. **(a-f)** To estimate this uncertainty on a cell by cell basis we defined, by visual inspection, the range of locations which would lead to an ambiguous classification between VPM and PO thalamus. Six example cases are shown (black line segments). We define the uncertainty as the width of this range along the line that passes through the recording site and is approximately perpendicular to the VPM/PO border (white line segments). **(g)** Histogram of the uncertainty ranges for all labeled recording sites (median = 80 µm).

References

Abdallah, K., Artola, A., Monconduit, L., Dallel, R., and Luccarini, P. (2013). Bilateral descending hypothalamic projections to the spinal trigeminal nucleus caudalis in rats. PLoS One *8*, e73022.

Ahissar, E., Golomb, D., Haidarliu, S., Sosnik, R., and Yu, C. (2008). Latency coding in POm: Importance of parametric regimes. Journal of Neurophysiology *100*, 1152-1154.

Ahissar, E., Sosnik, R., and Haidarliu, S. (2000). Transformation from temporal to rate coding in a somatosensory thalamocortical pathway. Nature *406*, 302-306.

Ahrens, K.F., Levine, H., Suhl, H., and Kleinfeld, D. (2002). Spectral mixing of rhythmic neuronal signals in sensory cortex. Proceedings of the National Academy of Sciences USA *99*, 15176-15181.

Alloway, K.D., Smith, J.B., and Beauchemin, K.J. (2010). Quantitative analysis of the bilateral brainstem projections from the whisker and forepaw regions in rat primary motor cortex. Journal of Comparative Neurology *518*, 4546-4566.

Alstermark, B., and Isa, T. (2012). Circuits for skilled reaching and grasping. Annu Rev Neurosci *35*, 559-578.

Amundsen Huffmaster, S.L., Van Acker, G.M., 3rd, Luchies, C.W., and Cheney, P.D. (2017). Muscle synergies obtained from comprehensive mapping of the primary motor cortex forelimb representation using high-frequency, long-duration ICMS. J Neurophysiol *118*, 455-470.

Arenkiel, B.R., Peca, J., Davison, I.G., Feliciano, C., Deisseroth, K., Augustine, G.J., Ehlers, M.D., and Feng, G. (2007). *In vivo* light-induced activation of neural circuitry in transgenic mice expressing channelrhodopsin-2. Neuron *54*, 205-218.

Arriaga, G., Macopson, J.J., and Jarvis, E.D. (2015). Transsynaptic Tracing from Peripheral Targets with Pseudorabies Virus Followed by Cholera Toxin and Biotinylated Dextran Amines Double Labeling. J Vis Exp.

Azim, E., Jiang, J., Alstermark, B., and Jessell, T.M. (2014). Skilled reaching relies on a V2a propriospinal internal copy circuit. Nature *508*, 357-363.

Bae, Y.C., Choi, B.J., Lee, M.G., Lee, H.J., Park, K.P., Zhang, L.F., Honma, S., Fukami, H., Yoshida, A., and Ottersen, O.P. (2002). Quantitative ultrastructural analysis of glycine-and γ-aminobutyric acid-immunoreactive terminals on trigeminal α-and γ-motoneuron somata in the rat. Journal of Comparative Neurology *442*, 308-319.

Barthas, F., and Kwan, A.C. (2017). Secondary Motor Cortex: Where 'Sensory' Meets 'Motor' in the Rodent Frontal Cortex. Trends Neurosci *40*, 181-193.

Batschelet, E. (1981). Circular statistics in biology, Vol 371 (London: Academic Press).

Berens, P. (2009). CircStat: A MATLAB toolbox for circular statistics. Journal of Statistical Software *31*, 1-21.

Berridge, K.C., Aldridge, J.W., Houchard, K.R., and Zhuang, X. (2005). Sequential super-stereotypy of an instinctive fixed action pattern in hyper-dopaminergic mutant mice: a model of obsessive compulsive disorder and Tourette's. BMC Biol *3*, 4.

Berryman, L.J., Yau, J.M., and Hsiao, S.S. (2006). Representation of object size in the somatosensory system. Journal of Neurophysiology *96*, 27-39.

Bonazzi, L., Viaro, R., Lodi, E., Canto, R., Bonifazzi, C., and Franchi, G. (2013). Complex movement topography and extrinsic space representation in the rat forelimb motor cortex as defined by long-duration intracortical microstimulation. J Neurosci *33*, 2097-2107.

Borke, R.C., Nau, M.E., and Ringler, R.L. (1983). Brain-stem afferents of hypoglossal neurons in the rat. Brain Research *269*, 47-55.

Bosman, L.W.J., Houweling, A.R., Owens, C.B., Tanke, N., Shevchouk, O.T., Rahmati, N., Teunissen, W.H.T., Ju, C., Gong, W., Koekkoek, S.K.E., *et al.* (2011). Anatomical pathways involved in generating and sensing rhythmic whisker movements. Frontiers in Integrative Neuroscience *5*, e1.

Bourassa, J., Pinault, D., and Deschênes, M. (1995). Corticothalamic projections from the cortical barrel field to the somatosensory thalamus in rats: A single-fibre study using biocytin as an anterograde tracer. European Journal of Neuroscience *7*, 19-30.

Bowden, R.E.M., and Mahran, Z.Y. (1956). The functional significance of the pattern of innervation of the muscle quadratus labii superioris of the rabbit, cat, and rat. Journal of Anatomy *90*, 221-227.

Brecht, M., Krauss, A., Muhammad, S., Sinai-Esfahani, L., Bellanca, S., and Margrie, T.W. (2004). Organization of rat vibrissa motor cortex and adjacent areas according to cytoarchitectonics, microstimulation, and intracellular stimulation of identified cells. J Comp Neurol *479*, 360-373.

Brodmann, K., and Gary, L.J. (2006). Brodmann's localisation in the cerebral cortex : the principles of comparative localisation in the cerebral cortex based on cytoarchitectonics (New York, NY: Springer).

Brown, A.R., and Teskey, G.C. (2014). Motor cortex is functionally organized as a set of spatially distinct representations for complex movements. J Neurosci *34*, 13574-13585.

Brown, A.W.S., and Waite, P.M.E. (1974). Responses in the rat thalamus to whisker movements produced by motor nerve stimulation. Journal of Physiology *238*, 387-401.

Buchthal, F., and Schmalbruch, H. (1980). Motor unit of mammalian muscle. Physiol Rev *60*, 90-142.

Caggiano, V., Leiras, R., Goni-Erro, H., Masini, D., Bellardita, C., Bouvier, J., Caldeira, V., Fisone, G., and Kiehn, O. (2018). Midbrain circuits that set locomotor speed and gait selection. Nature *553*, 455-460.

Carvell, G.E., Miller, S.A., and Simons, D.J. (1996). The relationship of vibrissal motor cortex unit activity to whisking in the awake rat. Somatosensory and Motor Research *13*, 115-127.

Castro, A., Raver, C., Li, Y., Uddin, O., Rubin, D., Ji, Y., Masri, R., and Keller, A. (2017). Cortical Regulation of Nociception of the Trigeminal Nucleus Caudalis. J Neurosci *37*, 11431-11440.

Chapin, J.K., and Nicolelis, M. (1994). Spatiotemporal structure of somatosensory responses of many-neuron ensembles in the rat ventral posterior medial nucleus of the thalamus. Journal of Neuroscience *14*, 3511-3532.

Crochet, S., and Petersen, C.C.H. (2006). Correlating membrane potential with behaviour using whole-cell recordings from barrel cortex of awake mice. Nature Neuroscience *9*, 608-609.

Cullen, K.E. (2004). Sensory signals during active versus passive movement. Current Opinion in Neurobiology *14*, 698-706.

Curtis, J.C., and Kleinfeld, D. (2009). Phase-to-rate transformations encode touch in cortical neurons of a scanning sensorimotor system. Nature Neuroscience *12*, 492-501.

Daunicht, W.J. (1983). Proprioception in extraocular muscles of the rat. Brain Research *278*, 291-294.

de Kock, C.P., and Sakmann, B. (2009). Spiking in primary somatosensory cortex during natural whisking in awake head-restrained rats is cell-type specific. Proceedings of the National Academy of Sciences USA *106*, 16446-16450.

Diamond, M.E., Armstrong-James, M., Budway, M.J., and Ebner, F.F. (1992a). Somatic sensory responses in the rostral sector of the posterior group (POm) and in the ventral posterior medial nucleus (VPM) of the rat thalamus: Dependence on the barrel field cortex. Journal of Comparative Neurology *319*, 66-84.

Diamond, M.E., Armstrong-James, M., and Ebner, F.F. (1992b). Somatic sensory responses in the rostral sector of the posterior group (POm) and in the ventral posterior medial nucleus (VPM) of the rat thalamus. Journal of Comparative Neurology *318*, 462-476.

Dieterich, M. (2007). Central vestibular disorders. Journal of Neurology *354*, 559-568.

Donoghue, J.P., and Parham, C. (1983). Afferent connections of the lateral agranular field of the rat motor cortex. Journal of Comparative Neurology *217*, 390-404.

Donoghue, J.P., and Wise, S.P. (1982). The motor cortex of the rat: Cytoarchitecture and microstimulation mapping. Journal of Comparative Neurology *212*, 76-88.

Erzurumlu, R.S., and Killackey, H.P. (1979). Efferent connections of the brainstem trigeminal complex with the facial nucleus of the rat. Journal of Comparative Neurology *188*, 75-86.

Esposito, M.S., Capelli, P., and Arber, S. (2014). Brainstem nucleus MdV mediates skilled forelimb motor tasks. Nature *508*, 351-356.

F., L.A.S., and S., S.C. (1917). OBSERVATIONS ON THE EXCITABLE CORTEX OF THE CHIMPANZEE, ORANG-UTAN, AND GORILLA. Quarterly Journal of Experimental Physiology *11*, 135-222.

Fee, M.S., Mitra, P.P., and Kleinfeld, D. (1996). Automatic sorting of multiple unit neuronal signals in the presence of anisotropic and non-Gaussian variability. Journal of Neuroscience Methods *69*, 175-188.

Fee, M.S., Mitra, P.P., and Kleinfeld, D. (1997). Central versus peripheral determinates of patterned spike activity in rat vibrissa cortex during whisking. Journal of Neurophysiology *78*, 1144-1149.

Ferezou, I., Haiss, F., Gentet, L.J., Aronoff, R., Weber, B., and Petersen, C.C.H. (2007). Spatiotemporal dynamics of cortical sensorimotor integration in behaving mice. Neuron *56*, 907-923.

Finn, I.M., Priebe, N.J., and Ferster, D. (2007). The emergence of contrast-invariant orientation tuning in simple cells of cat visual cortex. Neuron *54*, 137-152.

Francis, J.T., Xu, S., and Chapin, J.K. (2008). Proprioceptive and cutaneous representations in the rat ventral posterolateral thalamus. Journal of Neurophysiology *99*, 2291-2304.

Frederick, B.R. (1953). The cerebral cortex of man. By Wilder Penfield and Theodore Rasmussen. The Macmillan Company, New York, N.Y. 1950. 248 pp. American Journal of Physical Anthropology *11*, 441-444.

Friedman, D.P., and Jones, E.G. (1981). Thalamic input to areas 3a and 2 in monkeys. Journal of Neurophysiology *45*, 59-85.

Friese, A., Kaltschmidt, J.A., Ladle, D.R., Sigrist, M., and Jessell, T.M. (2009). Gamma and alpha motor neurons distinguished by expression of transcription factor Err3. Proceedings of the National Academy of Sciences USA *106*, 13588-13593.

Fritsch, G., and Hitzig, E. (2009). Electric excitability of the cerebrum (Uber die elektrische Erregbarkeit des Grosshirns). Epilepsy Behav *15*, 123-130.

Furuta, T., Nakamura, K., and Deschenes, M. (2006a). Angular tuning bias of vibrissa-responsive cells in the paralemniscal pathway. Journal of Neuroscience *26*, 10548-10557.

Furuta, T., Nakamura, K., and Deschenes, M. (2006b). Angular tuning bias of vibrissa-responsive cells in the paralemniscal pathway. J Neurosci *26*, 10548-10557.

Furuta, T., Timofeeva, E., Nakamura, K., Okamoto-Furuta, K., Togo, M., Kaneko, T., and Deschênes, M. (2008). Inhibitory gating of vibrissal inputs in the brainstem. Journal of Neuroscience *28*, 1789-1797.

Furuta, T., Urbain, N., Kaneko, T., and Deschênes, M. (2010). Corticofugal control of vibrissa-sensitive neurons in the interpolaris nucleus of the trigeminal complex. Journal of Neuroscience *30*, 1832-1838.

Ganguly, K., and Kleinfeld, D. (2004). Goal-directed whisking behavior increases phase-locking between vibrissa movement and electrical activity in primary sensory cortex in rat. Proceedings of the National Academy of Sciences USA *101*, 12348-12353.

Gentet, L.J., Avermann, M., Matyas, F., Staiger, J.F., and Petersen, C.C.H. (2010). Membrane potential dynamics of GABAergic neurons in the barrel cortex of behaving mice. Neuron *65*, 422–435.

Georgopoulos, A.P., Kalaska, J.F., Caminiti, R., and Massey, J.T. (1982). On the relations between the direction of two-dimensional arm movements and cell discharge in primate motor cortex. J Neurosci *2*, 1527-1537.

Gibson, J.J. (1962). Observations on active touch. Psychological Review *69*, 477-491.

Golomb, D., Ahissar, E., and Kleinfeld, D. (2005). Coding of stimulus frequency by latency in thalamic networks through the interplay of $GABA_B$-mediated feedback and stimulus shape. Journal of Neurophysiology *95*, 1735-1750.

Gonzalez-Joekes, J., and Schreurs, B.G. (2012). Anatomical characterization of a rabbit cerebellar eyeblink premotor pathway using pseudorabies and identification of a local modulatory network in anterior interpositus. J Neurosci *32*, 12472-12487.

Granit, R. (1970). The Basis of Motor Control (London: Academic Press).

Graziano, M.S., and Aflalo, T.N. (2007). Mapping behavioral repertoire onto the cortex. Neuron *56*, 239-251.

Graziano, M.S.A. (2016). Ethological Action Maps: A Paradigm Shift for the Motor Cortex. Trends Cogn Sci *20*, 121-132.

Graziano, M.S.A., Taylor, C.S.R., and Moore, T. (2002). Complex movements evoked by microstimulation of precentral cortex. Neuron *34*, 841-851.

Grinevich, V., Brecht, M., and Osten, P. (2005a). Monosynaptic pathway from rat vibrissa motor cortex to facial motor neurons revealed by lentivirus-based axonal tracing. Journal of Neuroscience *25*, 8250-8258.

Grinevich, V., Brecht, M., and Osten, P. (2005b). Monosynaptic pathway from rat vibrissa motor cortex to facial motor neurons revealed by lentivirus-based axonal tracing. J Neurosci *25*, 8250-8258.

Haidarliu, S., Kleinfeld, D., Deschênes, M., and Ahissar, E. (2015). The musculature that drives active touch by vibrissae and nose in mice. Anatomical Record *280*, 1347-1358.

Harrison, T.C., Ayling, O.G., and Murphy, T.H. (2012). Distinct cortical circuit mechanisms for complex forelimb movement and motor map topography. Neuron *74*, 397-409.

Hattox, A.M., Priest, C.A., and Keller, A. (2002). Functional circuitry involved in the regulation of whisker movements. Journal of Comparative Neurology *442*, 266-276.

Henneman, E. (1957). Relation between size of neurons and their susceptibility to discharge. Science *126*, 1345–1347.

Hill, D.N., Bermejo, R., Zeigler, H.P., and Kleinfeld, D. (2008). Biomechanics of the vibrissa motor plant in rat: Rhythmic whisking consists of triphasic neuromuscular activity. Journal of Neuroscience *28*, 3438-3455.

Hill, D.N., Curtis, J.C., Moore, J.D., and Kleinfeld, D. (2011a). Primary motor cortex reports efferent control of vibrissa position on multiple time scales. Neuron *72*, 344–356.

Hill, D.N., Mehta, S.B., and Kleinfeld, D. (2011b). Quality metrics to accompany spike sorting of extracellular signals. Journal of Neuroscience *31*, 8699–8705.

Hines, M. (1927). Nerve and muscle. The Quarterly Review of Biology *2*, 149-180.

Hira, R., Ohkubo, F., Ozawa, K., Isomura, Y., Kitamura, K., Kano, M., Kasai, H., and Matsuzaki, M. (2013). Spatiotemporal dynamics of functional clusters of neurons in the mouse motor cortex during a voluntary movement. J Neurosci *33*, 1377-1390.

Hira, R., Terada, S., Kondo, M., and Matsuzaki, M. (2015). Distinct Functional Modules for Discrete and Rhythmic Forelimb Movements in the Mouse Motor Cortex. J Neurosci *35*, 13311-13322.

Hires, S.A., Pammer, L., Svoboda, K., and Golomb, D. (2013). Tapered whiskers are required for active tactile sensation. Elife *2*, e01350.

Hollis, E.R., 2nd, Ishiko, N., Yu, T., Lu, C.C., Haimovich, A., Tolentino, K., Richman, A., Tury, A., Wang, S.H., Pessian, M., *et al.* (2016). Ryk controls remapping of motor cortex during functional recovery after spinal cord injury. Nat Neurosci *19*, 697-705.

Huang, C.S., Hiraba, H., Murray, G.M., and Sessle, B.J. (1989). Topographical distribution and functional properties of cortically induced rhythmical jaw movements in the monkey (Macaca fascicularis). J Neurophysiol *61*, 635-650.

Huet, L.A., Schroeder, C.L., and Hartmann, M.J.Z. (2015). Tactile signals transmitted by the vibrissa during active whisking behavior. Journal of Neurophysiology, in press.

Jacquin, M., Barcia, M., and Rhoades, R.W. (1989a). Structure-function relationships in rat brainstem subnucleus interpolaris: IV. Projection neurons. Journal of Comparative Neurology *282*, 45-62.

Jacquin, M.F., Golden, J., and Rhoades, R.W. (1989b). Structure-function relationships in rat brainstem subnucleus interpolaris: III. Local circuit neurons. Journal of Comparative Neurology *282*, 24-44.

Jacquin, M.F., Renehan, W.E., Rhoades, R.W., and Panneton, W.M. (1993). Morphology and topography of identified primary afferents in trigeminal subnuclei principalis and oralis. Journal of Neurophysiology *70*, 1911-1936.

Jacquin, M.F., and Rhoades, R.W. (1990). Cell structure and response properties in the trigeminal subnucleus oralis. Somatosensory and Motor Research *7*, 265-288.

Jacquin, M.F., Stennett, R.A., Renehan, W.E., and Rhoades, R.W. (1988). Structure-function relationships in the rat brainstem subnucleus interpolaris: II. Low and high threshold trigeminal primary afferents. Journal of Comparative Neurology *267*, 107-130.

Jacquin, M.F., Woerner, D., Szczepanik, A.M., Riecker, V., Mooney, R.D., and Rhoades, R.W. (1986). Structure-function relationships in rat brainstem subnucleus interpolaris. I. Vibrissa primary afferents. Journal of Comparative Neurology *243*, 266-279.

Jeong, M., Kim, Y., Kim, J., Ferrante, D.D., Mitra, P.P., Osten, P., and Kim, D. (2016). Comparative three-dimensional connectome map of motor cortical projections in the mouse brain. Sci Rep *6*, 20072.

Kakei, S., Hoffman, D.S., and Strick, P.L. (1999). Muscle and movement representations in the primary motor cortex. Science *285*, 2136-2139.

Kerr, F.W.L. (1970). The fine structure of the subnucleus caudalis of the trigeminal nerve. Brain Research *23*, 129-145.

Khatri, V., Bermejo, R., Brumberg, J.C., Keller, A., and Zeigler, H.P. (2009). Whisking in air: Encoding of kinematics by trigeminal ganglion neurons in awake rats. Journal of Neurophysiology *101*, 836-886.

Khatri, V., Bermejo, R., Brumberg, J.C., and Zeigler, H.P. (2010). Whisking in air: Encoding of kinematics by VPM neurons in awake rats. Somatosensory and Motor Research *27*, 11-20.

Kita, T., and Kita, H. (2012). The subthalamic nucleus is one of multiple innervation sites for long-range corticofugal axons: A single-axon tracing study in the rat. Journal of Neuroscience *32*, 5990-5999.

Klein, B., and Rhoades, R. (1985). The representation of whisker follicle intrinsic musculature in the facial motor nucleus of the rat. Journal of Comparative Neurology *232*, 55-69.

Kleinfeld, D., Berg, R.W., and O'Connor, S.M. (1999). Anatomical loops and their electrical dynamics in relation to whisking by rat. Somatosensory and Motor Research *16*, 69-88.

Kleinfeld, D., and Deschênes, M. (2011). Neuronal basis for object location in the vibrissa scanning sensorimotor system. Neuron *72*, 455-468.

Kleinfeld, D., Deschênes, M., Wang, F., and Moore, J.D. (2014). More than a rhythm of life: Breathing as a binder of orofacial sensation. Nature Neurocience *15*, 647-651.

Kleinfeld, D., Sachdev, R.N.S., Merchant, L.M., Jarvis, M.R., and Ebner, F.F. (2002). Adaptive filtering of vibrissa input in motor cortex of rat. Neuron *34*, 1021-1034.

Kobayashi, M., Masuda, Y., Fujimoto, Y., Matsuya, T., Yamamura, K., Yamada, Y., Maeda, N., and Morimoto, T. (2002). Electrophysiological analysis of rhythmic jaw movements in the freely moving mouse. Physiol Behav *75*, 377-385.

Komiyama, T., Sato, T.R., O'Connor, D.H., Zhang, Y.X., Huber, D., Hooks, B.M., Gabitto, M., and Svoboda, K. (2010). Learning-related fine-scale specificity imaged in motor cortex circuits of behaving mice. Nature *464*, 1182-1186.

Kurnikova, A., Moore, J.D., Liao, S.-M., Deschênes, M., and Kleinfeld, D. (2017). Coordination of orofacial motor actions into exploratory behavior by rat. Current Biology *27*, 1-9.

Lavallee, P., Urbain, N., Dufresne, C., Bokor, H., Acsady, L., and Deschênes, M. (2005). Feedforward inhibitory control of sensory information in higher-order thalamic nuclei. Journal of Neuroscience *25*, 7489-7498.

Leiser, S.C., and Moxon, K.A. (2007). Responses of trigeminal ganglion neurons during natural whisking behaviors in the awake rat. Neuron *53*, 117-133.

Lemon, R.N. (2008). Descending pathways in motor control. Annu Rev Neurosci *31*, 195-218.

Lemon, R.N. (2016). Cortical projections to the red nucleus and the brain stem in the rhesus monkey. Brain Res *1645*, 28-30.

Lim, D.H., Mohajerani, M.H., LeDue, J., Boyd, J., Chen, S., and Murphy, T.H. (2012). In vivo large-scale cortical mapping using channelrhodopsin-2 stimulation in transgenic mice reveals asymmetric and reciprocal relationships between cortical areas. Frontiers in Neural Circuits *6*, 1-19.

Mameli, O., Stanzani, S., Mulliri, G., Pellitteri, R., Caria, M.A., Russo, A., and De Riu, P. (2010). Role of the trigeminal mesencephalic nucleus in rat whisker pad proprioception. Behavior and Brian Function *6*, 1-12.

Mameli, O., Stanzani, S., Russo, A., Romeo, R., Pellitteri, R., Spatuzza, M., Caria, M.A., and De Riu, P.L. (2008). Hypoglossal nuclei participation in rat mystacial pad control. Pflugers Archives *456*, 1189-1198.

Mao, T., Kusefoglu, D., Hooks, B.M., Huber, D., Petreanu, L., and Svoboda, K. (2011). Long-range neuronal circuits underlying the interaction between sensory and motor cortex. Neuron *72*, 111-123.

Masri, R., Bezdudnaya, T., Trageser, J.C., and Keller, A. (2008a). Encoding of stimulus frequency and sensor motion in the posterior medial thalamic nucleus. Journal of Neurophysiology *100*, 681–689.

Masri, R., Bezdudnaya, T., Trageser, J.C., and Keller, A. (2008b). Reply to Ahissar et al. Journal of Neurophysiology *100*, 1155-1157.

Massion, J. (1994). Postural control system. Curr Opin Neurobiol *4*, 877-887.

Matthews, D.W., Deschênes, M., Furuta, T., Moore, J.D., Wang, F., Karten, H.J., and Kleinfeld, D. (2015). Feedback in the brainstem: An excitatory disynaptic pathway for control of whisking. Journal of Comparative Neurology *523*, 921-942.

Matyas, F., Sreenivasan, V., Marbach, F., Wacongne, C., Barsy, B., Mateo, C., Aronoff, R., and Petersen, C.C. (2010). Motor control by sensory cortex. Science *330*, 1240-1243.

McElvain, L.E., Friedman, B., Karten, H.J., Svoboda, K., Wang, F., Deschênes, M., and Kleinfeld, D. (2018). Circuits in the rodent brainstem that control whisking in concert with other orofacial motor actions. Neuroscience *368*, 152-170.

McNamara, A.M., Cleland, T.A., and Linster, C. (2004). Characterization of the synaptic properties of olfactory bulb projections. Chem Senses *29*, 225-233.

Mehta, S.B., Whitmer, D., Figueroa, R., Williams, B.A., and Kleinfeld, D. (2007). Active spatial perception in the vibrissa scanning sensorimotor system. Public Library of Science Biology *5*, 309-322.

Miri, A., Warriner, C.L., Seely, J.S., Elsayed, G.F., Cunningham, J.P., Churchland, M.M., and Jessell, T.M. (2017). Behaviorally Selective Engagement of Short-Latency Effector Pathways by Motor Cortex. Neuron *95*, 683-696 e611.

Mitchinson, B., Grant, R.A., Arkley, K., Rankov, V., Perkn, I., and Prescott, T.J. (2011). Active vibrissal sensing in rodents and marsupials. Philosophical Transaction of the Royal Society of London B - Biological Science *366*, 3037-3048.

Mitra, P.P., and Bokil, H.S. (2008). Observed Brain Dynamics (New York: Oxford University Press).

Moore, J.D., Deschenes, M., Furuta, T., Huber, D., Smear, M.C., Demers, M., and Kleinfeld, D. (2013). Hierarchy of orofacial rhythms revealed through whisking and breathing. Nature *497*, 205-210.

Moore, J.D., Mercer Lindsay, N., Deschênes, M., and Kleinfeld, D. (2015a). Vibrissa self-motion and touch are encoded along the same somatosensory pathway from brainstem through thalamus. Public Library of Science: Biology *13*, e1002253.

Moore, J.M., Deschênes, M., and Kleinfeld, D. (2015b). Juxtacellular monitoring of single neuronal units from sub-cortical brain structures in alert, head-restrained rats. Journal of Visualized Experiments, http://www.jove.com/video/51453.

Moore*, J.D., Deschênes*, M., Furuta, T., Huber, D., Smear, M.C., Demers, M., and Kleinfeld, D. (2013). Hierarchy of orofacial rhythms revealed through whisking and breathing. Nature *469*, 53-57.

Morecraft, R.J., Ge, J., Stilwell-Morecraft, K.S., McNeal, D.W., Pizzimenti, M.A., and Darling, W.G. (2013). Terminal distribution of the corticospinal projection from the hand/arm region of the primary motor cortex to the cervical enlargement in rhesus monkey. J Comp Neurol *521*, 4205-4235.

Mori, K., Manabe, H., Narikiyo, K., and Onisawa, N. (2013). Olfactory consciousness and gamma oscillation couplings across the olfactory bulb, olfactory cortex, and orbitofrontal cortex. Front Psychol *4*, 743.

Nguyen, Q.-T., and Kleinfeld, D. (2005). Positive feedback in a brainstem tactile sensorimotor loop. Neuron *45*, 447-457.

O'Connor, D.H., Clack, N.G., Huber, D., Komiyama, T., Myers, E.W., and Svoboda, K. (2010). Vibrissa-based object localization in head-fixed mice. Journal of Neuroscience *30*, 1947-1967.

O'Connor, D.H., Hires, S.A., Guo, Z.V., Li, N., Yu, J., Sun, Q.Q., Huber, D., and Svoboda, K. (2013). Neural coding during active somatosensation revealed using illusory touch. Nature Neuroscience *16*, 958-965.

Olsson, K.A., and Westberg, K.G. (1991). Integration in trigeminal premotor interneurones in the cat. 2. Functional characteristics of neurones in the subnucleus-gamma of the oral nucleus of the spinal trigeminal tract with a projection to the digastric motoneurone subnucleus. Exp Brain Res *84*, 115-124.

Olszewski, J. (1950). On the anatomical and functional organization of the spinal trigeminal nucleus. Journal of Comparative Neurology *92*, 401-413.

Oman, C.M., and Cullen, K.E. (2014). Brainstem processing of vestibular sensory exafference: Implications for motion sickness etiology. Experimental Brain Research *232*, 2483-2492.

Ono, T., Nakamura, K., Nishijo, H., and Fukuda, M. (1986). Hypothalamic neuron involvement in integration of reward, aversion and cue signals. Journal of Neurophysiology *56*, 63-79.

Oswald, M.J., Tantirigama, M.L., Sonntag, I., Hughes, S.M., and Empson, R.M. (2013). Diversity of layer 5 projection neurons in the mouse motor cortex. Front Cell Neurosci *7*, 174.

Overduin, S.A., d'Avella, A., Carmena, J.M., and Bizzi, E. (2012). Microstimulation activates a handful of muscle synergies. Neuron *76*, 1071-1077.

Peters, A.J., Chen, S.X., and Komiyama, T. (2014). Emergence of reproducible spatiotemporal activity during motor learning. Nature *510*, 263-267.

Pfaff, D., Ribeiro, A., Matthews, J., and Kow, L.M. (2008). Concepts and mechanisms of generalized central nervous system arousal. Ann N Y Acad Sci *1129*, 11-25.

Pierret, T., Lavallee, P., and Deschênes, M. (2000). Parallel streams for the relay of vibrissal information through thalamic barreloids. Journal of Neuroscience *20*, 7455-7462.

Pinault, D. (1996). A novel single-cell staining procedure performed in vivo under elecrtrophysiological control: Morpho-functional features of juxtacellularly labed thalamic cells and other central neurons with biocytin or Neurobiotin. Journal of Neuroscience Methods *65*, 113-136.

Pinganaud, G., Bernat, I., Buisseret, P., and Buisseret-Delmas, C. (1999). Trigeminal projections to hypoglossal and facial motor nuclei in the rat. Journal of Comparative Neurology *415*, 91-104.

Porter, J.D., Guthrie, B.L., and Sparks, D.L. (1983). Innervation of monkey extraocular muscles: Localization of sensory and motor neurons by retrograde transport of horseradish peroxidase. Journal of Comparative Neurology *218*, 208-219.

Poulet, J.F., Fernandez, L.M., Crochet, S., and Petersen, C.C. (2012). Thalamic control of cortical states. Narture Neuroscience *15*, 370-372.

Premack, D., and Shanab, M.E. (1968). Rats prefer the home cage to the runway following intermittent but not consistent reinforcement. Nature *125*, 288-289.

Rathelot, J.A., and Strick, P.L. (2009). Subdivisions of primary motor cortex based on cortico-motoneuronal cells. Proceedings of the National Academy of Sciences USA, 918-923.

Reep, R.L., Corwin, J.V., Hashimoto, A., and Watson, R.T. (1987). Efferent connections of the rostral portion of medial agranular cortex in rats. Brain Res Bull *19*, 203-221.

Rice, F.L. (1993). Structure, vascularization, and innervation of the mystacial pad of the rat as revealed by the lectin Griffonia simplicifolia. Journal of Comparative Neurology *337*, 386-399.

Richmond, F.J., Thomson, D.B., and Loeb, G.E. (1992). Electromyographic studies of neck muscles in the intact cat. I. Patterns of recruitment underlying posture and movement during natural behaviors. Exp Brain Res *88*, 41-58.

Rokx, J.T., van Willigen, J.D., and Jansen, H.W. (1984). Muscle fibre types and muscle spindles in the jaw musculature of the rat. Archives of Oral Biology *29*, 25-31.

Roucoux, A., Crommelinck, M., and Decostre, M.F. (1989). Chapter 28 Neck muscle activity in eye — head coordinated movements. In Afferent Control of Posture and Locomotion, pp. 351-362.

Saiki, A., Kimura, R., Samura, T., Fujiwara-Tsukamoto, Y., Sakai, Y., and Isomura, Y. (2014). Different modulation of common motor information in rat primary and secondary motor cortices. PLoS One *9*, e98662.

Sakurai, K., Akiyama, M., Cai, B., Scott, A., Han, **B.-X.**, Takatoh, J., Sigrist, M., Arber, S., and Wang, F. (2013a). The organization of submodality-specific touch afferent inputs in the vibrissa column. Cell Reports *5*, 87-98.

Sakurai, K., Akiyama, M., Cai, B., Scott, A., Han, B.X., Takatoh, J., Sigrist, M., Arber, S., and Wang, F. (2013b). The organization of submodality-specific touch afferent inputs in the vibrissa column. Cell Rep *5*, 87-98.

Semba, K., and Egger, M.D. (1986). The facial "motor" nerve of the rat: Control of vibrissal movement and examination of motor and sensory components. Journal of Comparative Neurology *247*, 144-158.

Sessle, B.J. (1977a). Identification of alpha and gamma trigeminal motoneurons and effects of stimulation of amygdala, cerebellum, and cerebral cortex. Experimental Neurology *54*, 303-322.

Sessle, B.J. (1977b). Modulation of alpha and gamma trigeminal motoneurons by various peripheral stimuli. Experimental Neurology *54*, 323-339.

Sherwood, C.C. (2005). Comparative anatomy of the facial motor nucleus in mammals, with an analysis of neuron numbers in primates. Anat Rec A Discov Mol Cell Evol Biol *287*, 1067-1079.

Shortland, P.J., DeMaro, J.A., and Jacquin, M.F. (1995). Trigeminal structure-function relationships: A reevaluation based on long-range staining of a large sample of brainstem a beta fibers. Somatosensory & Motor Research *12*, 249-275.

Simons, D.J., and Kyriazi, H.T. (1993). Thalamocortical response transformations in simulated whisker barrels. Journal of Neuroscience *13*, 1601-1615.

Skolnick, M.I. (1962). Introduction to RADAR Systems (New York: McGraw-Hill).

Smith, J.B., Watson, G.D., Alloway, K.D., Schwarz, C., and Chakrabarti, S. (2015). Corticofugal projection patterns of whisker sensorimotor cortex to the sensory trigeminal nuclei. Frontiers of Neural Circuits *9*.

Sosnik, R., Haidarliu, S., and Ahissar, E. (2001). Temporal frequency of whisker movement. I. Representations in brain stem and thalamus. Journal of Neurophysiology *86*, 339-353.

Sreenivasan, V., Karmakar, K., Rijli, F.M., and Petersen, C.C. (2015). Parallel pathways from motor and somatosensory cortex for controlling whisker movements in mice. European Journal of Neuroscience *41*, 354-367.

Stål, P., Eriksson, P.O., Eriksson, A., and Thornell, L.E. (1990). Enzyme-histochemical and morphological characteristics of muscle fibre types in the human buccinator and orbicularis oris. Archives of Oral Biology *3*, 449-458.

Stanek, E.t., Cheng, S., Takatoh, J., Han, B.X., and Wang, F. (2014). Monosynaptic premotor circuit tracing reveals neural substrates for oro-motor coordination. Elife *3*, e02511.

Szwed, M., Bagdasarian, K., and Ahissar, E. (2003). Coding of vibrissal active touch. Neuron *40*, 621-630.

Takatoh, J., Nelson, A., Zhou, X., Bolton, M.M., Ehlers, M.D., Arenkiel, B.R., Mooney, R., and Wang, F. (2013a). New modules are added to vibrissal premotor circuitry with the emergence of exploratory whisking. Neuron *77*, 346-360.

Takatoh, J., Nelson, A., Zhou, X., Bolton, M.M., Ehlers, M.D., Arenkiel, B.R., Mooney, R., and Wang, F. (2013b). New modules are added to vibrissal premotor circuitry with the emergence of exploratory whisking. Neuron *77*, 346-360.

Tennant, K.A., Adkins, D.L., Donlan, N.A., Asay, A.L., Thomas, N., Kleim, J.A., and Jones, T.A. (2011). The organization of the forelimb representation of the C57BL/6 mouse motor cortex as defined by intracortical microstimulation and cytoarchitecture. Cereb Cortex *21*, 865-876.

Timofeeva, E., Merette, C., Emond, C., Lavallee, P., and Deschênes, M. (2003). A map of angular tuning preference in thalamic barreloids. Journal of Neuroscience *23*, 10717-10723.

Tosolini, A.P., Mohan, R., and Morris, R. (2013). Targeting the full length of the motor end plate regions in the mouse forelimb increases the uptake of fluoro-gold into corresponding spinal cord motor neurons. Front Neurol *4*, 58.

Trageser, J.C., Burke, K.A., Masri, R., Li, Y., Sellers, L., and Keller, A. (2006). State-dependent gating of sensory inputs by zona incerta. Journal of Neurophysiology *96*, 1456-1463.

Tsai, P.S., Kaufhold, J., Blinder, P., Friedman, B., Drew, P., Karten, H.J., Lyden, P.D., and Kleinfeld, D. (2009). Correlations of neuronal and microvascular densities in murine cortex revealed by direct counting and colocalization of cell nuclei and microvessels. Journal of Neuroscience *18*, 14553-14570.

Urbain, N., and Deschênes, M. (2007a). Motor cortex gates vibrissal responses in a thalamocortical projection pathway. Neuron *56*, 714-725.

Urbain, N., and Deschênes, M. (2007b). A new thalamic pathway of vibrissal information modulated by the motor cortex. Journal of Neuroscience *27*, 12407-12412.

Veinante, P., and Deschênes, M. (1999). Single- and multi-whisker channels in the ascending projections from the principal trigeminal nucleus in the rat. Journal of Neuroscience *19*, 5085-5095.

von Holst, E. (1954). Relations between the central nervous system and the peripheral organ. British Journal of Animal Behavior *2*, 89-94.

Waite, P.M.E. (1973). The responses of cells in the rat thalamus to mechanical movements of the whiskers. Journal of Physiology *228*, 541-561.

Wang, Q., and Burkhalter, A. (2007). Area map of mouse visual cortex. J Comp Neurol *502*, 339-357.

Wang, X., Liu, Y., Li, X., Zhang, Z., Yang, H., Zhang, Y., Williams, P.R., Alwahab, N.S.A., Kapur, K., Yu, B., *et al.* (2017). Deconstruction of Corticospinal Circuits for Goal-Directed Motor Skills. Cell *171*, 440-455 e414.

Welt, C., and Abbs, J.H. (1990). Musculotopic organization of the facial motor nucleus in Macaca fascicularis: a morphometric and retrograde tracing study with cholera toxin B-HRP. Journal of Comparative Neurology *291*, 621-636.

Westberg, K., Clavelou, P., Sandström, G., and Lund, J.P. (1998). Evidence that trigeminal brainstem interneurons form subpopulations to produce different forms of mastication in the rabbit. Journal of Neuroscience *18*, 6466-6479.

Yamawaki, N., Radulovic, J., and Shepherd, G.M. (2016). A Corticocortical Circuit Directly Links Retrosplenial Cortex to M2 in the Mouse. J Neurosci *36*, 9365-9374.

Young, P.A., Young, P.H., Tolbert, D.L., and Young, P.A. (2015). Basic clinical neuroscience, Third edition. edn (Philadelphia: Wolters Kluwer).

Yu, C., Derdikman, D., Haidarliu, S., and Ahissar, E. (2006). Parallel thalamic pathways for whisking and touch signals in the rat. Public Library of Science Biology *4*, e124.

Zucker, E., and Welker, W.I. (1969). Coding of somatic sensory input by vibrissae neurons in the rat's trigeminal ganglion. Brain Research *12*, 134-156.